UNIVERSITÉ DE STRASBOURG

ÉCOLE DOCTORALE MSII

Laboratoire ICUBE

THÈSE présentée par:

Marouane BOUDHAIM

soutenue le : **26 septembre 2018**

pour obtenir le grade de: **Docteur de l'université de Strasbourg**

Discipline/ Spécialité: Énergétique

OPTICAL AND THERMAL PERFORMANCE OF COMPLEX FENESTRATION SYSTEMS IN THE CONTEXT OF BUILDING INFORMATION MODELLING

THÈSE dirigée par :

Mme SIROUX Monica	Professeur des universités, INSA de Strasbourg

RAPPORTEURS :

M. SALAGNAC Patrick	Professeur des universités, Université de La Rochelle
M. EL GANAOUI Mohammed	Professeur des universités, Université de Lorraine

---

AUTRES MEMBRES DU JURY :

M. CHAMAGNE Didier	Professeur des universités, Université de Franche-Comté

ACKNOWLEDGEMENTS

First and foremost, I want to thank my parents for many reasons I cannot summarize in a single paragraph. Moreover, I want to thank my little brother and sister, even though they are useless.

Secondly, I want to thank my PHD advisor, who trusted me for this great task, and went great lengths to ensure the smooth progress of this thesis.

I also want to thank my mentors, Bruno Bueno and Tilmann E. Kuhn, for the significant technical and scientific support they provided during these three years.

I also want to thank the rest of the ISE SOFA team for providing an enjoyable work atmosphere. With special thanks to Thibault Pflug, Christoph Maurer and Johannes Eisenlohr, who also provided scientific help. I also have to acknowledge the unlucky Jin Suk and Vladislav who had to read my programming code.

Finally, I want to thank Arconic Foundation, that has funded this PHD.

CONTENTS

List of Tables

List of Figures

List of Abbreviations and Acronyms

AEC architecture, engineering and construction

BIM Building Information Modelling

BRDF Bi-directional reflection distribution functions

BSDF Bi-directional scattering distribution functions

BTDF Bi-directional transmission distribution functions

CDA Continuous Daylight Autonomy

C_{ds} is a relatively more accurate contribution of the sky patches

CFS Complex Fenestration System

CGI CIE Glare Index

CIE International Commission on Illumination

CR contribution of the sun reflected from all room components without the window

CF direct contribution of the sun through the window.

Cres convective heat loss from respiration

D Daylight matrix

DA Daylight Autonomy

Dd is the day matrix without the outside environment's inter-reflections.

DF Daylight Factor

DGI Daylight Glare Index

DGP Daylight Glare probability

DHI Diffuse horizontal illuminance

DNI direct normal illuminance

e layer depth

E the evaporative heat exchange of the skin

e(x,x') intensity of emitted light from x' to x

EC the evaporative heat exchange at thermal neutrality feeling

eDGP Enhanced Simplified DGP

EN European Standard

Eres evaporative heat loss from respiration

ET* Effective Temperature

$\mathbf{F_{(A\rightarrow B)}}$ view factor from surface A to surface B

g(x,x') the factor for the geometrical occlusion of two points x and x'

GHI global

gu glazing unit

h convection heat transfer coefficient

H the dry heat loss

$\mathbf{h_r}$ linear radiative heat transfer coefficient

I(x,x') the intensity of light passing from x to x'

$\mathbf{i_m}$ total vapor permeation efficiency

IFC Industry Foundation Classes

LEED The Leadership in Energy and Environmental Design

LR the Lewi Ratio

M metabolic rate

MAE mean absolute error

MVD Model View Definition

$\mathbf{p_{(ET^*,s)}}$ the saturated vapor pressure at ET* in kPa

$\mathbf{p_a}$ water vapor pressure in ambient air

PMV Predicted Mean vote

PNTB Plan Transition Numérique dans le Bâtiment

PPD Predicted percentage dissatisfaction

r Spearman's rank correlation coefficient

R Thermal resistance of the CFS

Re Thermal resistance between the outdoor environment and the outer CFS layer

Ri Thermal resistance between the inner environment and the inner CFS layer

rMBE relative mean bias errors

RMSE relative root mean squared errors

S contact surface's area

Sd contains the luminance of the patches with direct sun component only.

sd shading device

SDA Spatial Daylight Autonomy

sDGP Simplified DGP

SET* Standard Effective Temperature

SHGC Solar Heat Gain coefficient

$\mathbf{s_{sun}}$ is the sky patches luminance, in relatively higher resolution.

t temperature

T Transmission matrix

$\mathbf{T_{(max,80\%)}}$ maximum operative temperature for 80% acceptability range

$\mathbf{T_{(max,90\%)}}$ maximum operative temperature for 90% acceptability range

$\mathbf{T_{(min,80\%)}}$ maximum operative temperature for 80% acceptability range

$\mathbf{T_{(min,90\%)}}$ maximum operative temperature for 90% acceptability range

$\mathbf{t_a}$ air temperature

$\mathbf{t_D}$ temperature of day D

$\mathbf{t_{mr}}$ mean radiant temperature

$\mathbf{t_{othe}}$ operative temperature

$\mathbf{T_{outdm}}$ mean outdoor temperature

$\mathbf{T_{com}}$ Comfort Operative Temperature

UDA Useful Daylight Autonomy

UGR Unified GLare Rating

v air velocity

V View matrix

VCF Visual Comfort Probability

$\mathbf{V_d}$ is the view matrix without the room's inter-reflections.

W mechanical work

w the skin wittedness

$\boldsymbol{\alpha_0}$ the outer layer absorbance

$\boldsymbol{\alpha_A}$ monochromatic absorption coefficient of surface A

$\boldsymbol{\alpha_i}$ the inner layer absorbance

$\boldsymbol{\lambda}$ thermal conductivity

$\boldsymbol{\rho}$ Pearson correlation coefficient

ρ(x,x',x") intensity of light scattered from x" to x through patch of surface at x'

$\boldsymbol{\sigma}$ Stefan–Boltzmann constant

$\boldsymbol{\varphi}$ heat flux

INTRODUCTION

1.1 Energy efficiency buildings

The building sector is responsible for a very high portion of the total energy consumption. In France, it is the biggest energy consumption sector and it produces 23% of CO2. In the European Union, it represents 40% of the energy consumption and 36% of CO2 emissions [EUR2017]. Improving the energy efficiency of the buildings can reduce the energy consumption by 5% to 6% and the CO2 emissions by approximately 5% [EUR2017]. In order to improve the energy efficiency, new buildings address this issue during the design phase. Energy simulations are performed to optimize the energy savings and building costs.

In France, the state has been working toward reducing greenhouse gas emissions in 2030 by 30% and in 2050 by 75% compared to 1990. As of the building's sector, it aims to reduce by 38% the energetical consumption between 2009 and 2020, going from 250 kWh/m² to 150 kWh/m², and to 100 kWh/m² in 2050. Such optimization of the energy efficiency of the buildings requires to study and optimize its energy related components.

The façade, as the interface between the exterior and interior space, plays a key role in the energy efficiency of a building. Better management of windows, which are usually the main daylighting and solar heat source in the room, has been demonstrated to provide both peak and average energy savings [CHO1984 and STE2013]. In this thesis we mainly focus on the estimation of the façade's role in the energetical performance of the building.

1.2 Complex Fenestration Systems

One of the most prominent technologies used in facades are Complex Fenestration Systems (CFS). CFS are non-opaque window technologies with at least one layer that is non-transparent or has switchable properties. They are used in order to optimize daylighting and energy savings. The performance of each CFS product is very case dependent. Therefore, in order to reliably estimate its performance and to use the most efficient product, accurate daylighting and energy analysis simulation on the building is required.

An accurate evaluation of the CFS impact is made from simulations that usually require information about building's geometry, opaque materials' thermal properties and the optical and thermal properties of transparent and translucent materials. It is traditionally handled by architects for common buildings, but more and more architecturally complex buildings prove to be a difficult challenge and get subcontracted to expert consulting.

1.3 The challenge of CFS performance estimation

These simulations prove to be a major challenge to even the field experts in practice. The thermal and optical characterization of the façade is usually insufficient. It requires the CFS properties to be either measured or calculated from highly detailed models that are often not provided, because they may be considered trade secret or may not even exist. And even when available they often represent the ideal design without the imperfections due to manufacturing. Measurements are usually the only way to get reliable data. For example, Deviation of ±5° has been observed between slats tilt angle [KAT2017] in some venetian blinds products.

Figure 1: Venetian blinds with major shape imperfections.

Moreover, in practical situations, the challenge goes beyond the modelling of the CFS itself. Modelling the building is a very time-consuming task. The preparation of the input can take up to 80% of the time spent in a project [Baz2001].

Recent efforts are switching toward the use of richer models as Building Information Modelling (BIM). Such models offer a great opportunity for automation and cost savings. Performance of multiple CFS models could be compared in the building's design phase in order to choose the most suitable product. Unfortunately, BIM suffers from many limitations. Using a BIM model in the current state as simulation input is not a trivial task. This thesis will discuss and evaluate BIM compatible methodologies for automated simulations of daylighting, optical comfort, thermal performance and comfort.

Therefore, our problem statement can be summarized as: **Is it possible to assess the thermal and optical performance of CFS from BIM?** This question involves several other questions:

- Are there BIM compatible models in literature that can be used? Which criteria should be used to choose the models?
- Is it possible to integrate existing models into BIM, and how?
- How accurate would such a workflow be?

1.4 Dissertation content

The **first chapter** of this thesis focuses on the introduction of the context of the and the main questions we will discuss. It presents the importance of energy efficiency buildings, before focusing on the Complex Fenestration Systems, and the questions we will try to answer in this thesis.

The **second chapter** discusses the subject on a deeper level and gives an overview of the state the art of the building's energy consumption. Afterwards it explains the concept of BIM, its definition, scope and limitations. Then it discusses the Complex Fenestration Systems. It explains its core concept and redefines its scope in our thesis. This chapter is then followed by an overview of the literature optical and thermal modelling of CFS. It also defines the concepts of thermal and visual comfort.

The **third chapter** explains a newly developed methodology that aims to represent the Building Information Modelling's architectural data in an energy/optics simulation software. It uses a set of algorithms and geometrical transformations to be able to assess the optical, visual comfort, energetical and thermal comfort performance of the Complex Fenestration Systems.

The **fourth chapter** assesses the accuracy of the optical models, that were chosen from literature in the second chapter, and linked to BIM with the third chapter's methodology. These models' accuracy is evaluated upon two aspects: daylight autonomy and visual comfort. It uses experimentally collected data.

The **fifth chapter** is analogous to the precedent chapter but focuses on the thermal aspect. It evaluates the thermal model on its ability to predict room temperature and the thermal comfort of the occupants. This assessment is based on a theoretical study where the model is compared to the current standard, ISO 15099.

The **sixth chapter** offers a case study, to show how are developed methodology can be used in real world scenario. Moreover, it shows an extension of the methodology applied to Building Integrated Photovoltaics, that has been successfully performed in real-world scenarios in collaboration with Fraunhofer ISE.

The **seventh chapter** is the conclusion of this thesis. It presents an overview of the presented work, along with perspectives of future work that can extend the research performed in this thesis.

1 CONTEXT OF THE STUDY

The evaluation of BIM compatible methodologies for automated simulations of daylighting, optical comfort, thermal performance and comfort of Complex Fenestration Systems in this thesis will start by defining the meaning and scope of these concepts, as long as present a summary of the current research and advancement in the field.

We will start by defining Building Information Modeling concept first, then we will define our subset of the study that is limited to complex fenestrations. Afterwards we will analyze the state of the art methodologies to thermally and optically evaluate CFS performance.

1.5 Building Information Modelling

1.5.1 Definition

Building Information Modelling has been defined by the National Building Specification as “a process for creating and managing information on a construction project across the project lifecycle. One of the key outputs of this process is the Building Information Model, the digital description of every aspect of the built asset. This model draws on information assembled collaboratively and updated at key stages of a project. Creating a digital Building Information Model enables those who interact with the building to optimize their actions, resulting in a greater whole life value for the asset.”

BIM is a new technology for the architecture, engineering and construction (AEC) that aims to remedy to many of the defects of the traditional CAD software for buildings design, management and coordination. CAD software has usually been used as 2d drawing tool to communicate building plans. While these plans have been used with success, it required human understanding. As a result, it was not computer processable for many other purposes. The main reason is that CAD software was originally designed to mainly convey geometry, therefore lacking strong semantical and topological information. To convey these information CAD software users resorted to the use of layers and annotations. Unfortunately, such methods can only convey a limited set of information and is not reliably processable by other software.

Building Information Modeling has been therefore developed with the CAD experience learned. It is now capable of designing the building as a rich and smart 3d model. Its scope is not only limited to modeling the building but can go beyond as a communication tool. The scope of BIM varies between industry actors. In order to distinguish between these visions, we will refer to the **Little Bim** and **Big BIM** terminology.

- **Little BIM** is the vision of BIM as an advanced model of the building. It is essentially a semantically and topologically rich model. Walls are aware that they are walls. A Slabs is aware that they it is inside a stem wall. The main benefit of this model is to provide an interoperable model between software.
- **Big BIM**'s vision extends beyond the limits of little BIM. It views the building model as one component of BIM. It additionally sees BIM as the modeling of the whole construction process. BIM is therefore a communication and coordination tool that is used between different actors in the creation, maintenance and destruction phase of the building lifecycle.

In this thesis, we will mainly focus in the little BIM vision to provide an interoperable exchange data format between architects' software and simulation tools. Therefore, the next section will discuss the little BIM technologies available.

1.5.2 Legal context of BIM [BED2017]

The European Union has been actively promoting Building Information Modelling. This effort has taken shape in the directive number 2014/24, adopted by the Council of the European Union "*For public works contracts and design contests, Member States may*

require the use of specific electronic tools, such as of building information electronic modelling tools or similar. ..."

French legislation took into account this directive with the ordinance "marchés publics" of the 23rd July 2015 and with the article 42 of the law number 2014-1545. Starting from 2017, all public markets require the inclusion of BIM. German legislation requires from 2020 the inclusion of BIM in all transportation construction projects.

1.5.3 BIM in France, Europe and worldwide

As much in the French level as in the international level, more and more regulations and development programs have started getting geared toward Building Informaiton Modelling [BED2017]. In **France**, the law Duflot/Pinel draw two main development axes:

- The group "Développer des matériaux innovants et inventer de nouvelles façons de construire" has been tasked with the construction and renovation of 500 000 housings and oriented its research toward Building Information Modelling
- BIM and heritage management with the group "Plan Bâtiment Durable"

Mr. Bertrand Delcambre has been nominated in 2014 as "ambassadeur du numérique dans le bâtiment" and has been made responsible of the Steering Committee "Plan Transition Numérique dans le Bâtiment" (PNTB).

The committee concluded that BIM can be a driving factor for the numerical transition to reduce the environmental impact mainly through cost reduction. It also suggested to better standardise BIM usage.

In the **United-Kingdom**, it has been decided that starting from 2006, all public markets have to use Building Information Modelling. The UK also required the usage of Industry Foundation Classes (IFC), a BIM format further discussed in 1.5.4 .

In **Nordic countries** (Finland, Norway and Denmark), huge BIM investment has been funded from 2002, before requiring it in every construction project in 2007.

The **Netherlands** have launched the Rijkswaterstaat BIM Program, that required Building Information Modelling for all major construction projects. It also mandated the usage of IFC format.

In **Spain,** in the community of Catalonia, BIM usage is required for public markets.

The **United State of America** require Building Information Modelling for all the Public Service Building and US Army building starting from 2007.

The **United Arab Emirates** require it for every public building in the municipality of Dubai from 2014.

In **China** in the municipality of Shangai, it is required to use BIM for every public building with a surface of 20 000m² or more.

In **Hong Kong** BIM is required for every new building project from 2014.

In **Australia** it is required from 2016 for every governmental project.

In **South Korea** it is required for every new project that is public or costs 50M $ or more.

In **Singapore** it is required from 2015 for every building project with 5 000 m² or more.

1.5.4 BIM formats

BIM has seen a lot of investment from the AEC industry, but currently only two software lead the BIM authoring software market: Autodesk Revit and ArchiCAD. This software uses their own proprietary format, only compatible with their own suite of software. These proprietary formats produce de facto a vendor lock-in, which goes against the philosophy of interoperability of BIM. Fortunately, this software also supports exportation to alternative open BIM formats:

- **Green building XML**: has been developed originally by Green Building Studio with the support of the California Energy Commission Public Interest Energy Research. It has been developed in order to facilitate the transition between the building model and energy software analysis tools.
- **Industry Foundation Classes** (IFC): is developed by BuildingSMART [BSM2017] to provide a collaboration format. It aims to provide a format interoperable between BIM software and software analysis tools used in the AEC industry.

In this thesis, we chose to use the IFC format for our BIM methodologies. This choice is motivated by its openness and goal to interoperability, and also by the fact that BuildingSMART is supported by many industry leaders, as the BIM software developers of Revit and ArchiCAD themselves. Which makes it the main candidate for being the BIM standard in the foreseeable future. It should be noted that its

specifications are now registered by ISO and are an international standard ISO 16739:2013.

1.5.5 IFC schema

IFC schema defines classes for each building component. FC format relies on the definition of multiple classes with an inheritance hierarchy. For example, it defines an IfcWall class to describe walls. This class has a parent class which is IfcBuildingElement. IfcBuildingElement is defined in ISO 6707-1:1989 : “Vertical construction usually in masonry or in concrete which bounds or subdivides a construction works and fulfils a load bearing or retaining function”. IfcWall is its child class because it inherits its attributes according to IFC specifications, while being restricted to walls in buildings. IfcWall has in turn a child class: IfcWallStandardCase. IfcWallStandardCase is a wall that is vertical with a fixed thickness.

IFC schema has a top-down approach. It has the benefit of the modifying the whole semantic stack when one value changes, preserving thus its integrity, at the cost of an additional layer of complexity [DONG2017]. This additional complexity makes it unsuitable for direct use by end users, as architects, but more geared towards experts, as software developers [BAZ1997]. Therefore, AEC industry users cannot usually rely on using IFC directly but have to rely on a prior work by experts. Unfortunately, IFC has many shortcomings that doesn’t permit a perfect mapping of current methodologies and practices into IFC. In the next section, we will discuss some IFC limitations that we encountered in our research.

1.5.6 IFC shortcomings

Despite BuildingSMART efforts, it should be noted that IFC suffer from real world limitations. This is mainly due to the fact that IFC is only an exchange data format, no BIM authoring software works natively with it. Some incompatibilities reside between the original platform and IFC philosophy. In our research, we faced the following limitations:

- **Geometry errors** : Most IFC files we dealt with had geometrical errors, such as misconnecting walls or misplaced windows. Other independent studies releved other errors as clash errors, space definition errors or boundary surface errors [LIL2015]

- **Classification errors** : Some IFC files had building components classified in the wrong category. For example slabs defined as walls.
- **Material errors** : Some building components' material has the wrong properties, resulting in transluscent walls.
- **Limited filtering means** : While IFC has a standard way to limit IFC export into a subset, called MVD (Model View Definition). Its capabilities are in practice limited to filtering out a whole class of building components. For example we can filter out doors, but we cannot filter out only internal doors and keep the external ones.
- **Non parametric design** : IFC doesn't keep the parameters responsible of the geometry, but only the resulting geometry. For example, it doesn't describe venetian blinds geometry as a function of the tilt angle, but only offer the geometry for an arbitrary tilt angle.
- **No query language** : There is no standard language or software to query IFC files. It is therefore hard to execute queries on the files as it is possible on databases. For example, there is no standard command to query the number of rooms in a build
- **Quantisation of space** : IFC can only represent a finite precision number for geometrical coordinates. We noticed some problems between software using the same IFC as they didn't use the same precision.
- **Inconsistency** : Some IFC files do not follow the same specification as others.
- **Level of detail** : BIM authoring software offer ways to choose the level of details, but for our study, none of the level of geometrical details was right. We end up always using higher level of detail than needed, resulting in slower processing.
- **Slow evolution** : IFC is developed by BuildingSmart. The main released versions have known a slow evolution. IFC 1.0 was released in 1997, and has known steady evolution until IFC2.3-TC1 realeased in 2007. Afterwards the IFC4 version was released 6 years later in 2013. The release of new features is dependant on the standardisation committee approval. Moreover, new versions aren't automatically supported by BIM software. In fact, the IFC2.3 version released more than 10 years ago is still only partially working. This slow

evolution makes it hard to accompany the innovation in building construction and to integrate innovant products.

These errors can be severely limiting the interoperability of IFC files. The biggest problem in our study was the geometrical errors, as they hardly human correctible. Complex Fenestration Systems performance is highly dependant on its geometry. Taking into account IFC limitations, the models to represent the CFS should encapsulate its geometry into a virtual model and not used it directly. In literature, there has already been some work to link IFC to energy simulation software, that we will present in the next section.

1.5.7 IFC related work

In the state of art, only few methodologies have been developed in order to create a Building Energy Model from BIM:

WoonSeong and JeongWook [WOO2016] proposed a methodology to convert IFC into object-oriented physical modeling-based energy modeling. They developed a BIM2BEM software that generate a BEM inside Modelica.

Rose and Bazjanac [COD2015] proposed a methodology to extract 2nd level boundaries [BAZ2010] from IFC. 2nd level boundaries are surface boundaries with information on what lay behind the surface. In order to generate them, graph traversal methods to calculate heat flow paths have been proposed. This methodology leads to a model usable in Energy Plus simulation software.

Lilis et al. [LIL2014] proposed an alternative method for 2nd level boundaries calculation. It relies on the use of "Binary Space Partition Tree" [FUC1980] combined with a new algorithm "Common Boundary Intersection Projection" to figure out the surface pairs and classify them.

These methodologies, while successfully recreating a BEM from IFC, did not focus on a detailed modelling of complex fenestration systems that can be standardized and used for most systems.

Moreover, these techniques were not pushed to be compatible with accurate daylighting and visual comfort analysis. In our study, we will try to suggest from literature, and validate, BIM-compatible methodologies that accurately describe the CFS and its daylighting, visual comfort, energy and thermal comfort performance.

In this dissertation, we will present a newly methodology to link these models with BIM (c.f. chapter 2). The suggested methodology is fully sufficient for optical simulations. For the thermal performance evaluation, this methodology provides an input that should further be processed with the methodology of Lilis et al. [LIL2014] or Cody et al. [COD015] in order to be compatible with the current energy simulation software.

The choice of the models takes into account the IFC shortcomings that were presented. Because of the BIM limitations, we think that there are three main characteristics that should be present in such models:

- **Independent of the geometrical data**: as BIM has currently several problems in practice with geometrical data, we believe that the model should imperatively reside in the semantical layer of the data and avoid the geometrical layer.
- **Generally applicable**: The models should not be limited to a narrow subset of CFS but apply as broadly as possible with minimalistic assumptions on the product.
- **Measurable**: The input data of the model should be fully measurable from the complex fenestration system. This characteristic is often necessary for models that aim to be compatible even with innovative product, as experimental data can be leveraged instead of assumptions. Moreover, in practical scenario, it has been noted that products diverge from ideal design because of the manufacturing process. Therefore, measurements remain as the only way to have reliable data.

Moreover, these models should be sufficiently accurate for their usage. The accuracy of the chosen models will be analyzed in this thesis (c.f. chapter 3 and 4).

In the next section, we will present complex fenestration systems and define the study's scope, before presenting the optical and thermal models developed in the scientific literature.

1.6 Complex Fenestration Systems

1.6.1 Definition and scope

Complex Fenestration Systems usually refer to any window technology that incorporates a light-scattering, light-redirecting or switchable layer. They have been defined [KLE1994a] as "windows with non-specular shading devices (such as shades, blinds, etc.)". In this thesis, CFS refers to the whole windows system, i.e. the glazing

unit(s) + the shading device(s). The studied methodologies, unless noted otherwise, are also valid for *simpler* fenestration systems without shading device.

CFS is in this research is limited in scope to passive windows technologies. Passive technologies are the technologies that do not use of mechanical and electrical devices [DOE2012], in contrast with active technologies as building integrated photovoltaics. In the next section, we will discuss which technologies we will consider in this thesis.

1.6.2 Classification

Complex Fenestrations Systems market incorporates many different technologies and products. Traditionally, CFS has been classified according to their glazing units and the shading typology [CAR2014]:

- Type of insulating glass: double or triple glazing unit, heat absorbing and solar control, etc.
- Type of opening: horizontal sliding, tilt and slide…
- Type of frame materials: wood, PVC…
- Type of spacers between the pane: aluminium, stainless steel…
- Air permeability
- Water tightness
- Wind resistance
- Thermal performance
- Glare performance

While these criteria have often been used to describe CFS, recent studies try to assess their characteristics by using a new methodology, based on the distinction between the **design space** and the **evaluation space** [KUH2017]. The concept behind these terms is very similar to the mathematical vector spaces.

Each space can be described with a vector base, called here parameters, which are orthogonal, i.e. independent. The design space is characterized by design parameters, and the evaluation space by the evaluation parameters. The design space contains the parameters that can be adjusted by the designer to shape the Complex Fenestration System. The evaluation space contains the metrics upon which we evaluate the performance of the CFS.

The author of this concept enumerates the design parameters for solar control systems. Following is a subset of this parameters limited to the scope of our study:

- Technology:
    - **Venetian blinds**

Figure 2: picture of venetian blinds (source: Direct Blinds)

    - **Awnings**

Figure 3 : Awning blinds (source: Westral)

    - **Vertical louvre blinds**

Figure 4 : Vetical blinds (source: EASi blinds)

- **Pleated blinds**

Figure 5: pleated blinds (source: www.pleated-blinds-direct.co.uk)

- **Roller shutters**

Figure 6: Roller shutters (source: The Shutter Guy)

- **Sun sails**

Figure 7: Sun sails (source: Argola)

- **Curtain panels**

Figure 8: Curtain panels (source: Crate and Barrel)

- **Individual slats**
- **Overhangs**

Figure 9 : Overhangs (source: Wikipedia)

- **Roller blinds**

Figure 10 : Roller blinds (source: Dunelm)

- **Solar control glass**

Figure 11: Solar control glass (source: Saint-Gobain Glass)

- Position:
  - **External**
  - **Integrated, between glass panes**
  - **Internal**
- Control:
  - **Manual control**

- **With central up-down commands**
- **Fully automated control**

For the evaluation spaces, the following criteria are considered:

- Daylighting
- Visual comfort
- Passive solar gain control
- Thermal comfort
- Influence on circadian and neuroendocrine regulation
- Outdoor colour specifications and colour uniformity
- Colour rendering of objects in a daylit room viewed from outdoors
- Outdoor glare
- Increased temperature of urban areas due to solar radiation absorbed by dark areas

In this thesis, for the design parameters, it is not possible to cover the whole enumerated space, as it is not possible to validate the methodologies across the whole spectrum due to the very high number of possible products. While the thesis aims to be as general as possible, the validation chapters will focus in practice on two main products: a double-glazing pane without shading device, a double-glazing pane with an external venetian. The control parameter of the fenestration is out of the scope of the thesis.

For the evaluation criteria, we are targeting the limited subset of: daylighting, visual comfort, passive solar gain control and thermal comfort. Therefore, in this thesis we will present models and methodologies that evaluate these criteria for Complex Fenestration System that can be integrated with Building Information Modelling.

In order to do choose the right methodologies, we have to take into account the BIM limitations that were discussed earlier (c.f. 1.5.6).

1.7 Optical performance assessment

1.7.1 Ray-tracing

Lighting simulations algorithms have always been a challenging problem in computer sciences. Current computers are not able to handle all modern light transport models,

such as quantum effects, and therefore rely on a subset of models with predictable optical behavior is implemented.

These models have known a steady evolution where Bi-directional reflection distribution functions (BRDF) have been specified for different materials, until the introduction of the currently most used algorithms, radiosity and ray-tracing [OCH2011].

In our choice of methodology, we have retained ray-tracing [KAJ1986] over radiosity as the latter make strong assumption about surface materials that is not always true. Radiosity assumes that all surfaces have a diffuse reflection, while such assumption is true in many cases, it is not suitable for our vision of BIM that provides a general method to cover most building cases.

Ray-tracing in the other has been validated for daylighting in multiple studies using real buildings [UBB1998, ASH2001 and GAL2002] or laboratory settings [MAR1995, KHO1996, FON1999, WIEN2004]. Moreover, research has actually pointed that ray-tracing provides better accuracy for energy-savings simulation programs [TSA2003]

Ray-tracing algorithm is an algorithm that solves the rendering equation [KAJ1986]:

$$I(x,x') = g(x,x')¿ \quad (1)$$

- x,x',x" are respectively the position of the camera or viewer position, the observed surface, and the light source.

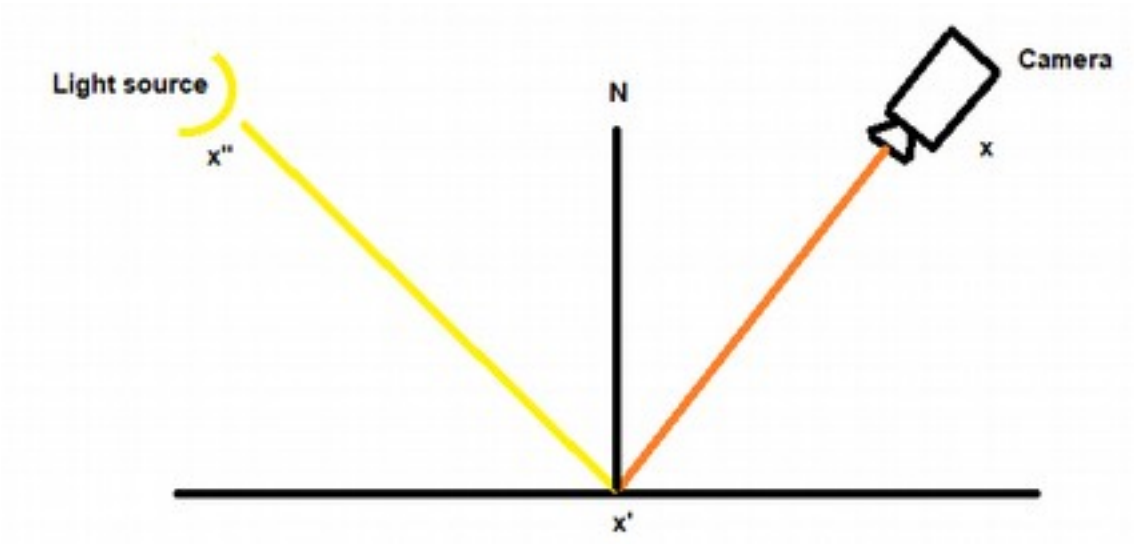

Figure 12 : Schema describing ray-tracing calculation from camera to light source.

- I(x,x') is the intensity of light passing from x to x'

- g(x,x') is a "geometry" term. If encapsulates the occlusion of the two points. If x and x' aren't mutually visible the term is equal to 0, otherwise it is equal to $1/r^2$ where r is the distance between x and x'
- e(x,x') is related to the intensity of emitted light from x' to x
- ρ(x,x',x") is related to the intensity of light scattered from x" to x through patch of surface at x'. This term is related to the Bi-directrional Reflectance Distribution Function of the material.

For a complete understanding of this rendering equation, it is important to understand the BRDF of different materials depending of the type of surface reflection. The BRDF in the general case is defined by the equation:

$$f(x, x', x) = \{dL(x,x')\} \text{ over } \{dE(\{x\} \wedge \{'\}, x)¿ \quad (2)$$

Materials are classified into three main categories depending of their reflection pattern:

- **Lambertian** surface : a surface that appears where the apparent brightness doesn't depend of the viewer's position. The associated BTDF function is :

$$f¿ \quad (3)$$

- **Specular** surface : a surface that has a mirror-lik reflection, where reflected ray goes in one direction symmetrical around the surface normal to the incident ray. The associated BTDF function can be described as :

$$f(x, x', x) = \text{Surface Albedo} * \delta(\text{widehat}\{x\ x'\ N¿, \widehat{Nx'x}) \quad (4)$$

- **Glossy** surface : a surface that isn't either perfectly lambertian nor perfectly specular. The BRDF function is usually hard to describe analytically. Some models exist to simulate it as Phong Model [PHO1975] or Blinn-Phong Moel [BLI1977].

In our study we want to focus on ray-tracing usage for daylighting. But there are multiple difficulties in using it in the traditional fashion:

- Getting CFS geometry and material in a digitalized format is hard. This data is often not available in the architect's model. It has usually to be requested from the manufacturer. The manufacturer may, or may not to keep trade secrets, provide the data. And when provided, the format is usually not the compatible with simulation software.
- Often the CFS geometry comes from a theoretical design that doesn't account for reality's imperfection.

- Even if we get the real CFS geometry and material, IFC has too much errors in this side to be reliable able to share this information.
- Ray-tracing can be very slow for complex building geometries.
- Ray-tracing is very input parameter dependent in practice, which needs an expert to use the ray-tracing engine.

Recent advancements in ray-tracing usage led to the development of new methodologies based on matrix calculation. For our case, two relevant methodologies are assessed in our study that theoretically answer all these questions: The **three-phase Method** and the **five-phase method**.

1.7.1.1 Three phase Method

The daylighting calculation will rely on the three-phase method [WAR2011] This method relies on the division of the space into 3 spaces: Outside the room, inside the window and inside the room. Moreover, it discretizes each part of this space, in order to generate 3 matrices:

- Daylight matrix (D) describes the results of ray-tracing outside the room to give the contribution of each part of the sky to each part of the window
- Transmission matrix (T) describes the ray-tracing results inside the window. It uses the bi-directional scattering distribution function (BSDF) as described by Klems [KLE1994 and KLE1994b].
- View matrix (V) describes the results of ray-tracing inside the room to give the contribution of each part of the window to each part of the room. To generate this matrix, calculation points are defined over the walls. This calculation points are called sensor points.

The luminance calculation is done by:

$$I=VTDs \tag{5}$$

Where s is a vector describing the luminance of each sky patch. Alternatively, we can use a matrix that is a concatenation of multiple vectors at different time points.

The resulting I here contains in our study the luminance of each pixel of the generated picture.

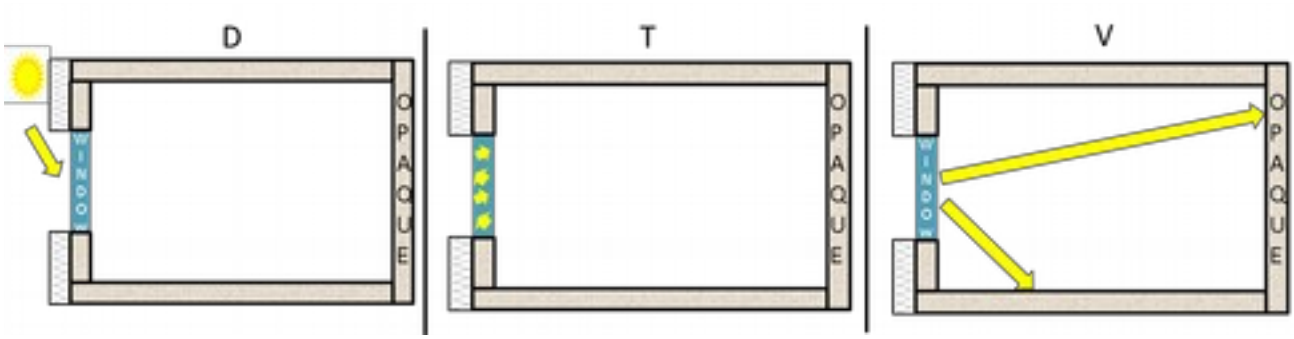

Figure 13: Illustration of the ray-tracing calculation of the D, T and V matrices from left to right

1.7.1.2 Five-phase method

The 5-phase method [MCN2013] is an extension of the the 3-phase method that enhances the direct radiation calculation. It is calculated by the following formula

$$I=VTDs - V_dTD_dS_d + C_{ds}s_{sun} \quad (6)$$

The first term of the calculation VTDs refers to the 3-Phase Method calculation.

The second term $V_dTD_dS_d$ is analogous to the first but for direct sun luminance component only:

- V_d is the view matrix without the room's inter-reflections.
- D_d is the day matrix without the outside environment's inter-reflections.
- s_d contains the luminance of the patches with direct sun component only.

The last term contains a more accurate calculation of the direct sun component:

- C_{ds} is a relatively more accurate contribution of the sky patches
- s_{sun} is the sky patches luminance, in relatively higher resolution.

Recent work [GEI2016] has improved the sun's contribution component C_{ds}. It split its calculation into two matrices. This is done in order to improve the accuracy of the contribution of the fenestration system, which now takes into account the scattering inside it:

$$C_{ds}=C_R+C_F \quad (7)$$

Where C_R is the contribution of the sun reflected from all room components without the window and C_F the direct contribution of the sun through the window.

1.7.2 Daylighting indices

The calculated luminance with the above methodologies has to be further processed in order to evaluate the performance of a CFS in daylighting. In literature, many indices exist:

- **Daylight factor** (DF) : defined by International Commission on Illumination (CIE) as :

$$DF = \frac{Ei}{Eo} x\, 100 \tag{8}$$

With Ei being the horizontal work plane illumination indoors and Eo the horizontal illumination on the roof of the building. Daylight Factor has been based on calculation with the overcast sky condition of CIE. DF values inferior to 2 are interpreted as not adequately lit, and needs artificial lighting, values between 2 and 5 as adequately lit but may need artificial lighting, values superior to 5 as well lit, but may suffer from glare.

- **Daylight autonomy** : is based on a dynamic simulation throughout the year [REI2001]. The daylight autonomy is the percentage of time where the horizontal luminance is above a defined target. The Leadership in Energy and Environmental Design (LEED) defines it as above 300 lux.
- **Continuous daylight autonomy** : is a variation of daylight autonomy that gives partial credit in dynamic simulations to timesteps where the horizontal luminance is below the target [REI2006].
- **Useful daylight autonomy** : is an other variation of daylight autonomy [NAB2006a and NAB2006b]. It fixes a minimum limit of 100lux and adds an upper limit of 2000 lux. This upper treshord is to prevent glare or overheating situations.
- **Spatial daylight autonomy** : is a variation that of daylight autonomy that takes into account the space repartion [HES2012]. Best values were found by setting a lower limit at 300 lux. Heshong's report assesses a room that meets spatial daylight autonomy with over 75% space that meets the 300 lux minimum as "preferred" by the occupant while a 55% to 74% is "nominally acceptable".
- **Annual sunlight exposure** : describes how much space receives too much light exposure causing glare or overheating.

In the state of art, none of these indices has made consensus as the best metric to use. In our study, we chose to use the **Daylight autonomy** to optically evaluate the performance of our CFS, in combination with a detailed glare analysis to prevent glare situation. In the next section we will define visual comfort parameters and how, specifically, glare is evaluated.

1.7.3 Visual discomfort

Visual comfort describes the well-being of subjects in accordance with the lighting conditions. In essence, it concatenates a number of parameters: “

- visual contact with the exterior,
- glare protection and avoiding reflections on computer screens,
- contrast between visual task and background,
- sufficiently high luminance values,
- color rendering of objects in the room.

” [KUH2017]

In our research we are going to focus on the glare aspect of visual comfort. Glare can be divided into multiple classes:

- **Glare causing health problems**: is cause by very high luminance, especially over a small solid angle, can cause permanent damage to the eye’s photoreceptors.
- **Disability glare**: impairs object vision by the subject. It is usually the loss of the retinal image contrast due to the light scattering inside the eye.
- **Discomfort glare**: “that causes discomfort without necessarily impairing the vision of objects” (CIE). It is a subjective rating that is not directly measurable but can be assessed with questionnaire [KUH2017]. It is usually reported under less bright situations than glare discomfort [WIEN2009]. It can be assessed in four ranges: Imperceptible, perceptible but not disturbing, disturbing but tolerable, intolerable.
- **Reflex glare:** reduces the contrast of objects. Which can hinder the visibility of display screens’ content.
- **Outdoor glare**: is a glare that impact the outside, as other rooms, street traffic or [KUH2017].

In this study we will focus on CFS performance mainly on the interior of buildings. The most common problems are disability, discomfort and reflex glare. Reflex glare is usually very dependent in practice on screen's technology and vary with production, and therefore will not be assessed. Disability glare is usually reported in less bright situations than discomfort glare, so it can be evaluated with the same glare indices as discomfort glare. In the next section, we will present glare indices that are relevant to our study.

1.7.4 Glare indices

In literature, many indices exist to evaluate glare, but none of them is an absolute referential:

- **Unified glare rating**: defined by the CIE [AKA1996] to evaluate how likely a luminaire can cause discomfort. It takes into account the luminance of the source and the relative position of the subject. It is defined by the equation:

$$UGR = 8\log\left[\frac{0.25}{L_b}\sum\frac{L^2\omega}{p^2}\right] \quad (9)$$

- **Visual comfort probability**: "The rating of a lighting system expressed as the percentage of people who, when viewing from a specified location and in a specified direction, will be expected to find it acceptable in terms of discomfort glare. Visual comfort probability is related to discomfort glare rating (DGR)" (IES). It is defined by the equation:

$$279 - 110 ¿¿ \quad (10)$$

- **CIE glare index**: is an index adopted by CIE as a standard and based on Einhorn's work [EIN1979]. The index goes from 10 (imperceptible glare) to 34 (intolerable glare). It is calculated by the following equation:

$$CGI = 8\log_{10}\left[\frac{2\left(1+\frac{E_d}{500}\right)}{E_d+E_i}\sum\frac{L_{s,i}^2\omega_{s,i}}{P_i^2}\right] \quad (11)$$

- **Daylight glare index**: is the IES glare index system which goes from imperceptible glare (<16) to intolerable (>28). It is calculated by the following equation:

$$DGI = 10 \log 0.478 \sum \frac{\Omega_{s,i}^{0.8} L_{s,i}^{1.6}}{L_b + (0.07\, \omega_{s,i}^{0.5} L_{s,i})} \quad (12)$$

- **Daylight glare probability** (DGP): [WIE2006] assesses that the probability that a subject suffers from glare. It is defined by the following equation:

$$DGP = c_1 . E_V + c_2 . \log\left(1 + \sum_i^n \frac{L_{s,i}^2 . \omega_{s,i}}{E_v^c . P_i^2}\right) + c_3 \quad (13)$$

In our study, we chose to used DGP to assess glare because of its overall relative performance. Some studies rate the DGP as the best index for evaluating glare from daylighting [SUK2016], other concluded that all existing metrics show bad performance after a statistical analysis [WYM2014], while other statistical studies show better overall performance for some indices, including DGP [WIE2017]. In the state of the art, evaluating glare perception is not a totally solved problem, but DGP is accepted in the literature as one of the best performing metrics.

The next section of our study will focus on how to assess the thermal performance of CFS.

1.8 Thermal performance assessment

In our study, we want to focus on the CFS thermal performance. The performance of the CFS is not independent of the rest of the buildings. Depending of the climate, building orientation and its thermal properties, the CFS performance may change drastically. We will therefore present an overview on how building energy simulation is conducted before diving in the detailed representation of the CFS.

1.8.1 Overview

1.8.1.1 Energy transfer

Building energy simulation simulate the heat transfer inside the building, in order to provide an estimate about its temperature, energy consumption and cooling/heat load. In

order to investigate the building energy models, it is important to understand first the main heat transport means:

- **Conduction** is the heat transfer occurring when two bodies are in contact. As temperature is a macroscopic representation of the average kinetic energy of the microscopic body components. Conduction occur when there is molecular collision between the two bodies, which lead to a transfer of an averaging of the temperature between the two bodies. The heat flux equation between two building components A and B is as follows in a steady system:

$$\varphi_{A\to B}=\frac{\lambda S}{e}(T_A-T_B) \qquad (0)$$

With φ the heat flux, λ the thermal conductivity, S the contact surface's area and e its depth, T is the temperature.

- **Convection** is the heat transfer occurring within fluids through bulk molecular movement. The term encapsulates both advection and diffusion phenomenon. We usually distinguish between two kinds of convections, natural and forced convection. Natural convection is a convection that happens because of the temperature gradient within the fluid. Forced convection happens when fluid movement is due to an external source. In our study, solar radiation is calculated through ray-tracing. Heat transfer radiation from building elements occur mainly in the far or long wave infrared. Heat transfer through convection between two building elements can be calculated by the following equation:

$$\varphi_{A\to B}=hS(T_A-T_B) \qquad (0)$$

With h the convection heat transfer coefficient.

- **Radiation** is the heat transfer through emission or transmission of energy in electromagnetic, acoustic, particle radiation or gravitation radiation waves. In the case of buildings, we mainly talk about electromagnetic waves. Heat transfer through radiation between two walls can be calculated by the following equation:

$$\varphi_{A\to B}=\alpha_B\sigma F_{A\to B}(T_A-T_B) \qquad (0)$$

With $\alpha_B$monochromatic absorption coefficient, σ Stefan–Boltzmann constant and $F_{A\to B}$ the view factor from surface A to surface B.

Building energy simulations are usually done through software that deal with the many complex parameters interactions in building. The façade is subject to solar radiation, the

windows provide a direct solar radiation to the interior, the walls exchange heat through radiation and conduction, while the air inside the room is responsible of convection. Different software handles the building's complexity through different abstracted models. There are currently two main approaches to solve the problematic:

- **The thermal model** where building elements are represented as thermal nodes. The building is therefore a thermal circuit made if these nodes. These nodes are characterized by a temperature and pressure. The energy heat balance equation is solved to calculate building's elements temperature.
- **The zonal model** is an approach that was developed to remedy one of the thermal models limitations. The assumption that air thermal nodes are homogeneous in temperature and pressure. This approach divides the room into zones with air that is homogeneous in temperature and mass volume and that has a hydrostatic pressure.

1.8.1.2 Energy types

In order to analyse the energy needs in a building, it is important to distinguish between three energy levels when we talk about energy consumption. In building and office space, there are four main levels:

- **Primary energy**: corresponds to the energy used from the nature source to provide it to the end user.
- **Secondary energy:** corresponds to the converted energy from the primary level and that should be transported to the end user.
- **Final commercial energy:** is the energy delivered to the end user, and is usually the one billed
- **Useful energy:** is the effective energy used by the end user.

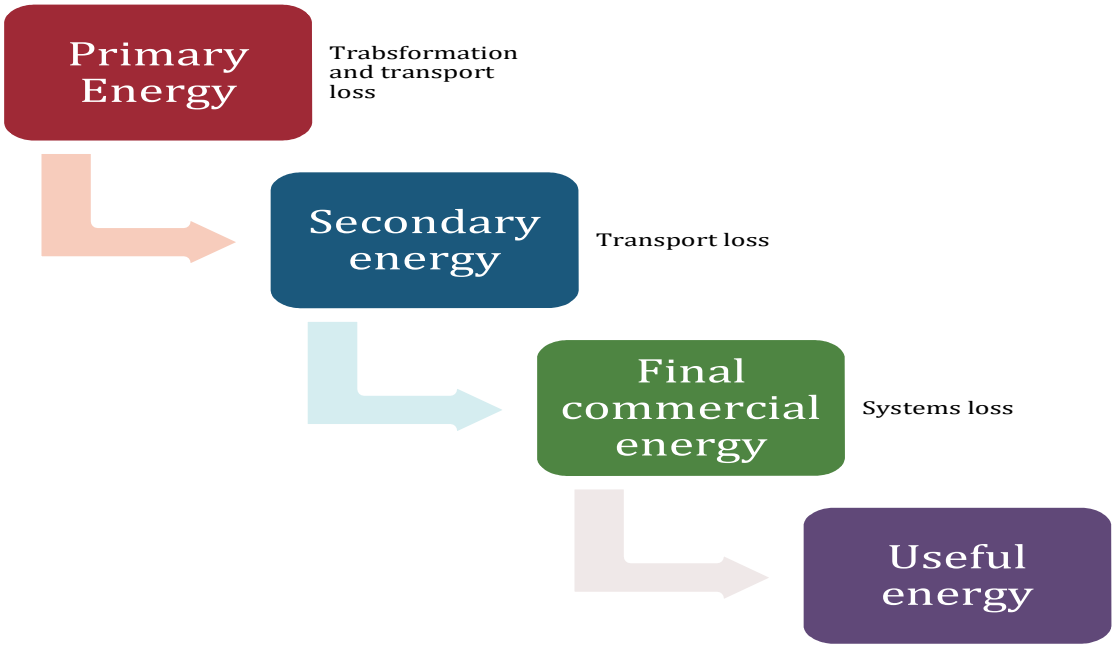

Figure 14: The different kinds of energy

1.8.2 CFS Models

1.8.2.1 Main models in literature

To represent the solar gain through the windows and heat gains/losses through conduction, many models have been proposed in the literature:

- **ISO 15099:2003** : is a nodal model where each layer of the fenestration system has calculated thermal resistance, solar and optical transmittance. The model focuses on calculating the front and back temperature and radiosity. It assumes that layers have a homogeneous temperature and heat transfer coefficients with a 2-dimensional heat flow.
- **EN 410:2011** : calculates the solar heat gain coefficient by calculating the transmitted radiation and the secondary heat gain. It assumes a constant heat transfer coefficients between glazings.
- **EN 673:2011** : The thermal resistance of the window is calculated by summing the resistances of its layers. It assumes that gas cavities temperature is 10°C and that heat transfer coefficient is constant in each layer.
- **Blackbox model [KUH2011]**: The model assumes that most Complex Fenestration System can be represented by two layers with data that can be measured, or calculated in some cases.

In our study, we chose to use the Blackbox model as it fits most of our criteria:

- **Doesn't rely on geometry**: which is mandatory for full BIM compatibility.
- **Tries to cover most CFS**: the model tries to make very minimal assumptions in order to fit a wide number of CFS.
- **Use measured data**: which proves to be critical to get data that takes into account manufacturing imperfections, missing data from manufacturer or cover innovative CFS. It should be noted that this data can be calculated for many existing CFS (example: double glazing unit with venetian blinds).

1.8.2.2 Blackbox model

The Blackbox model, also referred as Kuhn's model in literature, provides a 2-layer model usable in most simulation programs that relies on measured calorimetric data, or in some cases calculated, to represent the thermal behavior of a complex fenestration system. It is a work around to the problem of recent and complex fenestration systems that may not be possibly represented within current simulation program models. It also remedies to inaccuracy problems with manufactured systems that deviates a lot from their ideal design.

The use of a semi-empirical model leads to an easy and computationally light model to use in energy simulation programs without sacrificing accuracy for most complex fenestration systems.

In this model, each layer is characterized by an angular solar absorbance and the two are separated by a thermal resistance. It relies on some measured and/or calculated data as input:

- Angular g-value: measured with specific external and internal resistances.
- U-value: measured with the same external and internal resistances.
- Angular transmittance
- Angular reflectance (optional): to calculate the temperature of the external surface.

It is demonstrated that with this input the following absorbances can be calculated:

$$\alpha_{inner\,layer} = \frac{q_{tot}\left(R_e^{'} + R_s^{'}\left[T_{mean}^{'}\right] + R_i^{'}\right) - \propto R_e^{'}}{R_s^{'}[T_{mean}]} \quad (0)$$

$$\alpha_{outer\ layer} = \frac{q_{tot}\left(R_e^{'} + R_s^{'}\left[T_{mean}^{'}\right] + R_i^{'}\right) - \propto R_e^{'}}{R_s^{'}\left[T_{mean}\right]} \quad (0)$$

The Blackbox Model is then coupled with the 3-phase method in a simulation engine to simulate the radiative flux on the walls. This approach leads to an accurate representation of the transmitted irradiance distribution in the room.

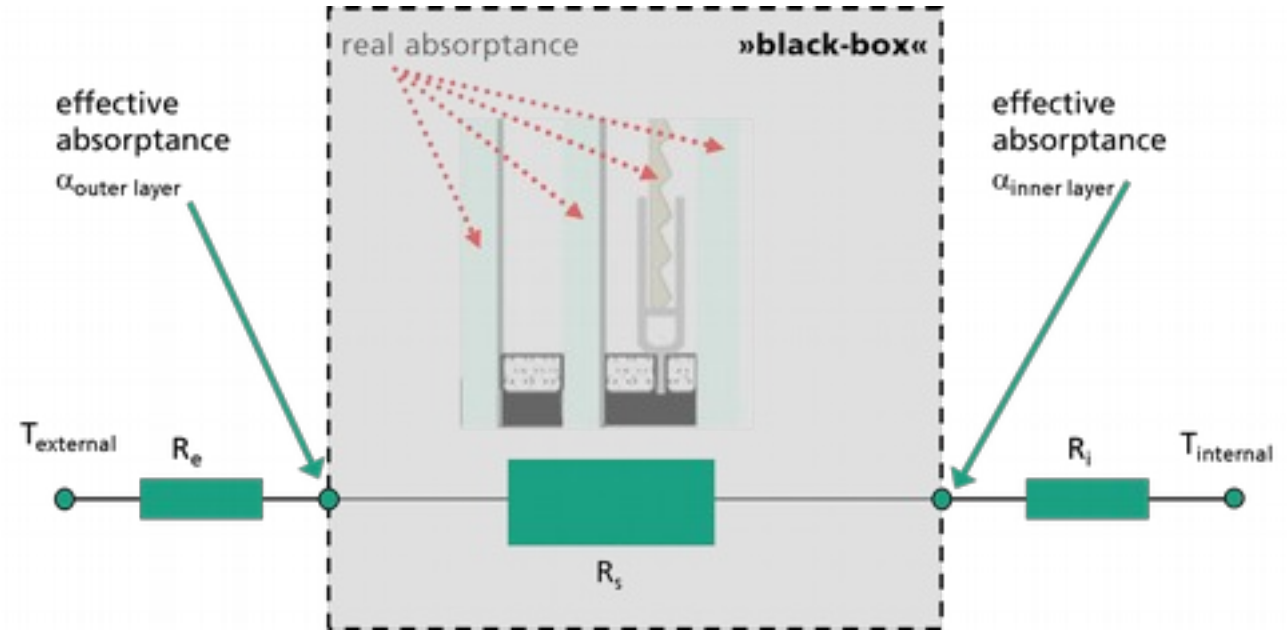

Figure 15:Blackbox model representation of a Complex Fenestration System

This model has been validated by comparing it to the ISO 15099 reference [BUE2015]. The validation focused on the air temperature and the heating/cooling energy demand. As we will see in the next chapter, these criteria are insufficient for thermal comfort modelling; further validation has therefore been studied in this thesis.

1.8.3 Thermal comfort

1.8.3.1 definition and factors

Thermal comfort is defined as “that condition of mind which expresses satisfaction with the thermal environment and is assessed by subjective evaluation” (ANSI/ASHRAE Standard 55-2010). Thermal comfort or discomfort is a physiological feeling triggered by thermal sensors and receptors in the skin and the brain [T. H. Benzinger 1979 cited in MAY1993]. Cold sensors are located in the skin and gives a local signal when the temperature falls under a certain threshold. Warm sensors are located in the brain and give a central non-directional signal when the temperature is above a certain threshold. Cold sensors exist in the brain too as do warm sensors in the skin, but don’t contribute

to the thermal comfort or discomfort sensation [MAY1993]. Traditionally, studying thermal comfort relies on the estimation of this thresholds, or the preferred body temperature. To do so, it is important to understand the factors that affect such body temperatures. These variables can be divided into mainly environmental and personal factors [AUC2007].

Environmental factors can be summarized into:

- **Air temperature** is the average temperature of the air surrounding the body. It is measured at the ankle, waist and head level (ASHRAE 55). It is measure by the dry-bulb temperature. It plays a key role in the heat dissipation by convection of the body.
- **Air movement** is measured by the velocity of the air. High speed velocity reduces the body or clothing's heat resistance as well as participates in the evaporation of skin
- **Air humidity** affects the moisture of the skin. High air humidity impedes the sweat's evaporation and therefore heat loss. Low humidity can also be uncomfortable due to its effect on the mucous membrane.
- **Radiation exchange** is the amount of heat transferred from a surface. It is estimated by using the mean radiant temperature which takes into account the environment surfaces temperature, emissivity and view factor. Its equation is defined as follow:

$$MRT = \sum \varepsilon_i T_i^4 F_i \qquad (14)$$

Where ε is the emissivity of the surface. Building materials emissivity is often approximated to 1. T is the temperature of the surface in Kelvin. F is the angle factor between the person and the surface.

On the other side, normal factors can be summarized in:

- **Metabolic rate** : the body continuously produces heat. Metabolic rate is made of the basal metabolic rate, which is the minimum energy expenditure of the body at rest, and the work carried by the muscles. ASHRAE 55 defines the metabolic rate by the energy expenditure, divided by the body surface and time.

- **Clothing** directly affects the thermal exchange between the body and the environment as it works as an insulating layer. A new unit has been developed to reflect it which is clo. 1clo=0.155 $m^2 \cdot K/W$.

Other contributing factors also play a role in thermal comfort:

- **Alimentation** has an impact on metabolic rate, depending of the amount and nature of the consumed food.
- **Body shape**, the more rounded the body shape, the lower is the ratio surface to volume. Resulting in a relatively higher body thermal resistance.
- **Subcutaneous fat** acts as an insulator, and thus augmenting the thermal resistance. Higher subcutaneous fat also correlates with more rounded body shape.
- **Age and gender** : Older people have smaller range of temperature tolerance, while women tend to prefer higher temperature than men.
- **State of health** : illness is a contributing factor to meatabolic rate.

Another factor that has been discussed in literature, is the ability of the body to adapt itself to its environment. There are short-terms adaptation of 20-30 min exposure, and long-term adaptations that take months. It can be distinguished into three [FOL1974, FOL1981, CLA1985, FRI1993, GOL1974 and ASHRAE RP-884]:

- **Behavioral adjustment** : which includes human's conscious or inconscious action to relieve from temperature change, as wearing heavier clothers or taking a nap during the hottest time of the day.
- **Physiological** : is the body's ability to adapt to different temperature. In high temperature, blood vessels dilatate to increase blood flow, skin temperature and heat dissipation [SZO2014]. Sweating is another efficient mecanism to cool the body. Cold temperature in the other side blood vessels constricts and body starts shivering.
- **Psychological** : is the subjective assessment of the temperature due to past experience and acclimatization. People acclimated to higher temperature and expeting it have higher thermal comfort set point.

Considering all these factors is a scientific challenge. In literature many indices have been developed to evaluate thermal comfort. We will present a comparison of the most relevant indices in the next section

1.8.3.2 Estimation indices

In the state of art, many indices exist to estimate thermal comfort, ranging from very simple ones as air temperature, to PMV/PPD model [FAN1970]. In the ASHRAE RP-884 study, they used a comprehensive database of field studies. They exclusively targeted field studies -i.e. not laboratory studies- because human thermal adaptation is mainly based on field research [DEA1998]. This database was assembled by the contribution of chosen thermal comfort researchers based on a data quality questionnaire. The final database included 160 building and 21 000 observations, from several locations. The data set included:

- Thermal questionnaire answers
- Clothing and metabolic estimate
- Concurrent indoor climate observations
- Recalculated thermal indices, which included: Mean radiant temperature, operative temperature, turbulence intensity, ET*, SET*, TSENS, DISC, PMV/PPD, PD draft risks.
- outdoor meteorological observations which comprehended daily temperatures, relative humidity.

The result of the study that only four indices to calcite comfort temperature, beside the developed adaptive model, had good correlation with the data set:

- **Operative temperature** (ISO 7726:1998) is based on mean air temperature, mean radiant temperature, and air velocity. It can be calculated with the following equation:

$$t_0 = \frac{h_r t_{mr} + h_{\square} t_a}{h_r + h_{\square}} \qquad (0)$$

Or

$$t_0 = \frac{t_{mr} + t_a \sqrt{10\,v}}{1 + \sqrt{10\,v}} \qquad (0)$$

With $h_{\square}$ convective heat transfer coefficient, h_r linear radiative heat transfer coefficient, t_a air temperature, t_{mr} mean radiant temperature and v air velocity.

- **Fanger's Model PMV/PPD** (ISO 7730): Fanger's model relies on two conditions. The skin temperature and the body's temperature should make up for a neutral thermal feeling, and the energy expended by the body (metabolic rate) is equal to the heat loss. This conditions translate into the body energy balance equation :

$$M - W = H + E + C_{res} + E_{res} \quad (0)$$

The Predicted Mean vote, the percentage number of users that would vote neutral thermal sensation can be derived from it:

$$PMV = \left(0.303 . e^{-0.036M} + 0.028\right)\left[(M - W) - H - E_c - C_{res} - E_{res}\right] \quad (0)$$

With M being the metabolic rate, and W the mechanical work, C_{res} convective heat loss from respiration, E_{res} evaporative heat loss from respiration, H the dry heat loss, E the evaporative heat exchange of the skin, E_C the evaporative heat exchange at thermal neutrality feeling.

As the PMV is based on the sensation of temperature neutrality, it suffers from the limitation of the case where the subject feels a warm or cool temperature but no discomfort. To consider these situations, the predicted percentage of dissatisfied has been developed (PPD).

- **Effective temperature** (ET*) is "The effective temperature is the temperature at 50% rh (relative humidity) that yields the same total heat loss from the skin as for the actual environment" (ASHRAE FUNDAMENTALS 2017). It is calculated by the following equation :

$$ET^{*} = t_o + w\, i_m\, LR\left(p_a - 0.5\, p_{ET^{*},s}\right) \quad (0)$$

With $t_o$the operative temperature, w the skin wittedness, i_m total vapor permeation efficiency, **LR** the Lewi Ratio (usually 6.5K/KPa indoor), $p_{ET^{*},s}$ the saturated vapor pressure at ET* in kPa, p_a water vapor pressure in ambient air.

- **Standard effective temperature** (SET*) has been developed as ET* depends on clothing and activity which makes it hard to use. It is defined as the effective temperature at 50% relative humidity, where a subject wearing standard clothes

for its activity has the same skin temperature and skin wettedness as in the environment (ASHRAE FUNDAMENTALS 2017).

- **Adaptive Model :** has been defined by AHRAE RP-884 on the basis of the data set collected. It aims to take into account the adaptation mechanism of human being to predict its thermal comfort temperature. The adaptive model, has been ported as a European standard EN 15251 and international standard ISO 7730. Although they do not implement the same formula but a variation of it. The ASHRAE standard 55 suggests the following equation :

$$T_{com} = 0.31\,T_{outdm} + 17.8 \quad (0)$$

With T_{com} the calculated comfort operative temperature, and T_{outdm} the daily mean monthly temperature.

In literature, there is no consensus over which is the best model to use. Recommendations go as to use the adaptive model for naturally ventilated building and PMV/PPD for mechanically ventilated buildings [HEL2006].

In this study, we chose to use the adaptive model. The PMV/PPD relies on many factors, some of them, as activity and clothes, cannot be implemented in a normalized way with IFC current capabilities.

We will develop and validate in this study a methodology that uses both the Kuhn's model for energy simulations, combined with the adaptive model for the thermal comfort, with a link to BIM. To the knowledge of the author, there has not been any prior study nor validation of the usability of Kuhn's model for thermal comfort. Previous studies only focused on air temperature, predicted thermal comfort relies on the operative temperature and thus also needs the mean radiant temperature of the room's surfaces.

2 Building Information Modelling to Building Energy Model

The presented work presents a methodology on how to transform a BIM model of a single room into explicit geometry. The external and internal surfaces are first distinguished, and calculation points (usually called sensor points) are created. The optical and thermal model are then extracted from IFC to load them in the simulation engine. The intended BEM relies on the use of the 3-phase method for ray-tracing coupled with the Blackbox Model to accurately model the daylight and thermal behavior of the CFS.

Our methodology relies on two independent phases that extract building's skeleton from the BIM and incorporate an accurate thermal model to IFC:

- Geometrical data extraction
- Extraction of thermal and optical properties.

2.1 Geometrical extraction overview

Our methodology relies on discretizing the surfaces to calculate the radiative flux. Sensors are points used as a discretization of the wall for this calculation. We need to split a building element into enough sensors to minimize the errors due to the discretization. Too much sensors can heavily slow down the simulation process. Choosing the right number of sensors is currently left to the user. We developed a methodology that creates sensors on a wall that relies in fixed distances between them according to the *X*, *Y* and *Z* axes, defined by the user as input.

The whole methodology is applied to closed spaces, containing one or multiple rooms. A room is described as a solid, represented by its bounding walls. Walls are made of two surfaces: surfaces visible from inside the room, called internal surfaces, and surfaces visible from outside the room, called external surfaces. The walls surface that are not visible (ie: intersection surfaces) are deleted in the final mesh.

The geometric processing of BIM's architectural view to get our BEM is then done in 6 steps:

1. Splitting the building into rooms as defined by the IFC input.
2. IFC's geometry transformation to Radiance/Fener geometry.
3. Distinguish template rooms
4. Distinguish inner surfaces and outer surfaces.
5. Create sensor points.
6. Translate to simulation engine's format.

2.2 IFC's geometry transformation

IFC geometric representation permits the modelling of a large number of geometries. They are stored as attributes of *IfcProduct*. *IfcProduct* has a *Representations* attribute that can hold one or many representations of theme product, as for example 2D and 3D representation of the wall. Only the possible 3D representations are of interest in this research, and they can be briefly summarized in the followings:

Construct solid geometry are derived from solid primitives as sphere or cube, or from the result of Boolean operations of primitives.

Shell and Boundary representation which describe the surfaces delimiting the solid.

2D surfaces that are either revolved or swept along a curve.

IFC format can store these geometric data either with the explicit coordinates of each points or the parameters for the outer surfaces equation. Simulation programs often need to use an explicit geometry (usually polygons with every vertex coordinate defined in the case of Radiance and Fener). Thus, a transformation from IFC's geometry classes to an explicit geometry format compatible with the simulation software is needed. This new geometry representation will serve as a skeleton for our new Building Energy Model. This conversion is done in 3 steps with the help of our newly developed library:

Figure 16: Simplified workflow of geometry processing from IFC.

The library primitives were developed to follow as closely as possible the possible geometries allowed by IFC in order to minimize data loss in this step. Once products geometries are loaded within the engine, they can be transformed into the simulation software format. In this research a conversion to rad files, used in Radiance and Fener, was developed. In the current status of the code, we only take advantage of the polygon primitive allowed in radiance. Every shape is transformed into triangles while keeping the associated material. Using rectangles or polygons with higher angle counts has been investigated but was not deemed possible. A recurring error in IFC files is that the vertices forming the polygon are not planar, leading to a wrong definition of the polygon. This why we default to triangles, as three points are always, by definition, planar.

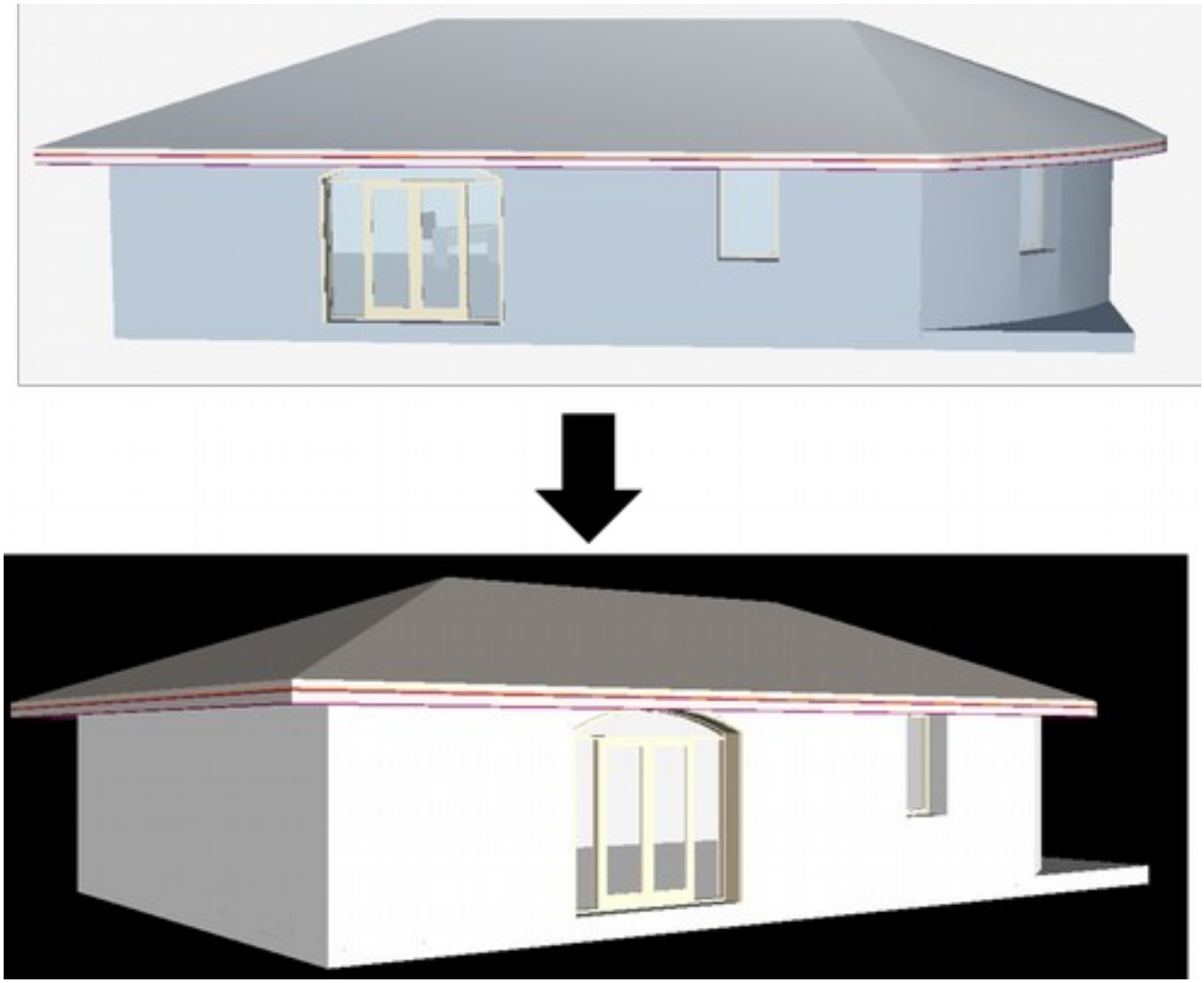

Figure 17: An Ifc file (top picture, visualised with ifcplusplus) transformed to a radiance file (bottom picture, visualised with rshow)

Generating the radiance files without any other processing did not allow for an automated simulation. Important information is missing. Other developed algorithms have therefore further processed the geometry in order to avoid human intervention.

Both Fener and Radiance, used with the 3-phase method, need sensor points location to calculate indoor luminance and irradiance. These sensor points are points with 3d coordinates that are evenly distributed in the wall. One difficulty related to these sensor points is that luminance calculation is only interesting inside a room. Irradiance calculation has to be done in both surfaces but we need to differentiate between them. We therefore need to eliminate non-visible surfaces and to distinguish between the outer surface of a wall and the interior one.

2.3 Removal of hidden surfaces

Many surfaces described in a building are not visible and therefore should be deleted from the final geometry. To achieve it we use Boolean operations between the solid representing each object. In practice, we added building elements to each other. So, they theoretically merge into one 3d element.

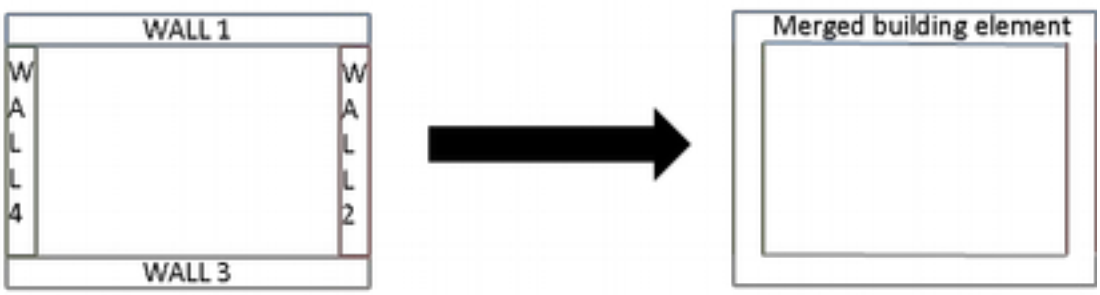

Figure 18: 2D example of merging of 4 walls of a room. The contact surfaces between walls have been deleted.

2.4 Distinguishing internal and external surfaces

In order to distinguish internal and external surfaces, we developed an algorithm that only need geometrical data with no topological information. Geometrical data is the description of shape's geometry. Topological data is the description of relation between shapes.

The developed algorithm relies on two important steps:

1. Get one external face: We need to identify at least one external face of the walls. It will serve as a reference to identify the other external faces
2. Split the list of polygons into smaller sublists of "touching polygons":

2.4.1 External face Identification

To get one external surface, a point outside the room and its building elements is first calculated:

The bounding box containing the simulation objects is calculated.

A point outside the *x,y,z* coordinates of the bounding box is then easy to find as its coordinates are superior (or inferior) to any other coordinates of the bounding box's vertices.

From this external point a ray is defined. The choice of the ray may be random, but a ray may fail to intersect the room. A ray between the exterior point and the center of the bounding box should always lead to correct results.

With ray tracing, we can find out the first polygon it intersects, which can only be an external surface. It may touch a vertex first. In this we would just take one of the polygons that contain this vertex.

2.4.2 Splitting of the list of polygons into smaller sublists of touching polygons

Let's call *P* the list of all polygons that bound the room, *L* a list of lists of polygons, a *li* a list of polygons included in *L*.

li should include only polygons that are in contact with each other. *i* is equal to the number of rooms included in simulation space. The definition of a polygon in contact with another polygon is the following: A polygon is bounded by an ordered list of edges. An edge is defined by a set of two points and contains every point between them. A general definition would be that two polygons *(polygon1,polygon2)* touch each other's if :

$$\exists \left(edg\, e_1, edg\, e_2\right) \in polygo\, n_1\, x\, polygo\, n_2 : edg\, e_1 \cap edg\, e_2 \neq \emptyset \qquad (0)$$

Only one of the sublists l_i contains the external polygon we have found above. It necessarily contains every external surface and only external surfaces. Thus, the other sublists contain internal faces only.

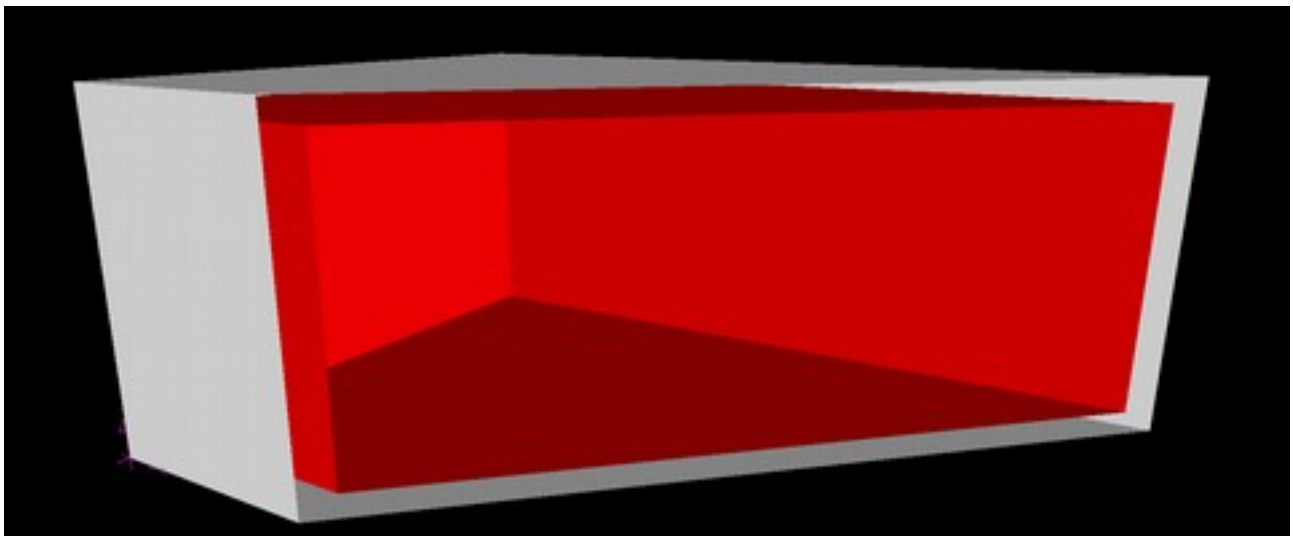

Figure 19: Theoretical room cut. Exterior faces are in white, interior faces in red

The simulation space has now been split into at least two lists of polygons, with only one of them being external. The latter category is used in the calculation of the V matrix of the 3-Phase-Method, while the former is used in the calculation of the D matrix.

Moreover, it should be noted that with this polygonal description of the rooms, we can use the existing methodologies [COD2015 and LIL2014] to generate 2nd level boundaries (cf. 1.5.7) and integrate the current model into simulation software as energy plus.

2.5 Creation of sensors

Sensor points are theoretical points covering the walls that will serve in the discretized calculation required in the 3-phase method.

The creation of the sensors may rely on multiple approaches:

Tessellation: it is the subdivision of a surface into non-overlapping bounded surfaces without gaps. We can then set a resolution by specifying a maximum surface and perimeters.

Triangulation: is a special case of tessellation with the transformation of a polygon to a set of triangles.

Regular grid: is the tessellation of space by congruent parallelotopes [MAT2017]. Parallelotopes are a generalization of parallelepiped in higher dimensions.

The method used in this research is an alternative one that can be easily implemented. It creates a uniform grid of points. The method is robust even in the case of polygons with holes or self-intersecting polygons. The methodology is applied on each polygon separately and not on the mesh as a hole.

The user gives as input *distX*, *distY*, *distZ* which are the distances between the sensors according to the *X*, *Y* and *Z* axes. The appropriate choice of distances is subject to a human intervention.

The polygon *P* is inside a plane *PL*.

A local coordinate system centred on the first point of the polygon is created an defined by the *X'*, *Y'* and *Z'* axes containing the unit vectors ***u***, ***v*** and ***w***. The plane *PL* is the *X'Y'* plane and the polygon normal is equal to Z'. The polygon normal is calculated with Newell's algorithm [TAM1992] to ensure robustness.

The plane PL is not necessarily parallel to any of the planes *XY*, *ZX* and *YZ*. The newly used distances *distX'* and *distY'* between the sensors that are used along the new (**u'**,**v'**) base will then be equal to:

$$distX' = \sqrt{u_x^2 * distX^2 + u_y^2 * distX^2 + u_z^2 * distX^2} \quad (0)$$

$$distY' = \sqrt{v_x^2 * distX^2 + v_y^2 * distX^2 + v_z^2 * distX^2} \quad (0)$$

We will calculate the bounding box of our polygon in the local coordinate system. It will be a rectangle that lays in the plane PL. We can now create our grid of sensors. The first sensor is put at a the point of coordinates $(\frac{dist\ X'}{2}, \frac{dist\ Y'}{2}, 0)$. The point located at the i^{th} line and j^{th} column is then located at $((i+\frac{1}{2}) * distX', (i+\frac{1}{2}) * distY', 0)$

The calculated grid covers the whole bounding box, but contains points that are not necessarily on our building elements. The winding number algorithm, as proposed by Sunday Dan [DAN2016] is used to check if each points is in the polygon or outside. The choice of this algorithm is motivated by both robustness and computation efficiency. If there is an insufficient coverage of the building element by the grid, as some sensor points that are missing in significant surface. User should lower the distances between points used as input.

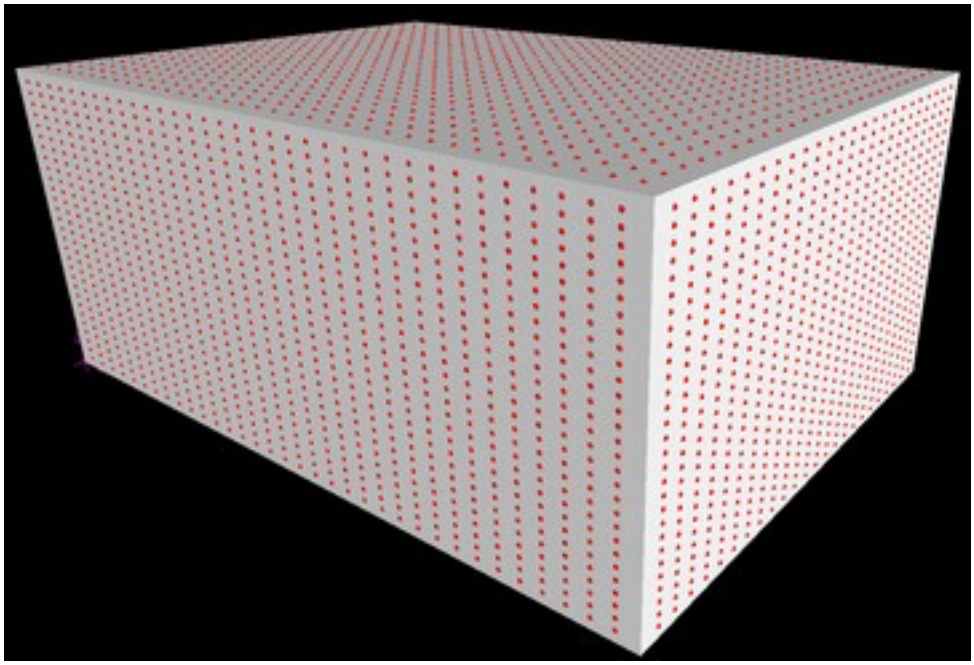

Figure 20: Theoretical 7mx5mx3m room seen from outside and covered with a regular sensor grid.

Sensors are created every 20cm, 20cm and 10cm according to X, Y and Z axes and are represented in red

2.5.1 Window data model

As seen in the blackbox model description, a complex fenestration system needs 3 inputs to be fully described:

Angular g-values: This is calculated from angular dependent g-values data.

U-value: This has to be expressed with the same internal and external resistance than the g-value

Angular solar transmittance: commonly contained in the BSDF dataset.

IFC format supports g-value, U-value and the solar transmittance, but does not natively support angular dependencies. One way to include angular dependency in IFC is IFC's complex properties named *IfcComplexProperty*.

IfcComplexProperty is an *IfcProperty* child that can hold multiple properties, either being *IfcSimpleProperty* or *IfcSimpleProperty*.. It makes possible to describe in the same property the parametric ranges of angles and the values as a list of data.

The description of a BSDF is for example integrated as follows:

Figure 21: BSDF description in IFC

This structure supports multiple wavelength and angular resolution. It can be generalized to any data that is wavelength- or angular-dependent. It can be used for angular dependent g-value in our case.

The *IfcProperty* that are generated can then be packed in an *IfcPropertySetDefinition*. Property set definitions are schemas intended to extend IFC's property capabilities based on a regional or project agreement. They are shared in xsd format, following the XML standard.

There is already a standard property set definition covering thermal and optical representation of glazing systems called "Pset_DoorWindowGlazingType", but it is not suited for the BlackBox model as it does not offer any mean to handle the newly added angular dependent data properties.

A new Property set definition will be created for this research that will be able to handle all of the requirements. The new property set definition can then be associated with a window. This association will be done manually, but will be automated in further development.

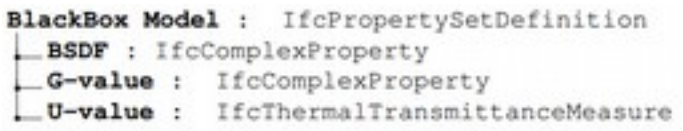

Figure 22 : Blackbox model description in IFC

This property set allow a full reconstructing of the blackbox model input insides an IFC file.

2.5.2 Opaque surface properties

For Building elements (e.g. walls, slabs, beams, floor), IFC already offers the means to set up the desired information:

Optical rendering related properties can be found in "IfcSurfaceStyleRendering".

Thermal properties needed are density, thermal transmittance, specific heat capacity and thickness. These properties can be found in "IfcThermalMaterialProperties", "IfcGeneralMaterialProperties" and "IfcMaterialLayer".

The data contained in this property sets can be with the geometry of the building geometry that has been generated with the methodology described above. The

combination of the geometry with the optical and thermal behavior description of building components will lead to the Building Energy Model.

2.6 Time saving opportunity

One of the main advantages of using such an automated workflow is to reduce human error and provide time savings, and thus cost savings, in a construction project. To evaluate this time saving opportunity, the author used this methodology on a real-world scenario where he was provided architect plans to use.

The project consisted of a building, with multiple levels, from which 12 different rooms chosen by the architect, had their energetical performance evaluated. The transmitted models were in the Portable Document Format, usually known as PDF. This format is human readable but not rich enough for automation.

The plan has therefore to be manually redrawn from scratch in a compatible format with the simulation's software. The provided plan was in German, a language that the author has no knowledge of, nor he has any experience with German conventions in architectural plans.

Redrawing the first room in a simulation software compatible format did take in practice two days. Two full days were necessary for the author to fully understand the plan, ask architect for missing data, and reproduce it in the right format. The subsequent rooms that had to be drawn took two hours in average. This time was mainly needed to both draw the room and ensure that there was no error in the drawing.

For the sake of comparison, an IFC model was redrawn afterward by the author of the thesis that corresponded to the room. The model was drawn and exported from the Archicad software. Translating the IFC model to the simulation software format was instantaneous, proving the potential of a huge time saving opportunity.

While the project still had remaining, as supervising the simulation in the simulation in the used software and analyzing the output. These steps only represented one third of the project time. Two-third of the time were mainly spent in understanding the plan, asking details from the architect and redrawing in the software. V. Bazjanac [BAZ2001] estimated that in practice, geometrical data's redrawing may represent up to 80% of the building's energy analysis. The author is therefore deeply convinced of the time and cost saving opportunity that such a methodology offers, on the top of human errors reduction.

2.7 Summary

In this chapter, we showed a full methodology to integrate IFC models with energy simulation software model. The methodology consists of two parts. The first part shows how we can fit the existing IFC's geometrical description within software simulation's limitations.

The developed methodology takes as input a building model. As the objective is to evaluate the CFS optical and thermal performance, the building is split into multiple rooms, in which the CFS performance is evaluated independently. The rooms are assumed opaque for optical simulations purpose, and adiabatic for thermal simulations. The algorithm could be extended, in a future research, to support simulation with multiple rooms at the same time if they aren't adiabatic or opaque.

Once these rooms are identified, the algorithm uses an internally developed geometry engine to interpret and process the data. It creates a set of surfaces that are either external (has contact at the outside environment) or internal to the room (has contact with the interior air). It moreover populates them with sensor points for the simulation purposes.

This methodology has been shown to offer important cost and time saving opportunities in real world project, compared to the traditional simulations based on architect plans that are only human readable.

This methodology has been developed and incorporated into programs called ifc2rad and ifc2fener. Possible applications and uses of the presented BIM workflow are presented in chapter 5.

On the top of the geometry, these programs also incorporate an optical and thermal model of the Complex Fenestration System. The accuracy and limitations of these models are evaluated in the next sections.

3 OPTICAL ASSESSMENT

In this research, we chose to use ray-tracing based methodologies to evaluate the optical performance of CFS. Accurate ray-tracing methodologies usually rely on the full description of the CFS geometry. For a methodology that should accommodate with BIM limitations and make possible to automate simulations, the authors are convinced that we have to rely on the Bi-directional Scattering Distribution Function (BSDF) of the CFS instead of its real geometry for several reasons:

- **BIM compatibility:** Building Information Modelling suffers for many practical limitations currently, making it unsuitable for the fenestration system's geometry modelling [BOU2016 and BOU2017]. Most important are the geometrical errors that affect geometry [LIL2015] and material errors that happen at the export time of the model from the BIM authoring software.
- **Data availability:** The 3D model of the Complex Fenestration system is not always available. Architects usually do not have this data. Manufacturers may have the 3D model designed in 3D software but may not be able to export it in the right format or choose not to do so to preserve trade secrets.
- **Data reliability:** The geometrical data usually used is theoretical. It only works on the basis that the manufactured product is closely conformed to the ideal design, which is often not the case.
- **Data quality:** It is currently difficult to ensure that the geometrical data, even measured from the manufactured product, is sufficiently accurate. It is hard to

predict the geometrical accuracy needed for a model. The same problem occurs when estimating the optical properties of the used materials.

- **Geometry's compatibility:** fenestration systems with many small sized geometrical details such as textile are sometimes impossible to use with a full-scale building geometry in some ray-tracing engines.
- **Simulation parameters:** Shading systems can have multiple small sized holes where many inter-reflections happen. For such cases, it is important to use highly accurate simulation parameters for the ray-tracing engine. To the knowledge of the authors, there is no way to automate the choice of such parameters.
- **Simulation time:** The many inter-reflections within the CFS layers have a high computational cost. It may result on impractical simulation times. For example, some glare indices rely on the rendered image from the subject's point of view. Generating such picture can take over an hour depending of the simulation case. Therefore, a one-year simulation with hourly intervals from 8 to 19 would need a 6 months long simulation.

The most used BSDF format is klems BSDF with 145*145 patches (Figure 23) and is usually used with the Three-phase method (c.f. 1.7.1.1). This model suffers from the relatively low number of patches. The patch cone has an apex angle that goes up to 13.5° [LEE2018], while the sun has an apex angle of 0.5°. Therefore, the sun's position can have up to 6° error when represented with Klems BSDF, which implies a significant error in the case where the subject is hit with direct irradiation. This limitation has been observed in prior studies [GEI2016 and LEE2018] where the three-phase method highly underestimates or overestimates the luminance. More some complex fenestration systems have peaks in transmittance/reflectance in small cones that cannot be correctly characterized by the CFS, leading to an averaged transmittance/reflectance over a small patch. To improve upon these limitations, tensor-tree [WAR2014] have been developed, to offer a variable resolution BSDF (Figure 24). These BSDF are often characterized by a higher resolution (in our research, we used 4096 patches) and by its variability over the hemisphere. This variability has been mainly developed to take into account the eventual peaks at small cone angles that characterize some CFS.

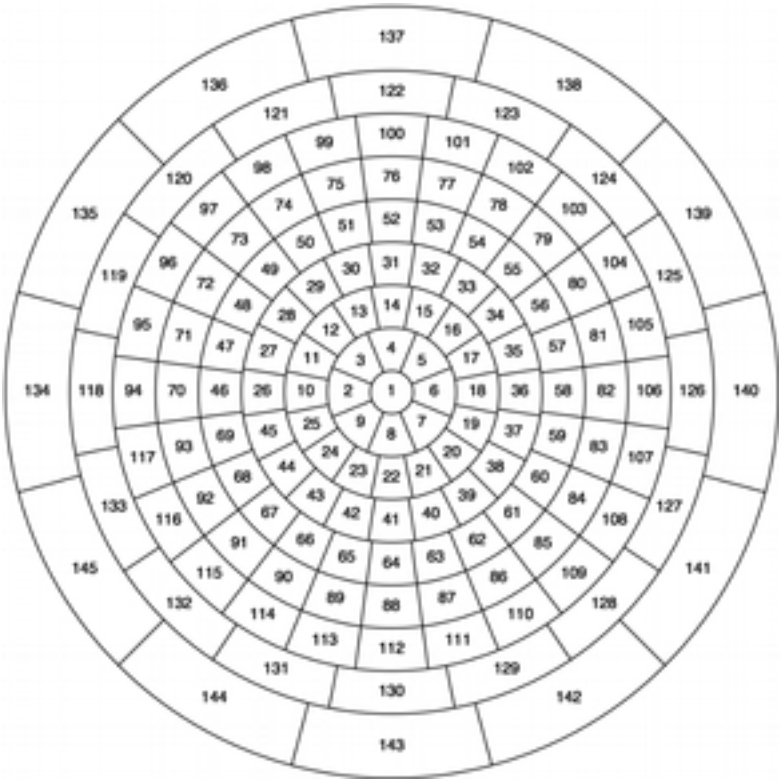

Figure 23 : Klems BSDF (source: https://andymcneil.gitbooks.io)

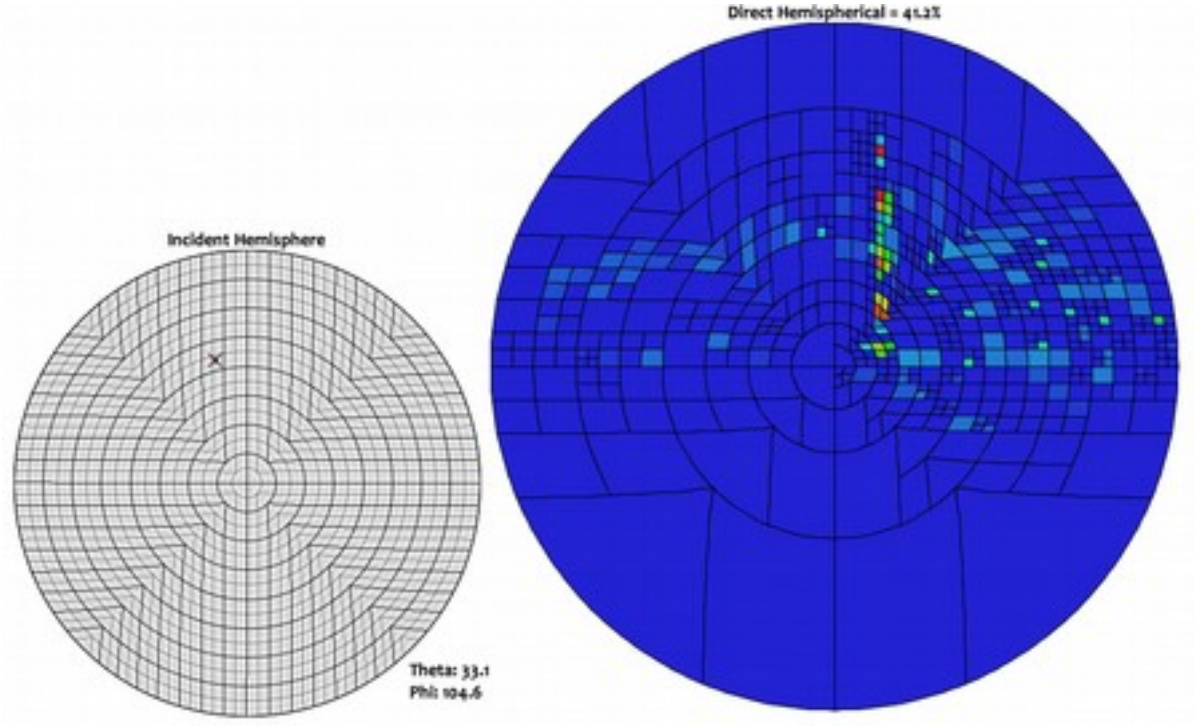

Figure 24 : Tensor tree BSDF incident hemisphere and transmitted hemisphere at polar coordinate (33.1°, 104.6°) (modified from: https://www.radiance-online.org)

In this section, we will therefore validate our developed methodology based on BSDF data. We will evaluate its relevance for two metrics: daylighting and visual comfort.

3.1 Daylight

3.1.1.1 Objective

Daylight calculation are usually reliant on the horizontal luminance (c.f. 1.7.2). Therefore, our research has focused on experimentally validating the accuracy of horizontal luminance calculation, and the accuracy of the deriver metric, daylight autonomy, which represents the percentage of annual daytime hours where an occupant, in a specified position,

3.1.1.2 Experimental setup

Our experimental setup is done in the Daylighting Laboratory at Fraunhofer ISE. It's located in Freiburg (Germany) which is at 48.018° North and 7.848° East.

The room is 3.65m wide, 4.6m deep and 3.0 high and is South-west oriented. The user has been close to the middle line of the window at average distance, looking south-west at the façade (Figure 25). The experimental setup was modeled in archicad and exported to ifc. Due to some errors in the resulting ifc file, due to the BIM software, the resulting file has been corrected by hand. Afterwards, we used the newly developed program ifc2rad to generate the room's geometry for radiance.

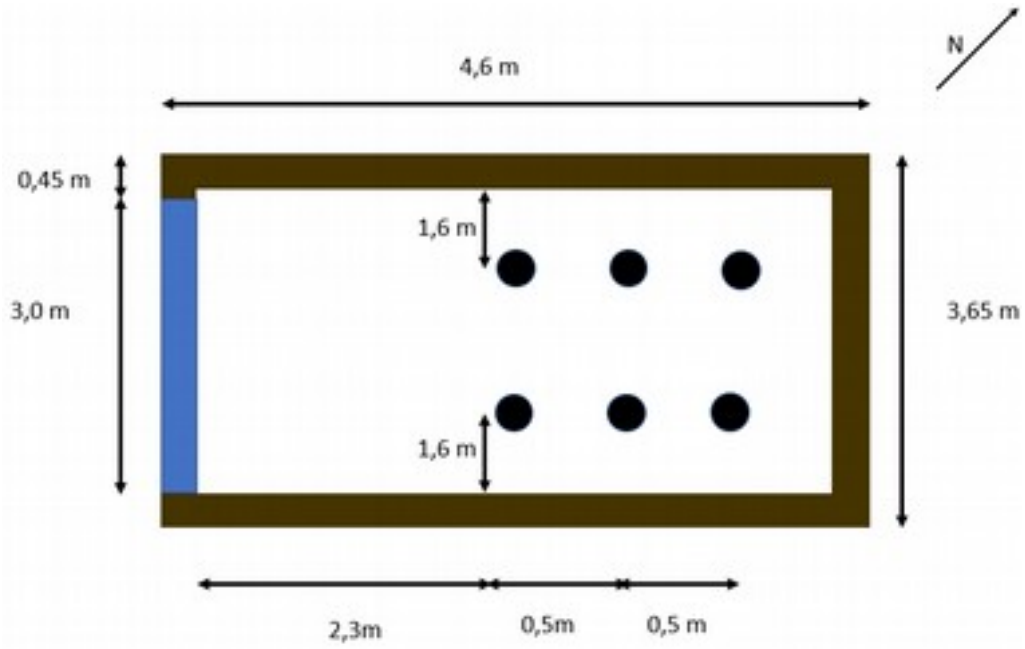

Figure 25 : room schema with the 6 used sensors.

Location	Freiburg
Latitude	48.018N
Longitude	7.848E
Orientation	South-West
Zone length	4.60
Zone width	3,65
Zone height	3.00
Wall reflectance	0.50
Ceiling reflectance	0.80
Floor reflectance	0.34
Ground albedo	0.20
Glazing visible transmittance	0.55
Glazing visible Reflectance (front)	0.19
Glazing visible Reflectance (back)	0.17

Table 1 :Room characteristics

We used six sensors (Hagner Model SD2) measuring horizontal luminance (directed upward). At the same time, weather data was collected with a SPN1 Sunshine Pyranometer. The SPN1 measured global and diffuse horizontal luminance data, that was used in our simulations. Data was collected at 12 seconds interval.

Measurements have been carried either without venetian blinds or with venetian blinds with the following characteristics (provided by the manufacturer):

- 8 cm depth
- 10,4 cm radius
- 7,2 cm between lamellas
- Color gray (55%)
- 1% specularity
- 6% roughness

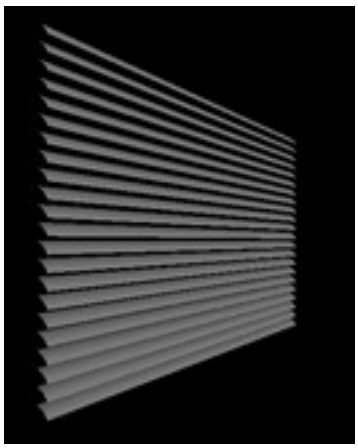

Figure 26 : generated geometry of venetian blinds in Radiance

The measurements were carried during the 13th, 18th and 25th march 2016 with the double-glazing unit without venetian blind, the 6th, 7th and 14th April with venetian blinds tilted downward at 5°, during the 1st April with 40° and from the 16th to the 19th April with 70°.

These measurements were performed by Angelina Katsifaraki at Fraunhofer ISE as a part of her PHD thesis.

3.1.1.3 Simulation description

As of the ray-tracing engine used in this study, we chose to use the Radiance Suite [GTY1989 and WAR1994]. It has been empirically validated in multiple studies [GEI2016, GRY1989, MAR1995, MAR2000, MAR2001, MCN2013, MCN2012 and REI2001]. Radiance uses a hybrid approach of Monte Carlo and deterministic ray tracing [WAR1994]. This hybrid approach is essentially solving Kajia's path tracing equation [KAJ1986]. Radiance suite incorporates many tools. The most notable for this study are:

- **Rtrace** which is used to trace the ray path.
- **Rfluxmtx** calculates a flux transfer matrix between a sender and a receiver surface by uniformly sampling rays at each surface over the chosen hemisphere in the parameters.
- **GenBSDF** computes a BSDF based a radiance description of the CFS. The resulting BSDF can be either the traditional klems BSDF or a tensor tree representation.

The horizontal luminance was calculated with radiance using different methodologies:

- **The three-phase method**: The BSDF has been generated with the genBSDF tool of Radiance suite using the default parameters. The result is a 145x145 matrix in accordance with Klems hemisphere directions.
- **The five-phased method**: The tensor tree has been generated with the genBSDF tool of Radiance suite using the parameter "-t4 6 -c 40960". This option provides a hemisphere with 4096 regions and 10 ray samples per region in average.
- Traditional backward ray-tracing: that uses the same tensor tree as in the 5-phase method. We will call it for the sake of conciseness **Rtrace_ttree**, as it relies on both the Rtrace tool of Radiance, and the tensor tree supplied as BSDF material.

The two BSDF (klems BSDF and the tensor tree) were both generated using the the whole complex fenestration system, i.e. using both the double-glazing unit with the venetian blinds (if used). To model the double-glazing unit, we used the Roos model [ROO2001] with manufacturer provided data as a function describing the window's material in radiance.

As of the measured weather data, it consists of the global (GHI) and the diffuse horizontal illuminance (DHI). For our simulations, we needed to provide radiance with direct normal illuminance (DNI). DNI was therefore calculated as follow:

$$DNI = \frac{GHI - DHI}{\sin(solar\ altitude)} \qquad (0)$$

Sun altitude was calculated using pysolar [PYS2018] program, which uses Bretagnon's VSOP 87 theory [BRE1988]. It was validated against ephemeris code maintained by the United States Naval Observatory with a standard deviation of 0.0795 degrees.

With the Direct Normal Irradiance and Direct Horizontal illuminance, the sky was modelled according to Perez Model [PER1990 and PER1993].

Internally, radiance calculates the radiance flux from the sky's, or other light sources if available, to a sensor. A sensor is a virtual point defined by its position and view direction. To translate the irradiance to luminance, we must take into account the photosensitivity of the eye depending of the light spectral band. Therefore, luminance is calculated as follow [PER1990].

$$Luminance = ¿ * 47 + ¿ * 117 + ¿ * 14.7 \qquad (15)$$

3.1.1.4 Horizontal luminance validation

The measured horizontal luminance has been compared to the horizontal luminance calculated by either the three-phase method, five-phase method and rtrace_ttree. To evaluate the overall accuracy and uncertainties of these methodologies, we use the relative mean bias error and the relative squared error. Relative mean bias error is usually used to detect if the models have an inherent bias toward overestimating or underestimating the estimated physical quantity. They are defined as:

$$rMBE = \frac{1}{N}\sum_{i=1}^{N}\frac{Observation - Measurement}{Measurement} \quad (16)$$

$$r\,MSE = \sqrt{\frac{1}{N}\sum_{i=1}^{N}\left(\frac{Observation - Measurement}{Measurement}\right)^2} \quad (17)$$

Overally, the tensor tree-based methods (Rtrace_ttree and Five-phase method) show better accuracy than the three-phase method (Table 2). The main limitation of the Three-phase method comes for the usage of the klems BSDF with 145x145 patch. It showed an always negative relative mean bias error, especially in the case without glazing and at 70° tilt angle (-11% and 13%), whereas the 5° and 40° have very low rmbe (-1.8% and -1.9%). These rmbe are relatively low, moreover, in literature both positive and negative rmbe have been reported. They are mainly due to the direct sun irradiation and its position in its klems patch. Tensor tree-based methods had rmbe closer to 0, between -6% and -7%. Overall, we do not think there is a systematic bias inherent to these methodologies.

As of the accuracy, the tensor tree-based methods have a relative mean square error between 9% and 14%, with no significant difference between the two. Therefore, the discretization of the sky in the Five-phase method doesn't seem to have any significant impact on the calculation's accuracy. As of the three-phase method, the root mean square error was relatively worse. It is mainly attributed to the direct irradiation cases. The error is usually significant during mid-day, where the sun can be visible through the fenestration depending on the tilt angle. In the case of double glazing unit, the large luminance observed form 10h to 16h is also accompanied with a large relative error (Figure 27).

The observed errors are due to multiple factors, that are relevant both to horizontal luminance calculation and glare (c.f 3.2). The errors in these methodologies are partially due to the usage of BSDF:

- BSDF doesn't account for the spatial distribution of the light but only its angular average.
- Moreover, for the three-phase method, the error of the Klems BSDF low's resolution is not negligible according to our results. The sun's apex cone angle of 0.5° is a lot smaller than the 13.5° apex angle of the Klems BSDF. We suspect that is why the error for the three-phase is a lot higher when the subject is hit by direct irradiation.

Beside the BSDF itself, some other sources of errors are present:

- We didn't model the room's interior.
- Perez's sky model, is known to have a sub-optimal sky representation in the case of non-uniform clouds.
- The CFS's characteristics and BSDF weren't measured but calculated from manufacturer's data.

Another hypothesis usually assumed in literature is the discretization of the building, sky and environment. In our comparison between the Five-phase method and rtrace_ttree (c.f. Table 2, 3.2.5.1 and 3.2.6.1), we notice that the accuracy of each the two methods is very similar. Therefore, we deduce that this factor doesn't have a significant impact tin practice.

To understand if these errors are in practice significant, we will investigate the Daylight autonomy to see if these errors have a significant impact on the prediction of sufficient/insufficient daylight situations.

Case	Methodology	Relative mean square error (%)	Relative mean bias error (%)
No shading	Three-phase	22	-11
	Five-phase	11	-6
	Rtrace_ttree	9	-7
5° tilt angle	Three-phase	24	-1.8
	Five-phase	13	-2.0
	Rtrace_ttree	14	-2.3
40° tilt	Three-phase	10	-1.9
	Five-phase	9	0.5

Case	Methodology	Relative mean square error (%)	Relative mean bias error (%)
Angle 70° tilt angle	Rtrace_ttree	10	0.3
	Three-phase	25	-13
	Five-phase	12	-3
	Rtrace_ttree	11	-2

Table 2 : Accuracy of the BSDF based methodologies to calculate horizontal luminance

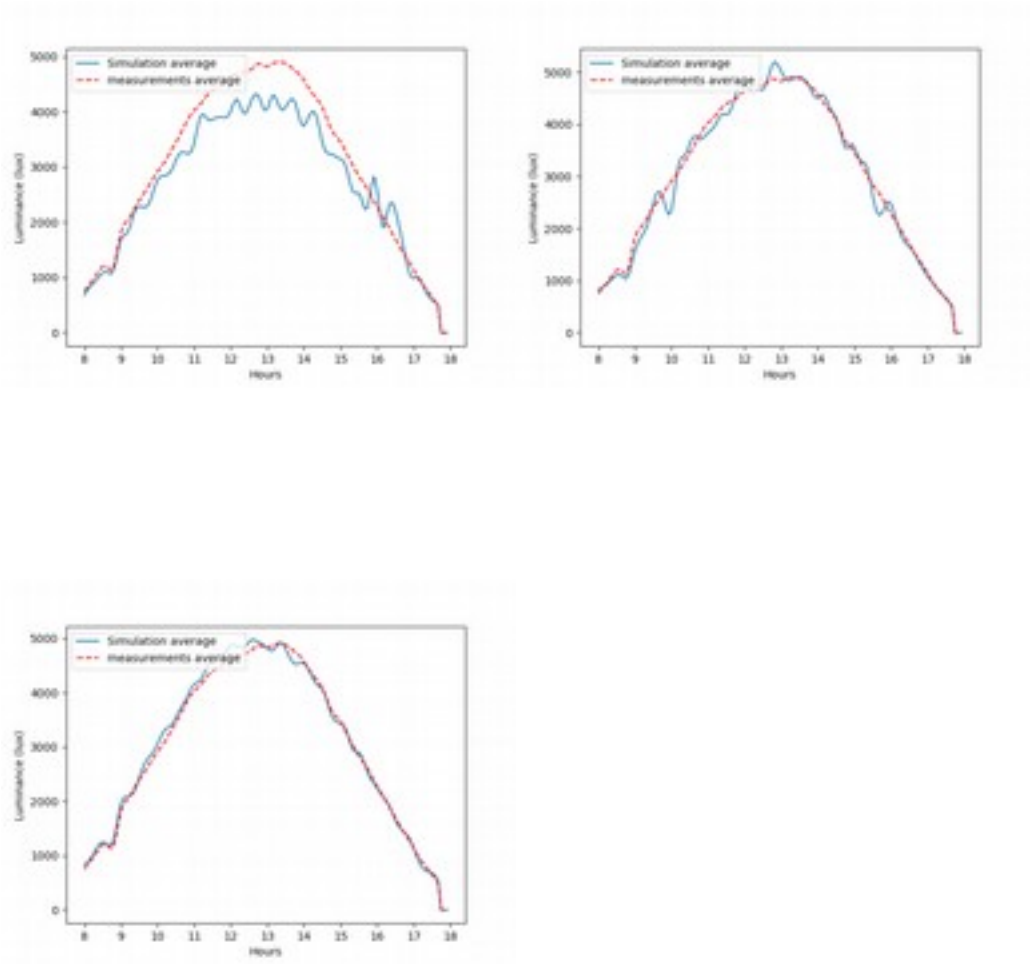

Figure 27 : Horizontal luminance average of the 6 sensors for the 3-pm (left), 5-pm (right), rtrace_ttree (bottom) the 25th march 2016 without shading.

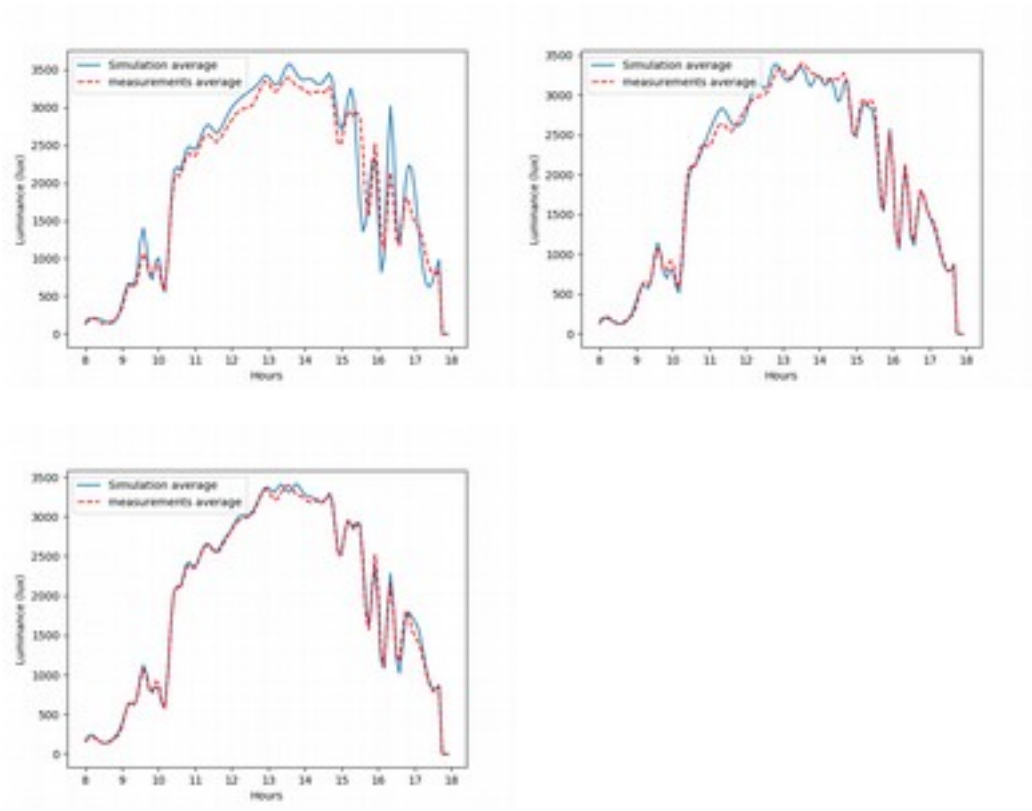

Figure 28 : Horizontal luminance average of the 6 sensors for the 3-pm (left), 5-pm (right), rtrace_ttree (bottom) the 6th april 2016 with 5° tilt angle.

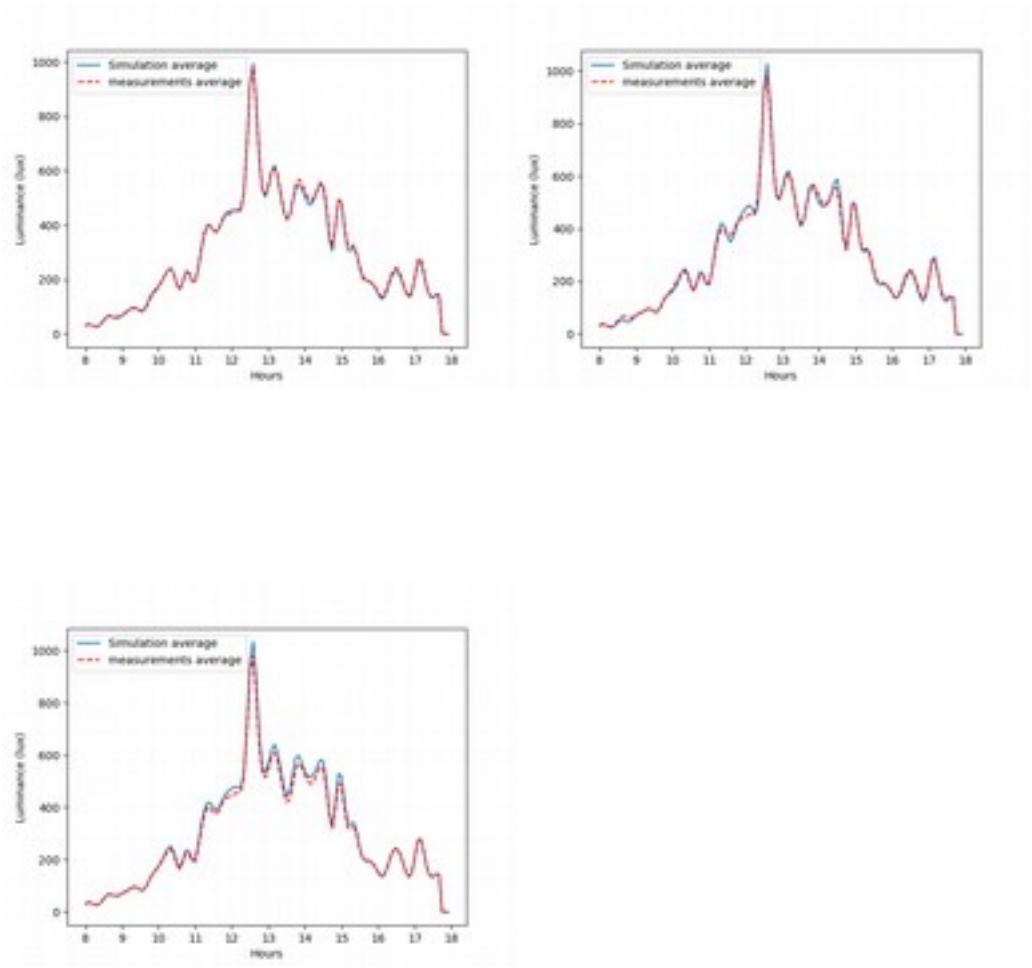

Figure 29 : Horizontal luminance average of the 6 sensors for the 3-pm (left), 5-pm (right), rtrace_ttree (bottom) the 1st april 2016 with 40° tilt angle.

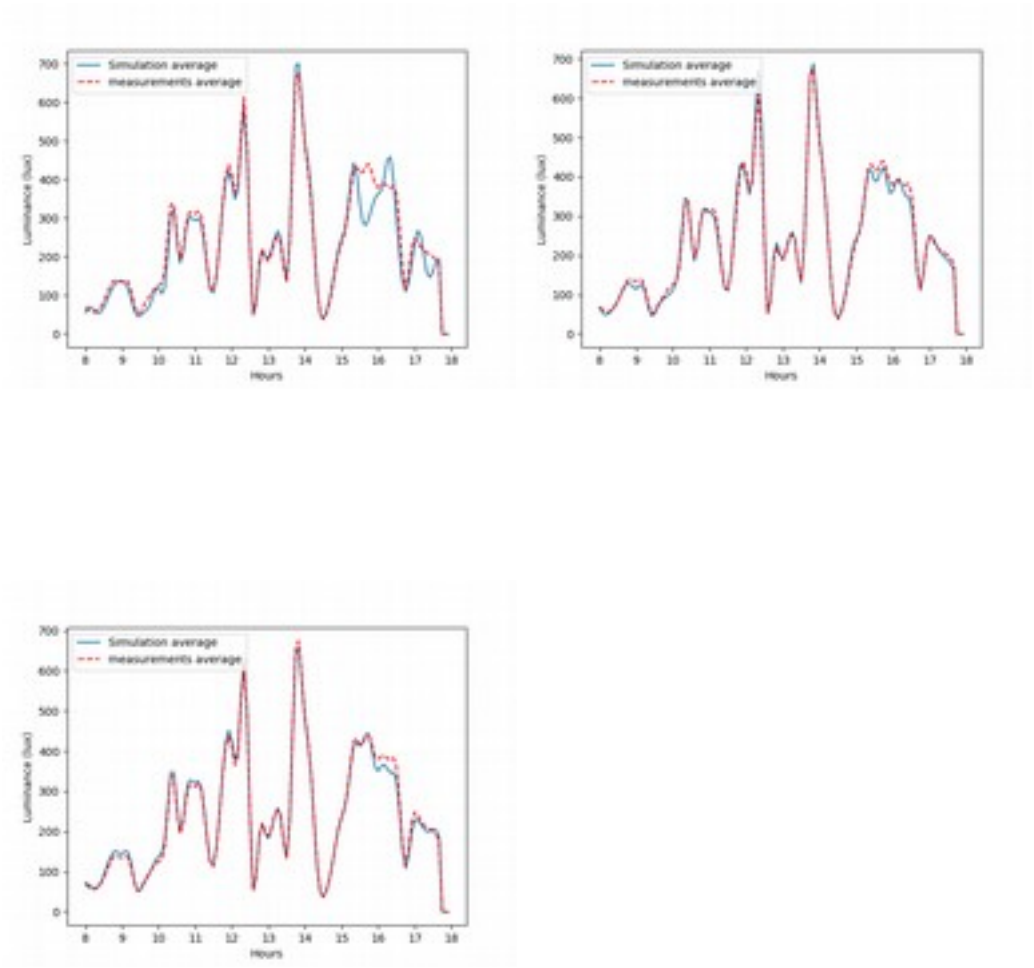

Figure 30 : Horizontal luminance average of the 6 sensors for the 3-pm (left), 5-pm (right), rtrace_ttree (bottom) the 16th june 2016 with 70° tilt angle.

3.1.1.5 Daylight autonomy

To assess the daylight autonmy accuracy of these methodologies, it is important to know the probability of predicting the wrong situation, i.e. the probability to predict a sufficient daylighting while it is not, or the probability to predict an insufficient daylighting while it is. To do so, we conducted a binary classification test. A binary classification test calculates two metrics:

- **Sensitivity**: true positive rate. The percentage of positive situations identified as such.
- **Specificity**: true negative rate. The percentage of negative situations identified as such.

Our gathered results show that in every case (double glazing unit with or without venetian blinds), the BSDF based methods predict very reliably the daylight autonomy. All these methods had less than 1% error rate. One admitted limitation of these methods

is the relative low number of measured situations without enough daylighting. Usually this situation occurred before 10h and after 16h (Figure 27 Figure 28 Figure 29 Figure 30).

	Three-phase method		Five-phase method		Rtrace_ttree	
No shading device	Positive	Negative	Positive	Negative	Positive	Negative
True	>99%	>99%	>99%	>99%	>99%	>99%
False	<1%	<1%	<1%	<1%	<1%	<1%
5° tilt angle						
True	94%	>99%	>99%	>99%	>99%	>99%
False	<1%	<1%	<1%	<1%	<1%	<1%
40° tilt angle						
True	>99%	>99%	>99%	>99%	>99%	>99%
False	<1%	<1%	<1%	<1%	<1%	<1%
70° tilt angle						
True	>99%	>99%	>99%	>99%	>99%	>99%
False	<1%	<1%	<1%	<1%	<1%	<1%

While BSDF based methods show that they are accurate enough for daylight autonomy and represent a viable alternative to geometry-based simulations, it is also important to take into account glare metrics for choosing the right ray-tracing methodology. In the next section, we will present a study for glare, which in contrast to daylight autonomy, uses vertical luminance as main input instead of horizontal luminance.

3.2 Visual comfort

3.2.1 Objective

This research focuses on the assessment of visual comfort based on BSDF-based methods to calculate glare situation probability in buildings. It considers three possible metrics: DGP, Enhanced Simplified DGP (eDGP) and Simplified DGP (sDGP). It compares three different methods: Three-phase method, Five-phase method and

Rtrace_ttree (picture rendering of the scene with tensor tree layer to represent the CFS instead of geometry).

We will calculate and compare the accuracy and calculation time of each combination of metric and method for different fenestration systems. The first two fenestration systems used consists of a double-glazing unit and its combination with interior venetian blinds. For these systems, the results of the simulations will be compared with measurements carried out at the Daylighting Laboratory at Fraunhofer ISE (Germany). The analysis will then consider other fenestration geometries at a theoretical level, for which measurements are not available.

The simulations calculate and compare the following metrics:

- Daylight Glare Probability
- Enhanced simplified DGP
- Simplified DGP

Calculating these metrics requires a rendered picture and vertical luminance as input. The input data is calculated, with the same parameter as the the daylighting simulations, with:

- Three-phase method
- Five-phase method
- Rtrace_ttree

3.2.2 Computation cost

All the simulations are performed on a 2x Intel(R) Xeon(R) CPU E5-2697 with 28 threads each clocked at 2.6GHz and 40GB of RAM. It should be noted that the exact simulation times given in this paper are mainly relevant for a same configuration computer. The main interest of the numbers is the relative computation speed between the different metrics and methodologies that should remain valid for most configurations. This is mainly due that simulation times depend on many parameters, such as processor frequency, core numbers, cache size and supported instructions and RAM size, bandwidth and latency. Other factors can have a role as the disk speed if data can’t fit in RAM.

Moreover, the simulation was performed with a shoebox geometry representing the laboratory’s test room, without modelling the interior. The outside environment was not

modeled. This model isn't heavy on details but is traditionally used to estimate building performance on the planning and design phase.

3.2.3 Experimental setup

Our experimental validation was carried inside the same laboratory as the previous study (c.f. 3.1.1.2).

In our study, we used a previously calibrated CCD Camera to capture the pictures of a theoretical user's view, which would serve as a basis for DGP calculation. The camera is a TechnoTeam LMK 98-2. It was mounted on a tripod, with a vertical luminance sensor to measure eye luminance level (Figure 31). DGP was then calculated from both the picture and the measured vertical luminance with the evalglare tool [WIEN2004].

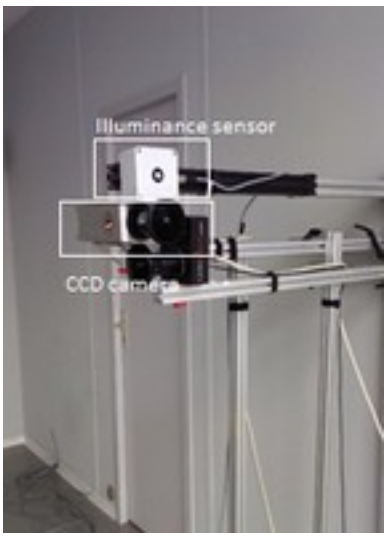

Figure 31 : picture of the CCD camera and luminance sensor.

A separate exterior meteorological station located on the roof recorded global total and diffuse luminance (LMT BAP30, Hagner ELV641) and irradiance (Kipp & Zonen CM 11) measurements. These measurements have been carried in sunny days. They have been carried with venetian blinds from the 3rd to the 6th June 2015 and without shading the 4th and 5th September 2015 (Figure 32).

These measurements were performed by Mahdieh Abravesh at Fraunhofer ISE as a part of her PHD thesis.

Figure 32: Fenestration system used. With and without venetian blinds.

With the measured data, we were able to calculate DGP with the Evalglare tool. We only kept the data set involving a non-null DGP. The measured DGP data are presented below:

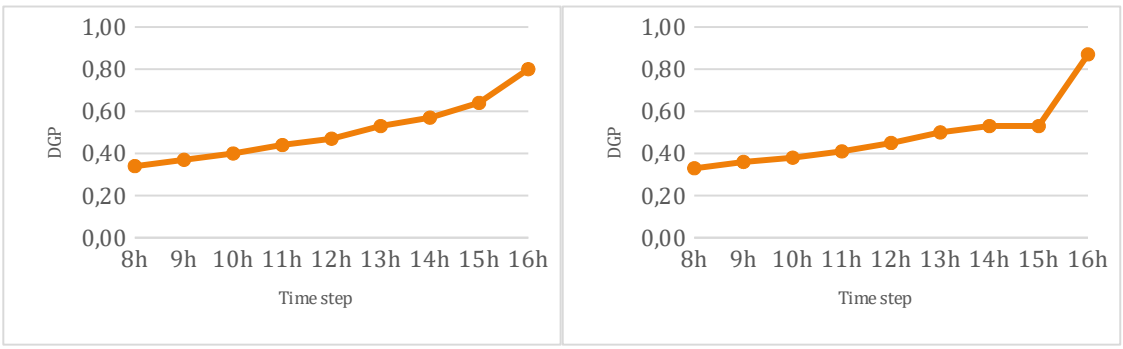

Figure 33 : Measured DGP the 03/06/2015 (left) and 04/06/2015 (right)

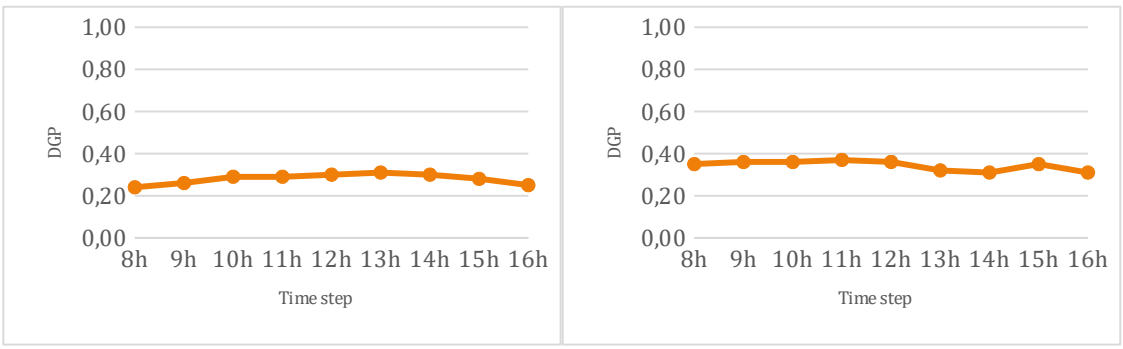

Figure 34 : Measured DGP the 05/06/2015 (left) and 06/06/2015 (right)

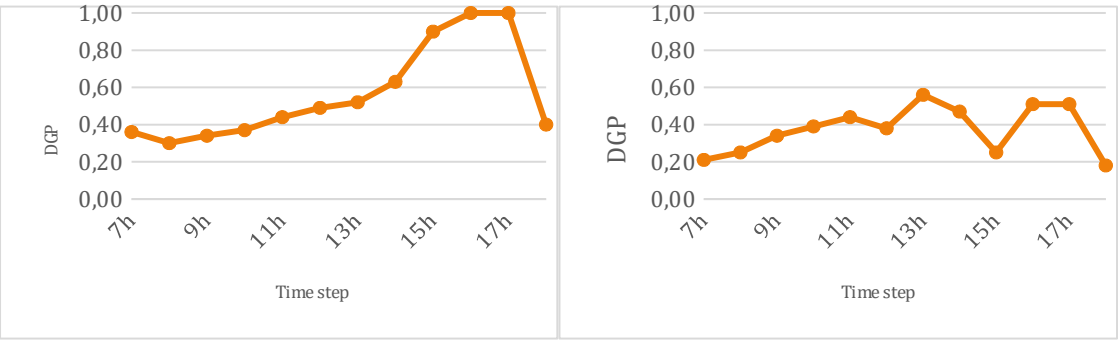

Figure 35 : Measured DGP the 04/09/2015 (left) and 05/09/2015 (right)

In our measured data, DGP ranges between 0.14 and 1 for the days without shading. With the venetian blinds, it goes from 0.29 to 0.94.

3.2.4 The three-phase method

3.2.4.1 Accuracy

In our simulations, we used the 3-phase method with a sky divided into 5185 sky patches following Reinhart MF:6 sky distribution, as it did provide considerably better results than the usual Reinhart MF:4 sky distribution with 2305 patches. To the knowledge of the authors, all the other studies with the 3-phase method involved the 2305 sky patches.

We also have set the number of ambient bounces for the View matrix calculation to 8, which in our case study, did also provide more consistent values than the lower values ambient values recommended in some Radiance tutorials [RAD2017]. Higher values didn't seem to provide any benefit though. It should be noted that in the first Five phase method tutorial [RAD2018], the author advices to use -ab 10 in the general case. The advised parameters in this tutorial provided satisfying results.

For our DGP calculation, we rendered the image according to the 3-phase method. For simplified DGP we calculated the vertical luminance following the 3-phase method's equations. For the Enhanced simplified DGP, we used the same vertical luminance methodology as for the simplified DGP, the simplified picture was rendered with the direct view and direct daylight matrices used usually in the Five-phase method. The simulations were carried with the following parameters:

Radiance command	Radiance parameter	D matrix for fully	V matrix for fully	D matrix for simplifie	V matrix for simplifie	D matrix for vertical	V matrix for vertical

		rendered picture	rendered picture	d picture	d picture	luminance	luminance
-ab	Ambient bounces	8	6	0	0	8	6
-ad	Ambient divisions	65536	8192	65536	8192	65536	8192
-as	Ambient supersamples	65536	8192	65536	8192	65536	8192
-ar	Ambient resolution	16384	1024	16384	1024	16384	1024
-lw	Minimum weight of each ray	10-6	10-6	10-6	10-6	10-6	10-6
-lr	Maximum number of reflections	12	8	12	8	12	8

Table 3 : 3-phase method simulation parameters

We compared the estimated DGP from the 3-phase method with the measured one.

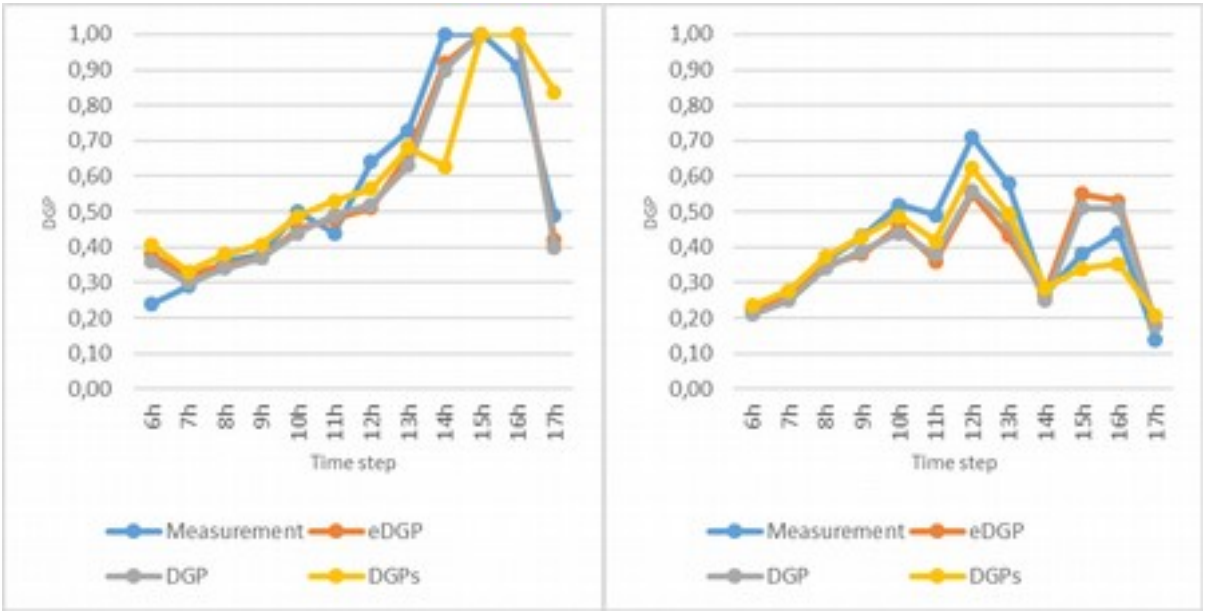

Figure 36 : Calculated DGP/eDGP/sDGP with 3-PM and measurements the 03/06/2015 on the left, and the 04/06/2015 on the right.

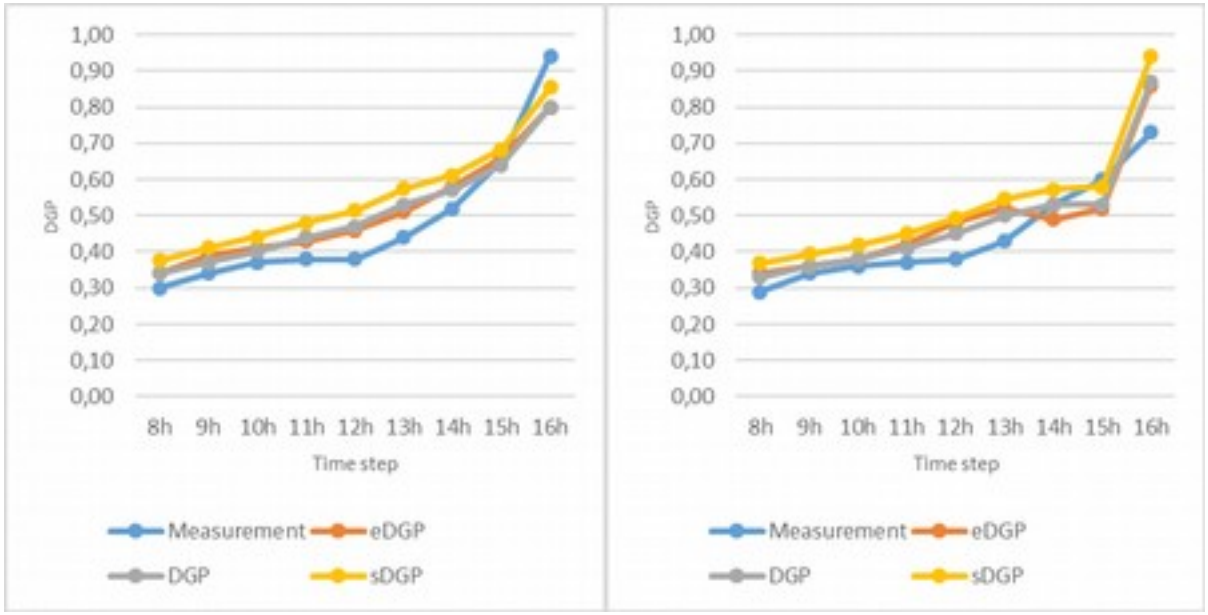

Figure 37 : Calculated DGP/eDGP/sDGP with 3-PM and measurements the 05/06/2015 on the left, and the 06/06/2015 on the right

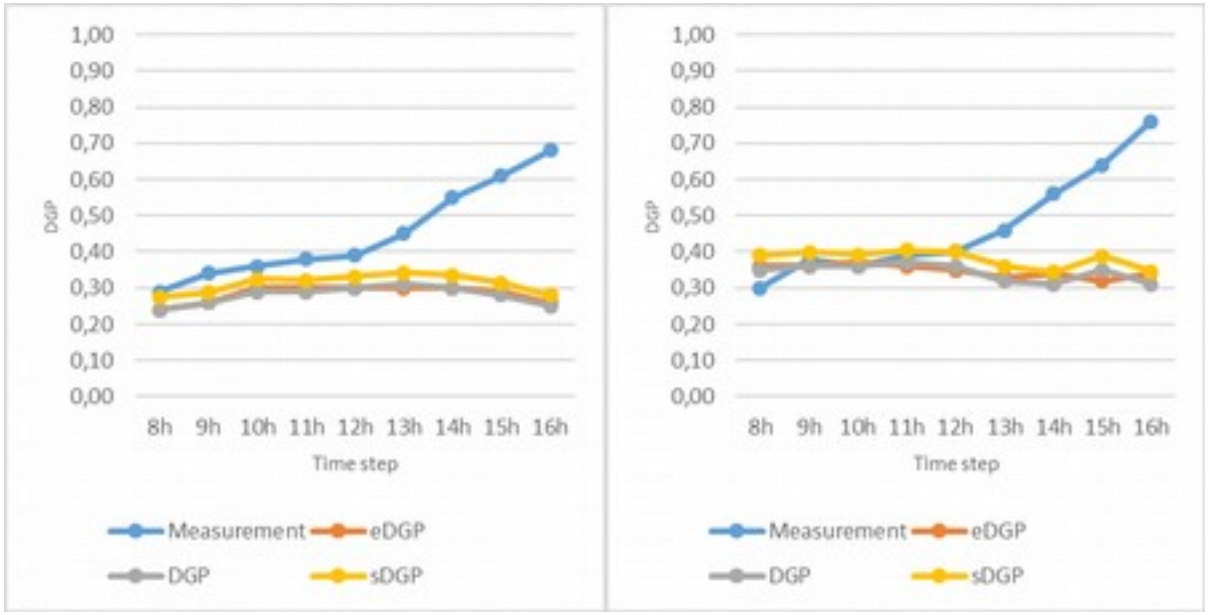

Figure 38: Calculated DGP/eDGP/sDGP with 3-PM and measurements the 04/09/2015 on the left, and the 05/09/2015 on the right

In most time steps, both DGP and eDGP have very close value. Simplified DGP in the other hand show more divergences compared to them. To evaluate the overall accuracy of these different metrics, the relative root mean squared errors (RMSE) and the averages of the averages of the relative mean bias errors (rMBE) are usually used to describe the errors compared to the reference method. They are defined as:

$$rMBE = \frac{1}{N}\sum_{i=1}^{N}\frac{DGP_i - DGP_{ref}}{DGP_{ref}}$$	(18)
$$rRMSE = \sqrt{\frac{1}{N}\sum_{i=1}^{N}\left(\frac{DGP_i - DGP_{ref}}{DGP_{ref}}\right)^2}$$	(19)

	DGP	eDGP	sDGP
rMBE	-6%	-5%	1%
RMSE	23%	25%	25%
Maximum relative error	50%	58%	70%
Minimum relative error	-63%	-62%	59%

Table 4 : Summary of the accuracy of the 3-phase method

Globally, the three metrics show approximately the same accuracy, with an rMSE of 23% for DGP, and 25% for eDGP and sDGP. RMBE is very low, ranging from -6% for DGP and -5% for eDGP, to 1 for sDGP. The maximum absolute error goes up to 70% for sDGP, while DGP and eDGP are limited respectively to 63% and 62%. In the case of the 4th and 5th September (Figure 38) we can see a clear divergence between the three-phase method and measurements. In these days, the subject is hit by direct irradiance at 15:00. Direct luminance is one of the main limitations of the three-phase method as observed for horizontal luminance too (c.f. 3.1.1.4). An other limitation, which is related only to this case, is that the low BSDF resolution smoothen the luminance over a large angle, which directly impacts DGP calculation.

The main advantage of the three-phase method is that it does not require a tensor tree BSDF, and its calculation speed.

3.2.4.2 Calculation time:

For calculation time, we will mainly use three parameters:

- N=number of CFS
- S= number of scenes. A scene is a combination of material and geometry. In our paper, when we refer to a scene, it is for a unique combination of the outside environment and inside space. The CFS is not counted in the scene.
- T=number of time steps used in simulation.

In our time calculation formulas, we use the little-o notation "o(X)" to refer to a neglectable parameter in calculation time.

In our simulations, the most significant portion of the computation time was due to the calculation of the View and Daylight matrix. From our experience, matrix multiplication has always had negligible time. We assume that BSDF data is already calculated from measurements. Therefore, we do not take into account the potential time it would take to generate it.

	Calculation time formula
DGP	$C_S * S + o(T) + o(N)$
eDGP	$C'_S * S + o(T) + o(N)$
SDGP	$C''_S * S + o(T) + o(N)$

Table 5 : Calculation time of the 3-phase method

The three-phase method, in each of its variation scales linearly with the number of scenes. In our simulations, we obtained the following numbers:

- C_S=30 min
- C'_S= 4 min
- C''_S= 20 sec

As it can have theoretically predicted, calculation of DGP is always slower than eDGP calculation which is in turn is always slower than SDGP calculation. In order to better evaluate the impact of these calculation on the methodology, we discussed different possible use cases in Section 4, where these calculation times are compared to the other methodologies' result.

3.2.5 The Five-phase method

3.2.5.1 Accuracy

In our simulations, we used the Five-phase method with the same matrices, and therefore the same parameters, as in the Three-phase Method. The other components of the equation used the following parameters:

Radiance command	Radiance parameter	$C_{F\text{-}ds}$	C_{IR-ds}	M
-ab	Ambient	1	1	0

Radiance command	Radiance parameter	$C_{F\text{-}ds}$	C_{IR-ds}	M
	bounces			
-ad	Ambient divisions	5000	5000	-
-dj	Direct jittering	0	0	-
-dt	Direct threshold	0	0	-
-lw	Minimum weight of each ray	10-4	10-4	-
-dc	Direct certainty	1	1	-
-ps		-	-	1
-av		-	-	0.31831 0.31831 0.31831

Table 6 : 5-phase method simulation parameters.

The simplified eDGP image picture has been rendered by keeping only the direct component of the Five-phase method. It was rendered following the equation:

$$I = V_d T D_d s_d + (C_{R\text{-}ds} + C_{F\text{-}ds}) s_{sun} \quad (20)$$

With these parameters, we compared the different estimations of DGP calculated with the 5-phase method with the experimental data:

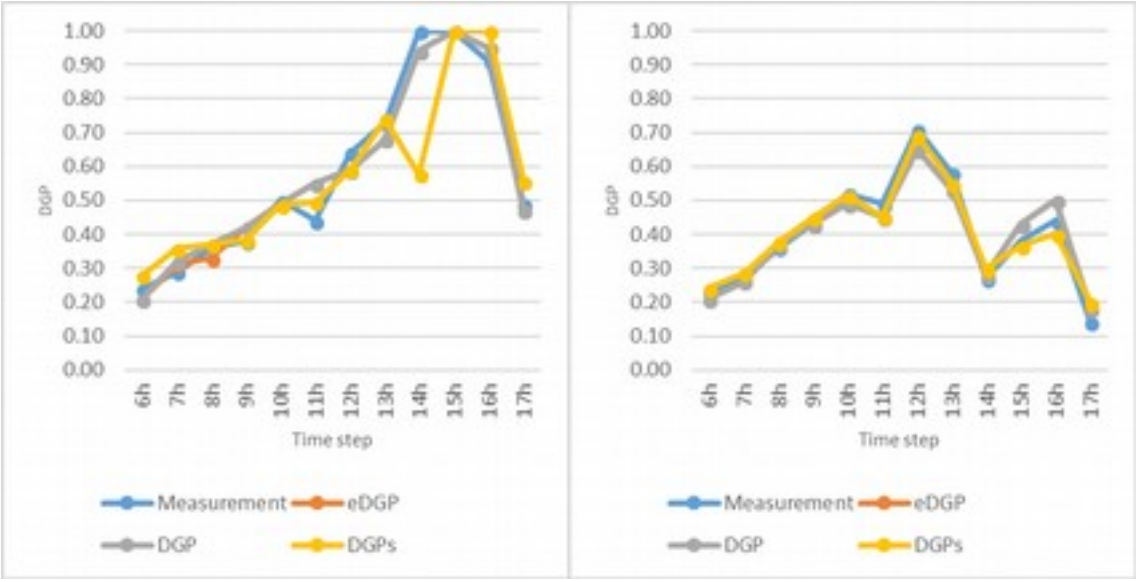

Figure 39 : Calculated DGP/eDGP/SDGP with 5-PM and measurements the 03/06/2015 on the left, and the 04/06/2015 on the right.

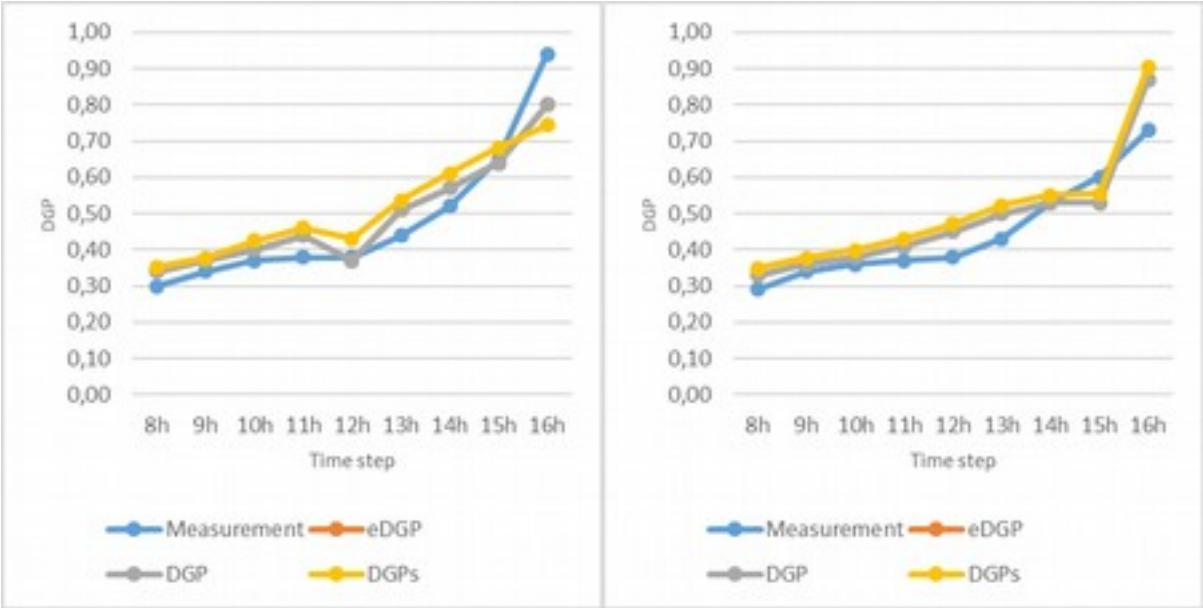

Figure 40 : Calculated DGP/eDGP/SDGP with 5-PM and measurements the 05/06/2015 on the left, and the 06/06/2015 on the right

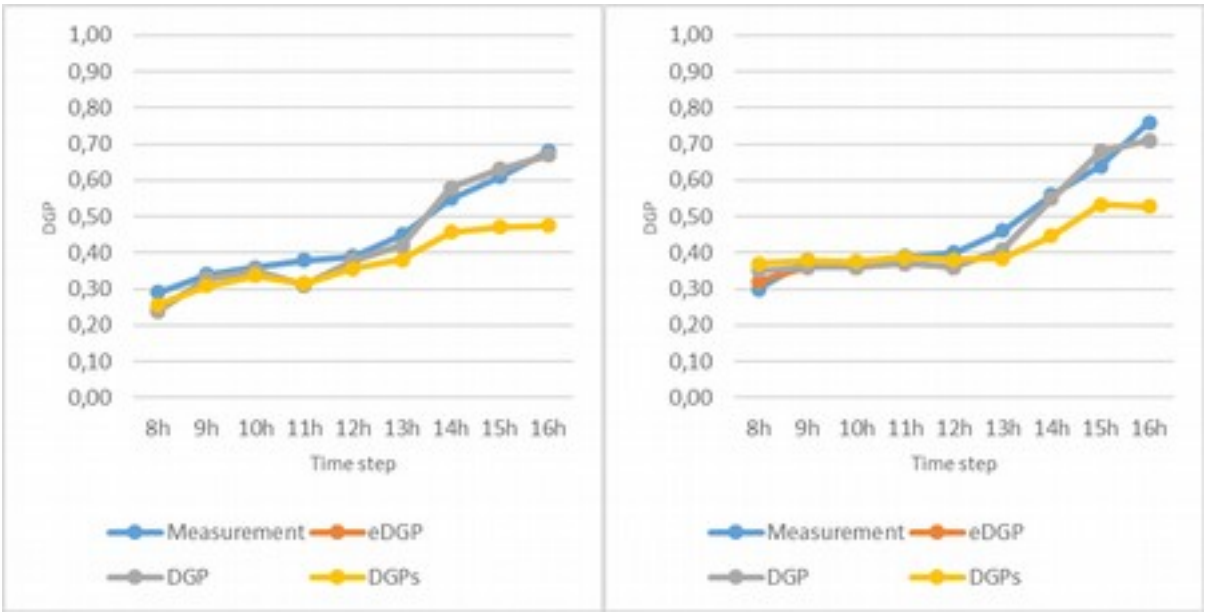

Figure 41: Calculated DGP/eDGP/SDGP with 5-PM and measurements the 04/09/2015 on the left, and the 05/09/2015 on the right

With the 5-phase method, the error in the calculation of the DGP and eDGP is very close in most of the time steps. Globally, the DGP has a 11% accuracy while eDGP has 10%. They have the same maximum absolute relative error of 29%. SDGP in the other performed relatively worse, with 16% accuracy and 43% maximum relative error. The relative mean bias error is low for the three metrics. These results are analogous to the horizontal luminance calculation. The five-phase method performs better than the three-phase method in the case of direct irradiation, which can be seen in Figure 44 where the calculated DGP is still close to the measured DGP even after 14:00.

	DGP	eDGP	SDGP
rMBE	2%	1%	2%
rRMSE	11%	10%	16%
Maximum relative error	29%	29%	43%
Minimum relative error	-18%	-18%	-42%

Table 7 : Summary of the accuracy of the 5-phase method

3.2.5.2 Calculation time:

In our simulations, the main calculation came from the calculation from the calculation of the direct sun coefficient matrix. As of our experience with the Three-phase method, matrix multiplication has always had negligible time.

	Calculation time formula
DGP	$C_S * S + C_{SN} * S * N + o(T)$
eDGP	$C_S^{'} * S + C_{SN}^{'} * S * N + o(T)$
SDGP	$C_S^{\} * S + \{C\} rsub \{SN\} rsup \{} * S * N + o(T)$

Table 8 : Calculation time of the 5-phase method

From our simulations, we got the following numbers:

- C_S=40 min and C_{SN}=300 min
- C'_S=14 min and C'_{SN}=305 min
- C''_S=1 min and C'_{SN}=5 min

In the case of the Five-phase method, the time function doesn't only grow linearly with the number of scenes as the 3-phase method, but also with the product of the number of scenes and number of CFS. It is due to the direct sun coefficient component which depends on the scene and fenestration system combination.

3.2.6 Rtrace_ttree

3.2.6.1 Accuracy

To generate pictures, we used rtrace combined with rview. As for the other methodologies, we generated 180° fish eye lense pictures with an 800x800 resolution.

We used the following parameters:

Radiance command	Radiance parameter	Full picture	Simplified picture	Vertical luminance
-ab	Ambient bounces	12	1	12
-ad	Ambient divisions	5000	5000	65536

-as	Ambient super-samples	5000	5000	65536
-ar	Ambient resolution	2000	2000	-
-aa	Minimum weight of each ray	0.15	0.15	0
-lw	Minimum weight of each ray	10^{-4}	10^{-4}	10^{-4}
-lr	Maximum number of reflections	12	12	12

Table 9 : rtrace_ttree simulation parameters.

With these parameters, we compared the different estimations of DGP with the experimental data:

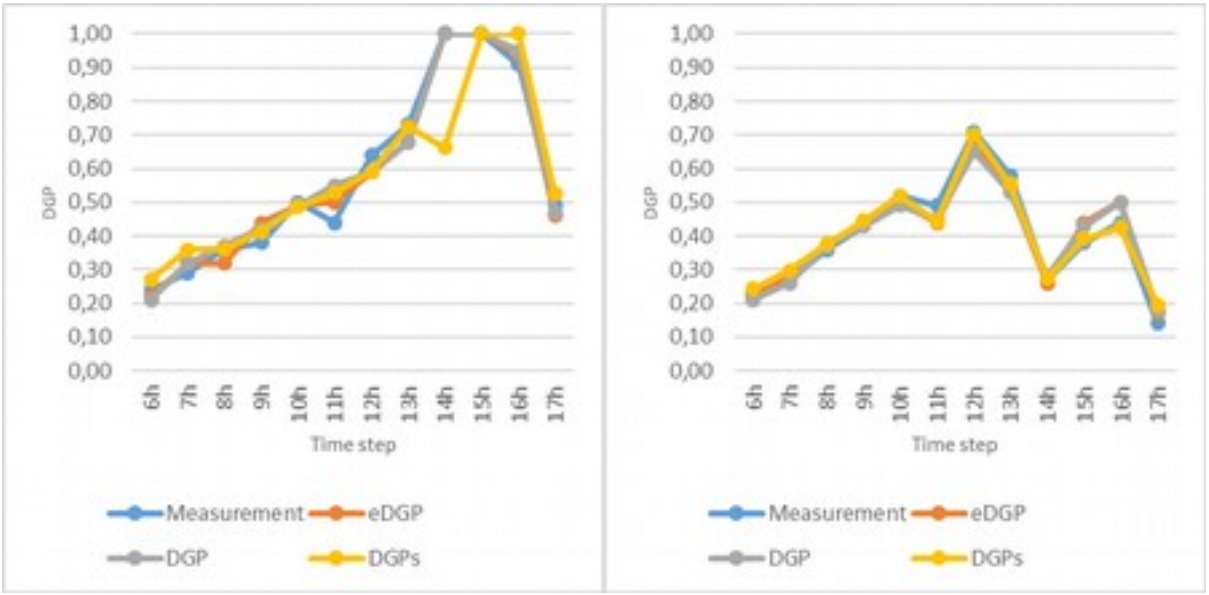

Figure 42 : Calculated DGP/eDGP/SDGP with rtrace_ttree and measurements the 03/06/2015 on the left, and the 04/06/2015 on the right.

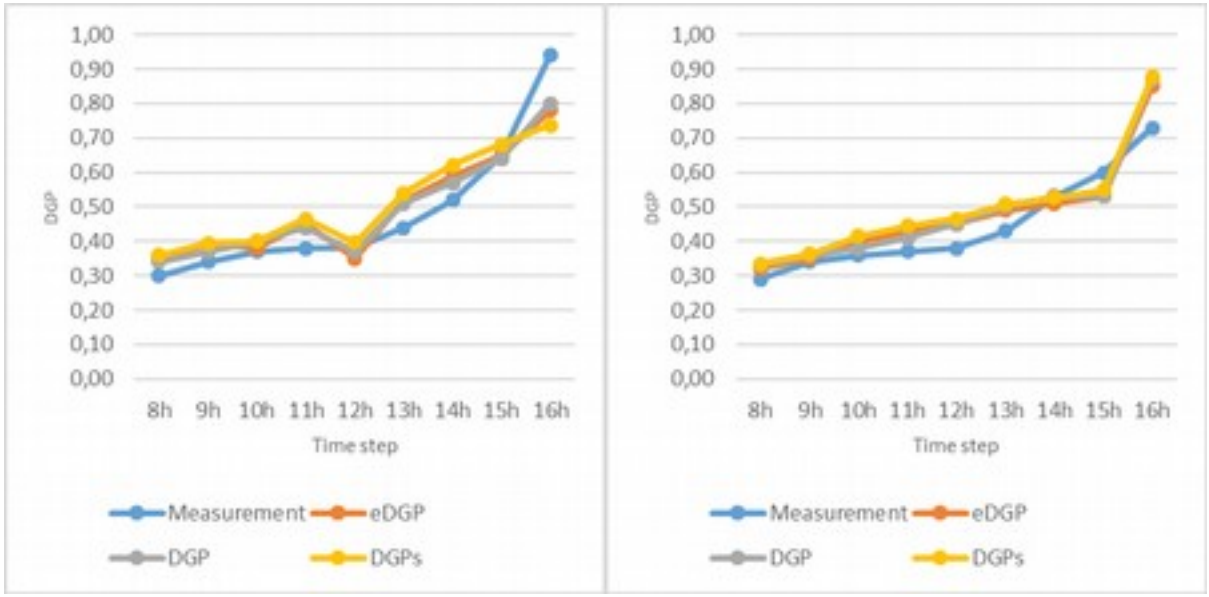

Figure 43 : Calculated DGP/eDGP/SDGP with rtrace_ttree and measurements the 05/06/2015 on the left, and the 06/06/2015 on the right

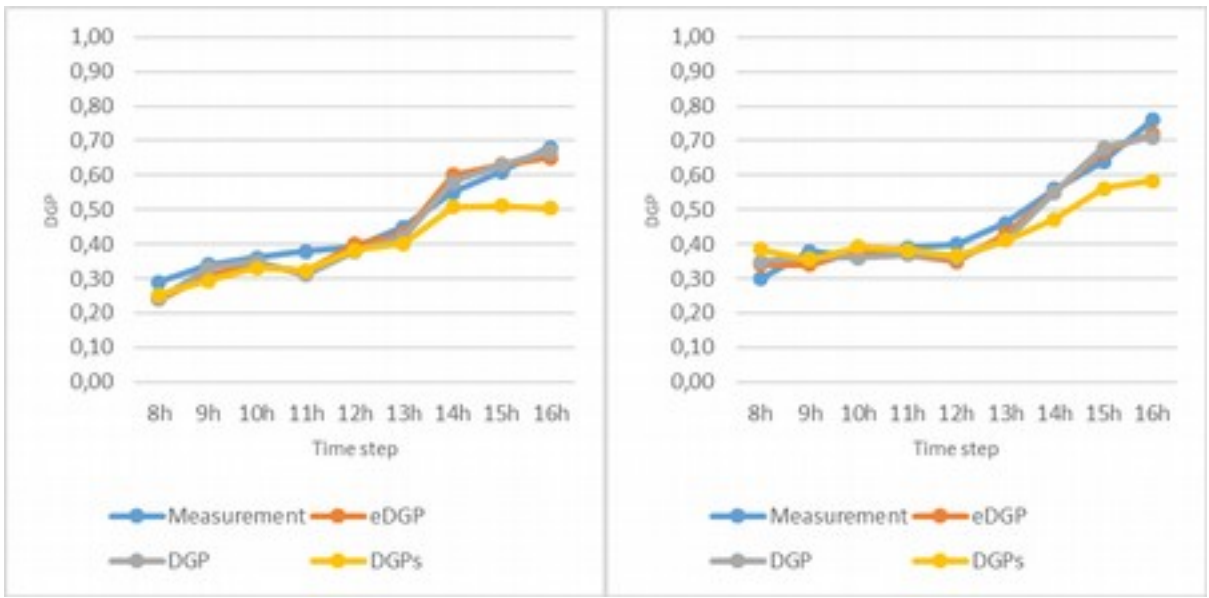

Figure 44: Calculated DGP/eDGP/SDGP with rtrace_ttree and measurements the 04/09/2015 on the left, and the 05/09/2015 on the right

With the rtrace_ttree method, the error in the calculation of the DGP and eDGP is very close in most of the time steps. Globally, the DGP has a 11% accuracy while eDGP has 10 and has 15% accuracy. The relative mean bias error is at 2% for the three metrics. In this regard the behavior is very similar to the 5-PM methodology. The maximum absolute relative error is only 21% for eDGP in this methodology, in 5-PM it was 29%.

While our dataset is admittedly limited, and therefore can't demonstrate that 5-PM and rtrace_ttree behaves the same way in regards of DGP for every case, it still hints, the MF:6 discretization of the sky doesn't have much impact on the accuracy of DGP calculation.

	DGP	eDGP	SDGP
rMBE	2%	2%	2%
rRMSE	11%	10%	15%
Maximum relative error	29%	21%	39%
Minimum relative error	-18%	-17%	-34%

Table 10 : Summary of the accuracy of rtrace_ttree

3.2.6.2 Calculation time:

As of the calculation time, it is very dependent on the input parameters. Especially the ambient accuracy parameter which has a very strong impact on the calculation time.

	Calculation time formula
DGP	$C_{NST} * N * S * T$
eDGP	$C'_{NST} * N * S * T$
sDGP	$C_{NST}^{\} * N * S * ¿}$

Table 11 : calculation time of rtrace_ttree.

From our simulations, we got the following numbers:

- C_{NST}=45 min
- C'_{NST}=1 min
- C'_{NST}=6 sec

In this case, the simulation has to be repeated for each time step, fenestration and scene. Consequently, the time function scale with the product of the three parameters.

3.2.7 Theoretical comparison

We mainly noticed in the previous experimentation that the Five-phase method and rtrace_ttree results agreed in most time steps. As our data set is limited, we chose to conduct a theoretical study where we modify some optical parameters of the venetian blinds, in order to see if our results remain the same. Simulations will be carried in the case of a sun corresponding to the clear sky standard of CIE.

In our study, we chose to modify three parameters:

- Peak angle amplitude: Venetian have a peak angle Θ, which is the incident angle of maximum direct-direct transmittance. The direction is usually in the vertical plane orthogonal to the window, at a profile angle equal to the tilt angle for venetian blinds. Moreover, venetian is characterized by a cut-off angle. When the incident's ray profile angle is superior to Θ + ΔΘ or inferior to Θ – ΔΘ, where ΔΘ depends of the CFS geometry, the direct-direct transmittance becomes null. A small peak angle amplitude means that the light is only visible from a specific position and we have an luminance peak. This factor is important to consider, especially that ΔΘ may be way small than the BSDF patches and may result in these peaks being smoothed out. Low angles amplitudes are unusual for venetian blinds, they are more common in the case of textile or perforated blinds.

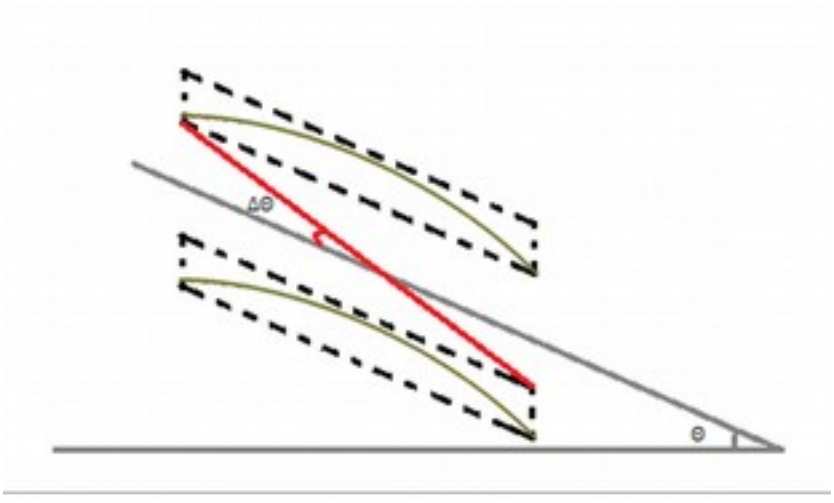

Figure 45: 2D representation of Θ and ΔΘ in the case of venetian blinds.

- Direct-direct transmittance of incident rays at peak angle: Most heterogeneous CFS as venetian blinds contain one heterogeneous layer that is made of a pattern

of opaque and void spots. At peak angle, depending on the ratio of opaque and void spots surfaces, the maximum direct-direct transmittance value varies.

- Scale: venetian blinds' depth is in the order of magnitude of 10cm. While textile yarns' diameter is usually sub-millimetric. Blinds with 8 cm depth are considered in this study as reference. They therefore have a scale of 100%. A blind of 4 cm would have a scale of 50% and a blind of 0.8 mm has 1% scale and can be assimilated to a textile. Very small-scale geometries can be perceived by the eye as homogeneous. It is usually the case with textiles seen from far.

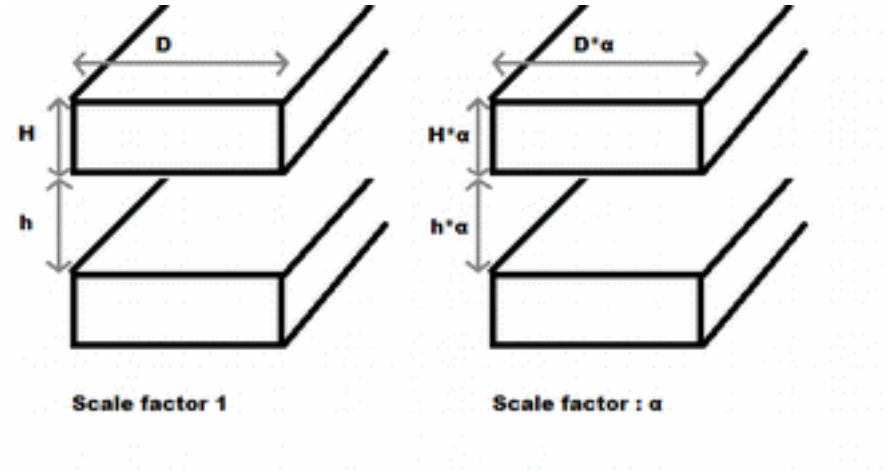

Figure 46 : scale factor influences on a cuboid based CFS. These cuboids may represent the bounding box of textile yarns or venetian blinds.

For the scale's case, we noticed that changing the scale always resulted in the same BSDF calculated, bearing a negligible margin of error. This result could have been theoretically predicted, as angular properties are independent of scale, therefore we will only present the results of the two other parameters.

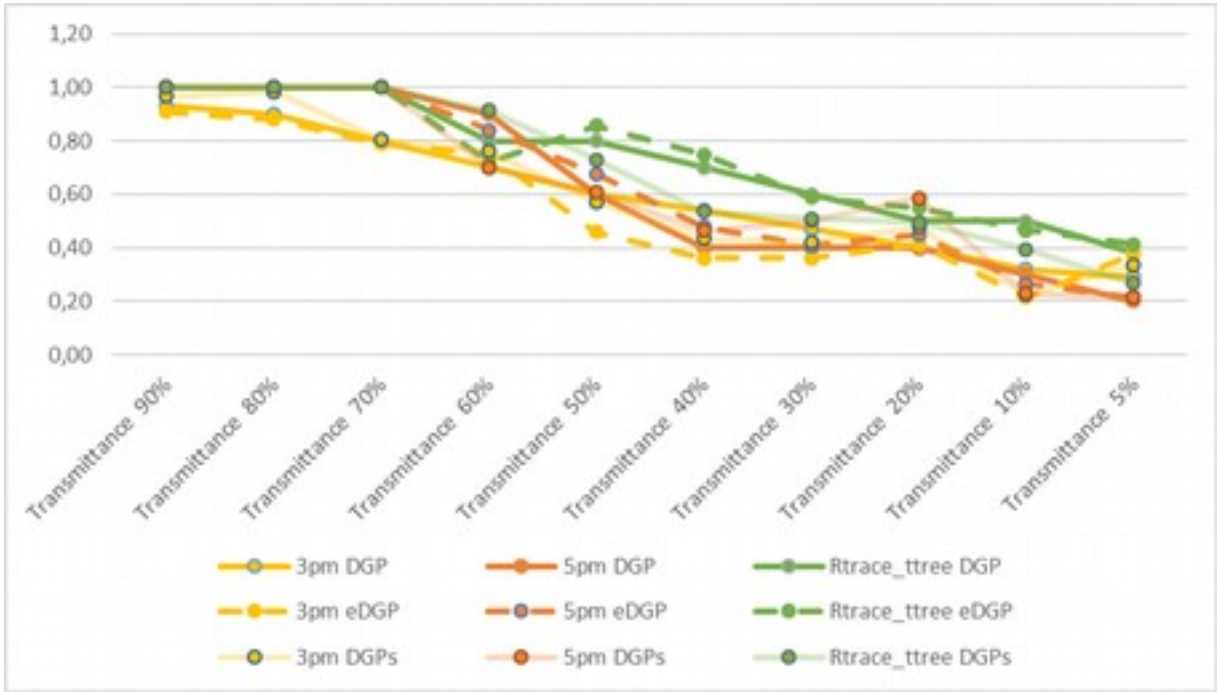

Figure 47 Calculated DGP relatively to the direct-direct transmittance

From the trend of the graph, we can notice that the five-phase method and rtrace_ttree's DGP mainly diverge at low direct-direct transmittance, while they follow the same trend at higher direct-direct transmittance. The error can go as high as 50% in the lowest transmittance. Five-phase method scales linearly's DGP scales linearly with direct-direct transmittance while rtrace_ttree calculates higher DGP.

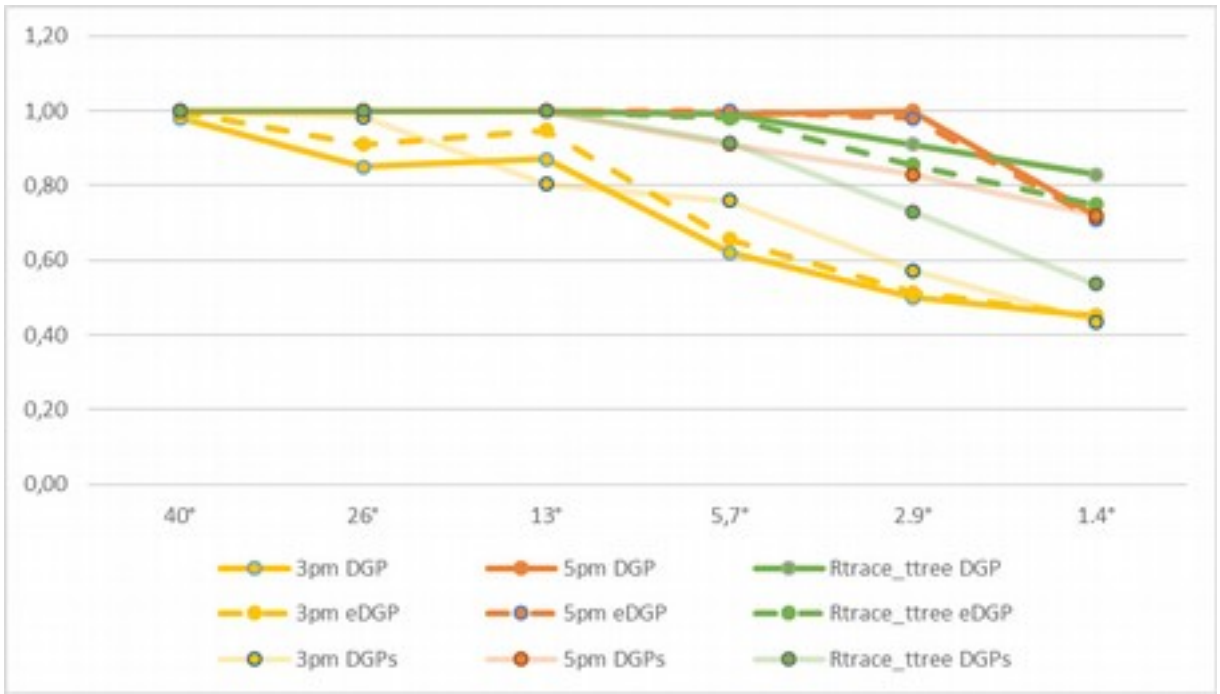

Figure 48 : Calculated DGP relatively to the peak angle amplitude

The difference between the Five-phase method and rtrace_ttree method doesn't vary much according to peak angle amplitude. However, the three-phase method seems to diverge a lot more at lower amplitude angle. The limited resolution of Klems BSDF is the main limitation when dealing with such small angles.

	3pm DGP	5pm DGP	Rtrace_ttree DGP	3pm eDGP	5pm eDGP	Rtrace_ttree eDGP	3pm sDGP	5pm sDGP
Direct-direct transmittance	40	50	0	60	50	10	50	50
Peak angle amplitude	46	13	0	46	14	10	48	13

Table 12: maximum relative error with the DGP from rtrace_ttree taken as reference.

3.2.8 Discussion

In order to compare the accuracy/time calculation trade-off these methodologies offer, we shall consider the following cases:

- Case 1: One CFS, in a single scene, simulated over a single day with ten timesteps.
- Case 2: One CFS, in a single scene, simulated over a year with 10 time steps each day.
- Case 3: 5 different CFS, 3 building orientations (and thus, 3 scenes), simulated over a single day with ten timesteps.

While some cases may not seem realistic as we use a high number of CFS, we hope that in the next decade, usage of Building Information Workflow will be more pervasive, and a CFS product database would be established, which would make such a comparison possible.

	3PM			5PM			Rtrace_ttree		
	DGP	eDGP	sDGP	DGP	eDGP	sDGP	DGP	eDGP	sDGP
rMSE	23%	25%	26%	11%	10%	16%	11%	10%	15%
Case 1	3	0.4	0.03	28	26	0.6	45	1 *10 min*	0.1
Case 2	0.008	0.001	0.0001	0.07	0.07	0.001	45	1 *3650 min*	0.1
Case 3	0.60	0.08	0.04	31	31	1.7	45	1 *150 min*	0.1

Table 13 : Summary of the accuracy and calculation time of the 3-phase, 5-phase and rtrace_ttree methods.

Overall, the 3-phase method has a worse DGP accuracy than the other methodologies but better calculation time. To use the optimal methodology, the methodology choice depends on the number of time steps:

- If the number of time steps is high, approximately 6 times more time steps than tested CFS with a single scene, it is advantageous to use the 5-Phase method to calculate full DGP over the enhanced simplified DGP with rtrace_ttree. Enhanced simplified DGP with 5-phase method didn't seem to offer any foreseeable advantage in this case.
- If the number of time steps is low, it is more advantageous to use eDGP with rtrace_ttree. Unfortunately, using the enhanced simplified DGP relies on the assumption that there is no specular material involved.
- In the case of a scene involving specular material, it is important to note that it is outside of the assumptions of eDGP and sDGP. Moreover, the accurate direct sun component of the five-phase method doesn't take into account specular reflection. Therefore, the safest choice would be to use full DGP with rtrace_ttree.

As of the three-phase method, it offers excellent calculation time at the cost of accuracy. It is only recommended to use it if tensor-tree data is unavailable. If tensor-tree is available, simplified DGP with the 5-PM or rtrace_ttree offer a better alternative with a small calculation time and better accuracy. An alternative research path would be to use a higher resolution matrix BSDF, which might answer drastically improve the 3-PM calculation's accuracy.

4 THERMAL ASSESSMENT

In our BIM implementation, we rely on Kuhn's model to represent the CFS (1.8.2.2). Kuhn's model has been implemented in FENER [BUE2015], a simulation engine that relies for thermal simulations on the Blackbox model, coupled with the Three-phase method to calculate irradiance.

4.1 Blackbox Model

The blackbox model is a virtual model that encapsulates the complexity of the CFS in a two-layers system. Its main advantage is that its input is totally measurable, therefore it should be able to remain accurate even new technologies by making minimal assumptions. In contrast with other models, it doesn't assume for example that the layers are parallel or homogeneous. The model relies on the following data as input:

- U-value of the system
- Directional g-value
- Bi-directional scattering distribution function

The resulting two-layer systems are characterised by their own absorbance.

According to the EN410:2011, the relation between the U-value of a two-layer system and the absorbance of its layers can be written as follow:

$$\frac{1}{U} = R_e \alpha_0 + \left(R_e + R\right) \alpha_i \tag{21}$$

With R_e and R_i the outdoor and indoor thermal resistance to the convective and conductive heat exchange between the wall and the environment, R the system's resistance, α_0 the outer layer absorbance and α_i the inner layer absorbance. The U-value is dependent on the temperature and is expressed as a linear function of the latter.

The resistance values retained are based on the EN410 results:

- $Ri = 0.13\ m^2\ KW{-}1$
- $R_e = 0.04\ m^2\ LW{-}1$

The absorbance of each layer is then calculated as follow:

$$\alpha_i = \frac{1}{R}\left(\frac{q_i}{U} - \alpha R_e\right) \quad (0)$$

$$\alpha_0 = \frac{1}{R}\left(\alpha\left(R_e + R\right) - \frac{q_i}{U}\right) \quad (0)$$

With q_i the secondary heat gain coefficient

The equations 34 and 35 are dependent on the incident angle and are solved with BSDF data.

The direction solar heat gain coefficient of the system in this model can also be calculated, instead of directly measured, from the BSDF and directional solar heat gain coefficient of the glazing unit (gu) and the shading device (sd).

$$g = \tau_{sd}\, g_{gu} + \frac{\alpha\, \Delta_{ext}}{\Delta_2} + \frac{\tau_{sd}\left(1 - g_{gu}\right)\Delta_{ext}}{\Delta_1} \quad (0)$$

With $\Delta_2 = 18\, W\, m^{-1} K^{-1}$ and $\Delta_1 = 6\, W\, m^{-1} K^{-1}$ similarly to EN13363-1. And

$$\Delta_{ext} = \left(\frac{1}{U_{gu}} + \frac{1}{\Delta_1} + \frac{1}{\Delta_2}\right)$$

In the case of internal shading device, the formula becomes:

$$g = \tau + g_{gu} - \tau_{gu} + \frac{\left(1 - \kappa\right)\tau_{gu}\alpha_{gu,diffuse}\,\rho_{sd}}{1 - \rho_{sd,diffuse}\,\rho_{gu,diffuse}} + \tau_{gu}\alpha_{sd}\,¿ \quad (0)$$

The coefficient κ represents the fraction of the outward going energy that is reflected by the shading device and absorbed by the glazing. [KUH2011] showed that a value of 0.4 can be used in the case of venetian blinds if it is not possible to measure it. This formula has been used for our calculation and its impact is discussed in 4.3.

The Blackbox model has been implemented in Fener software [BUE2015]. Fener is a software that works with shoebox geometries to simulate CFS performance in isolated

rooms. It uses the energy balance method between outdoor and inner surfaces. It accounts for conduction, convection and radiation [BUE2017].

Convection and longwave radiation are calculated with $q=h \Delta T$ with h the heat transfer coefficient. The indoor convective coefficient is the same as Energy plus [DOE2018]. The outdoor convective coefficient is calculated from wind speed. Radiative heat transfer is linearized from Stefan-Boltzmann equation. The transient heat conduction between surfaces is calculated with the finite difference methods

4.2 Theoretical setup

In this research, we tried to validate our methodology that uses the blackbox model as a representation of the CFS thermal behavior. To do so, we compare it to the state-of-art reference, the ISO 15099.

In our comparison we will compare estimation based on FENER's model, and Energy plus used with the ISO 15099 model, on the basis of the following metrics:

- Air temperature
- Interior window surface temperature
- Interior walls surface temperature

In order to do so, we consider a shoebox room, where only the façade is exposed to the exterior (Figure 49). The room is 5m x 4m x 3m from the interior. The fenestration system is 4m wide, frame included. The setup is similar to an average office room.

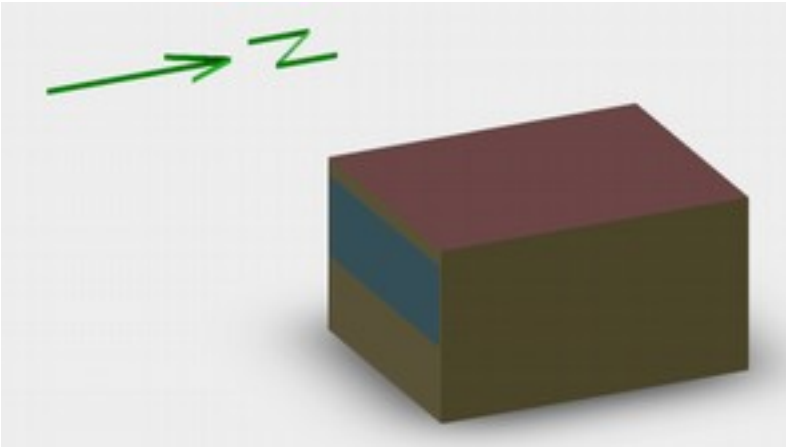

Figure 49: 3d visualization of the room with the façade oriented south.

In order to extensively validate the Blackbox model and avoid bias related to our theoretical setup, many characteristics of this room have been altered in the different

simulations. All the simulations were hour by hour simulations over a year (8760 hours simulated each year). The room has been tested over 8 different orientations: South, South-East, East, North-East, North, North-West, West and South-West. 4 different locations were used in order to use different climates (Figure 50): Frankfurt (Moderate climate), Alicante (Dry), Accra (Tropical) and Houlton (Continental). These 4 locations have, expectedly, different average temperatures during the year (Table 14).

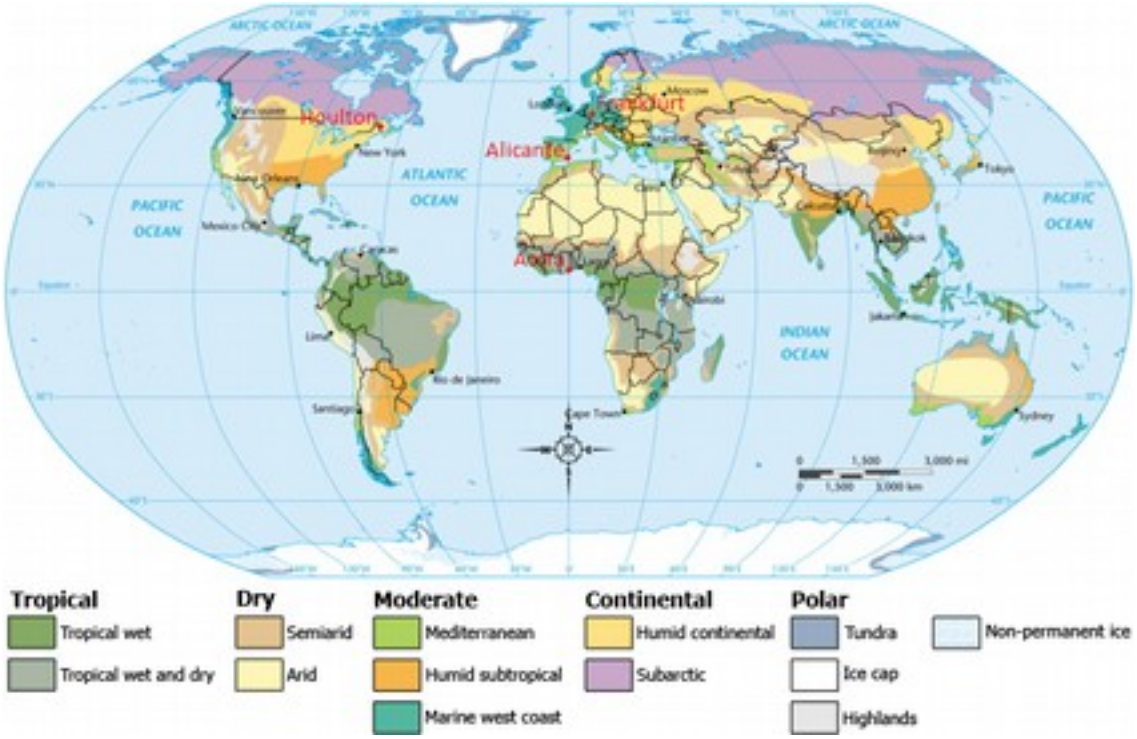

Figure 50: Worldwide climate classification (source: Wikipedia)

Location	Average yearly temperature (° C)	Average yearly temperature during work time (° C)
Houlton	4.9	7.7
Frankfurt	10.1	12.3
Alicante	17.9	20.1
Accra	26.9	28.4

Table 14 : Average temperature in each location

Moreover, we used 4 different fenestration systems: Double glazing unit, double glazing unit with external blinds, double glazing unit with external shade and double-glazing unit with internal shade. We therefore have collected a dataset of 8 760 * 8 * 4 * 4 = 1 121 280 rows.

Interior length	5 m

Interior width	4 m
Interior height	3 m
Sky view factor	0.5
Ground albedo	0.2
Wall reflectance	0.5
Ceiling reflectance	0.7
Floor reflectance	0.2
Infiltration/ventilation	0.5 ACH
Equipment heat gain during work time	$8.0 W/m^2$
Occupation during work time	1 person
Work time	8:00 – 18:00
People radiant fraction	0.5
Interior finish conductivity	$0.25\ W.m^{-1}.K^{-1}$
Insulation layer conductivity	$0.03\ W.m^{-1}.K^{-1}$
Massive material conductivity	$2.3\ W.m^{-1}.K^{-1}$
Exterior finish layer	$2.3\ W.m^{-1}.K^{-1}$
Window dimension	3m x 1.5m
Fenestration systems	Double glazing unit Double glazing unit with external blinds Double glazing unit with external shade Double glazing unit with interior shade
Locations	Accra (Ghana) Alicante (Spain) Houlton (USA) Frankfurt (Germany)
Orientation	**South** South-East East North-East North North-West West South-West

Table 15: Room characteristics.

4.3 Data processing

In order to compare the results concerning the air temperature and surfaces temperature, we first started by removing outlier values in the beginning of the year (Figure 51). These outlier values are characterized by a large difference on predicted temperature between Fener and Energy plus (Figure 52). They are due to different boundary condition between Fener and Energy plus during the warm up phase that preceded the simulation. This behavior is the same in all simulations, independently of the room characteristics (CFS used, location and orientation)

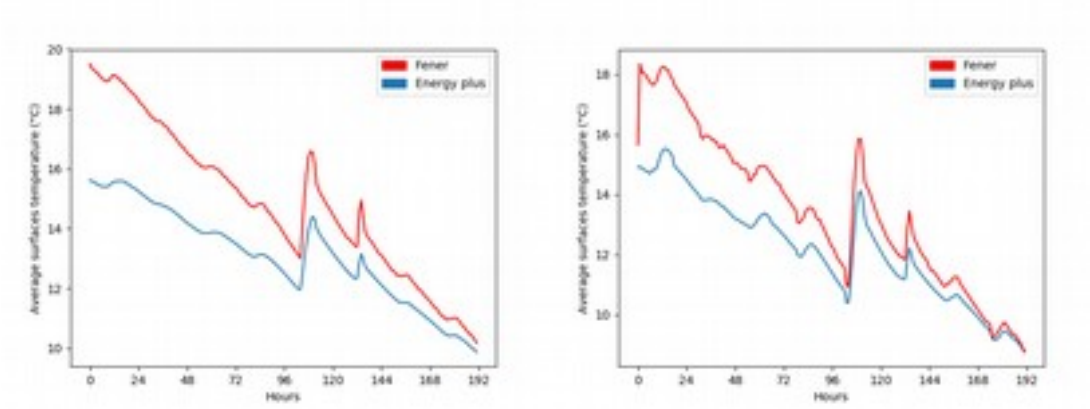

Figure 51 : Predicted average wall temperature (left) and air temperature (right) during first week of the year, with room oriented south in Frankfurt with Double glazing unit

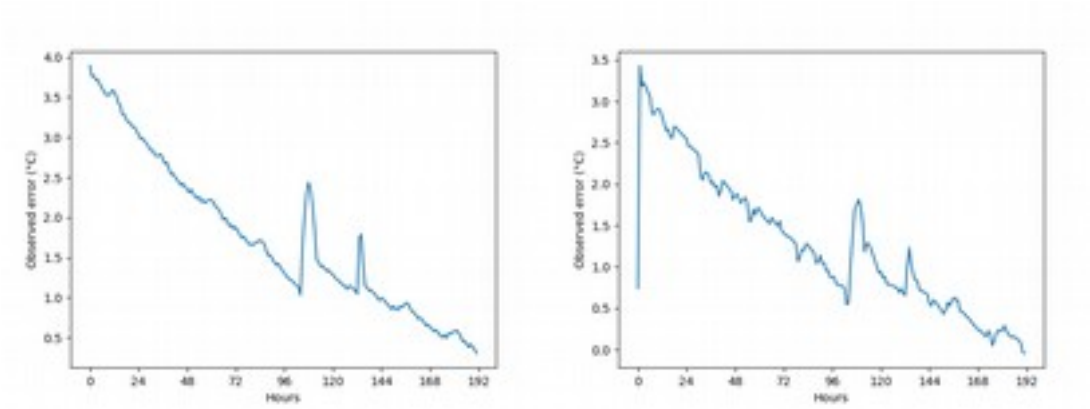

Figure 52 : Observed error on average wall temperature (left) and air temperature (right) during first week of the year, with room oriented south in Frankfurt with Double glazing unit

In order to clean the data and get rid of the outlier values, we chose to calculate the mean absolute error (MAE):

$$MAE = \frac{\sum_{1}^{n} \left| T_{i,Energyplus} - T_{i,Fener} \right|}{n} \quad (0)$$

The mean absolute error is 0.5°C. This error is reached during the sixth or seventh day in every simulation. Therefore, we will only keep the data from the eighth day and onward. We can notice that it has a significant impact on the root mean square error.

Metric	Root mean square error before correction (° C)	Root mean square error after correction (° C)
Air temperature	0.9	0.6
Walls average temperature	1.0	0.6
Window temperature	1.8	1.7

Table 16 : Impact of the exclusion of the seven first days from the dataset

All the temperatures had a root mean square error of approximate 1°C and went down to 0.6°C (Table 16). A notable exception is the window's temperature. The window's temperature error is unexpectedly high when compared to the air or other surfaces.

We identified that Energy plus and Fener do not consider the same surfaces when it comes to windows. Fener uses the Blackbox model which models the whole complex fenestration system as two layers. These two layers are virtual layers that were analytically deduced. In the case of Energy plus, the reported temperature corresponds to a weighted average between the glazing and the shading device, based on the openness of the shading device. In 4.5.1, we will see that this error is highly dependent on the relative shading device's position to the glazing.

4.4 Data analysis

From the retained data, we will calculate the accuracy of the different quantities and analyze whether it correlates with any of the room's characteristics (CFS, location and orientation). We will therefore analyze the three different temperatures (air, walls average and inner window surface). Moreover, we will see if the meteorological data have an impact on accuracy.

For the correlation purpose with the meteorological data, we will use two different metrics: Pearson correlation coefficient (ρ) [PEA1895] and Spearman's rank correlation coefficient (r) [SPEA1904]. They are defined as follow:

$$\rho_{x,y} = \frac{E\left(\left(X - E(X)\right) * \left(Y - E(Y)\right)\right)}{\sqrt{\left(E\left(X^2\right) - E^2(X)\right) * \left(E\left(Y^2\right) - E^2(Y)\right)}} \quad (0)$$

$$r_{x,y} = 1 - \frac{6\sum_{1}^{n} rank\ difference^2}{\sqrt{\left(E\left(X^2\right) - E^2(X)\right) * \left(E\left(Y^2\right) - E^2(Y)\right)}} \quad (0)$$

Pearson and spearman are usually to find correlation, although they differ on their meaning. Pearson benchmarks linear correlations between two variables, while spearman identifies monotonic relationships (monotonic functions are always increasing or decreasing functions).

Moreover, this coefficient will be coupled with a significance test by calculating the P-value. P-value is the probability of seeing a result at of such magnitude or larger even if the hypothesis was false. For statistical significance, p-value < 0.05 is considered sufficiently significant.

$$P = 1 - \frac{6\sum_{1}^{n} rank\ difference^2}{\sqrt{\left(E\left(X^2\right) - E^2(X)\right) * \left(E\left(Y^2\right) - E^2(Y)\right)}} \quad (0)$$

4.5 Temperature error analysis

4.5.1 Complex Fenestration System Impact

First comparison scenario is between air temperature calculated by the Blackbox model and ISO 15099 (Figure 53) for each Complex Fenestration System. The air temperature's accuracy is between 0.5°C and 0.6°C independently of the CFS used. The same conclusion can be made about the average temperature of walls whose root mean square error is also between 0.5°C and 0.6°C. The mean bias error show that the shades have in overall more bias than the systems without shadings or venetian blinds. Air temperature shows -0.4°C mean bias error with either internal or external shades, while external venetian blinds system have 0.1°C and the no shading device has -0.2°C. The

walls temperature shows a bias between -0.3°C for external shades and 0.2°C for external venetian blinds. Overall, the bias regarding the air and walls temperature is considered low independently of the CFS used, moreover the accuracy of air and walls temperature is considered sufficient for many usages. Its usage in thermal comfort is discussed later in 4.8.

As of the window's inner surface temperature, the conclusion is different. The system shows a very high dependence on the CFS used. It depends highly on the position of the shading device.

The cases where there is no shading device or an external device have an error between 0.8°C (no shading device) and 1.2°C (external shades). CFS with interior shades show an error as high as 2.8°C in the average case. As of the bias, it is significantly higher for the cases when used with external shades.

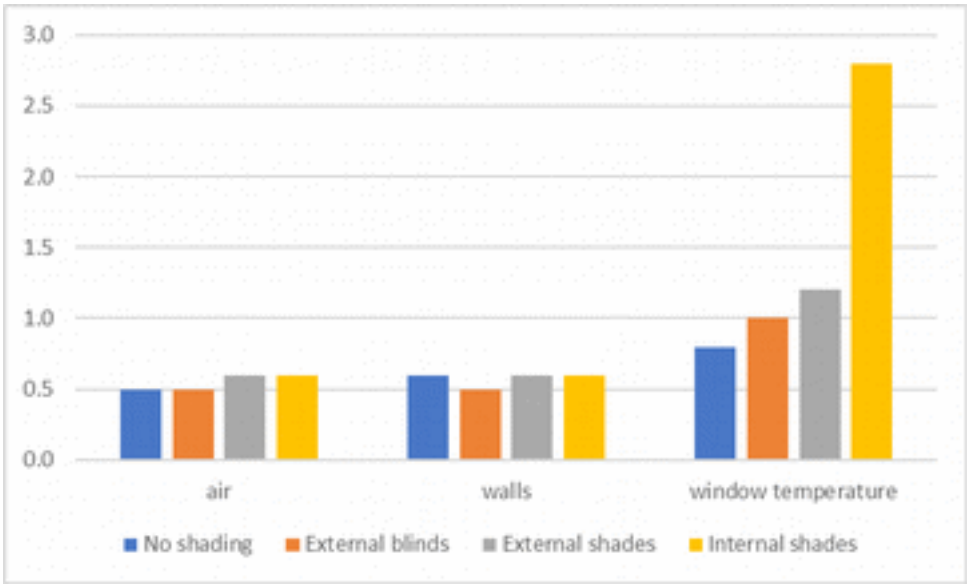

Figure 53 : Root mean square error of the temperature (°C) depending on the complex fenestration system used.

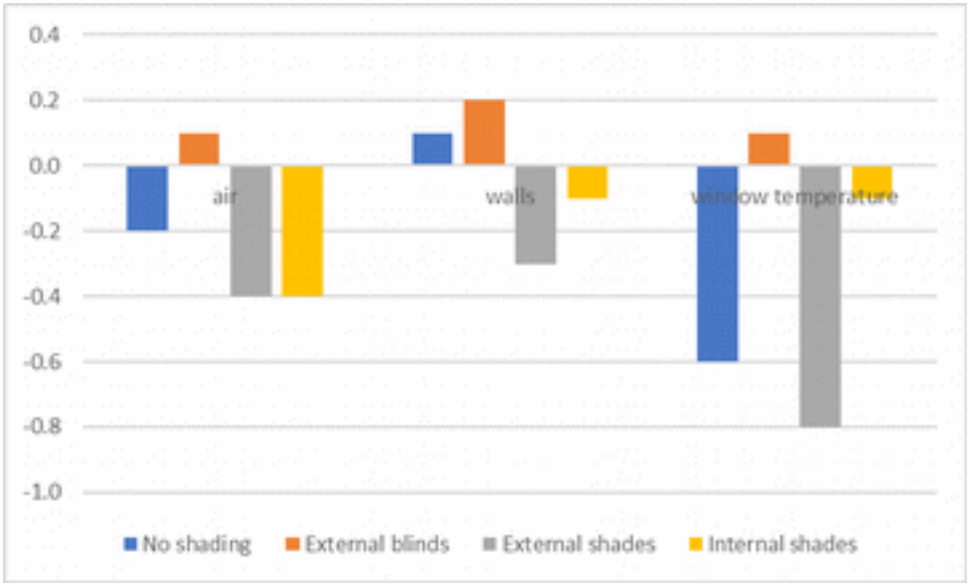

Figure 54 : Mean bias error of the temperature (°C) depending on the complex fenestration system used.

The high window's inner temperature uncertainty, when using an internal shading device, has been discussed in previous research [BUE2017]. The uncertainty is linked to the relatively high secondary heat gain coefficient when an internal shading device is used. The error is assumed to be due to two factors:

- The lower dependence on the boundary conditions of the black box model, compared to the ISO 15099.
- The usage of the default parameter κ with a value of 0.4. Further calibration may provide better accuracy of the model.

In any calculation involving the window's inner surface temperature, we will distinguish between the two following cases:

- External or no shading device.
- Internal shading device.

The air and wall temperatures' accuracy do not show a similar dependence on the position of the shading device.

4.5.2 Orientation impact

In this second case, we compare the 8 usual building orientations to estimate its impact on the accuracy of air, wall and the window's inner layer temperature as calculated with the Blackbox Model.

The air and walls temperature's uncertainty are independent of the orientation (Figure 55). The window's inner surface temperature, with an external or no shading device, slightly depends on the orientation, ranging from 0.8°C for North orientation to 1.1°C for orientation from East to South-West. When the Blackbox Model is used with an internal shading device, façades that are subject to a higher direct irradiance have a significantly worse accuracy. North orientation has an error of 1.5°C, while South-west orientation goes up to 3.5°C.

As of the model's bias, the air temperature's bias is low in low irradiation orientation, and has no bias in higher irradiation orientations (Figure 56). Walls's temperature bias depends on the orientation. It goes from -0.3°C North to 0.2°C South.

The inner surface of windows has a significantly more important bias. For CFS with external or no shading device, the bias is always negative, going from -0.3°C to -0.6°C North. Windows with internal shading device have a bias on the inner temperature surface that is negative in low irradiation surface, -0.5°C for North case, and positive in the high irradiation surface, 0.3°C for North case. Inner shading device's bias has therefore a significantly higher dependence on the irradiation received on the façade. In high irradiance scenarios, the Blackbox model tends to underestimate the layer's temperature.

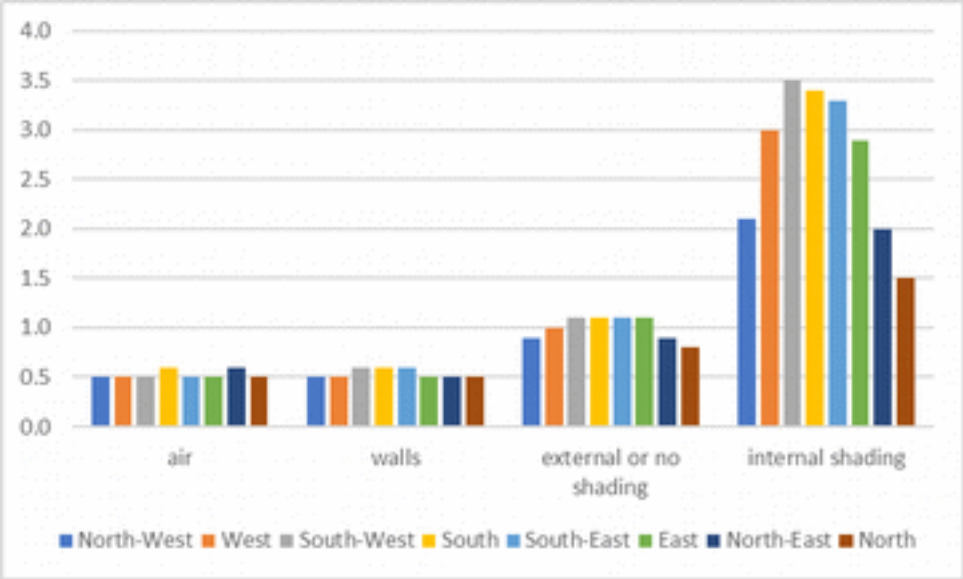

Figure 55 : Root mean square error of the temperature (°C) depending on the building orientation

Figure 56: Mean bias error of the temperature (°C) depending on the building orientation.

4.5.3 Climate impact

The third study focused on the impact of the location, and thus the climate, on the accuracy of the method. The simulations were performed for four different locations:

- Accra: Tropical wet and dry, the yearly average temperature is 28.4°C during office time, with a maximum of 47.6°C and a minimum of 18°C.
- Alicante: Mediterranean climate, the yearly average temperature is 20.1°C during office time, with a maximum of 35.6°C and a minimum of 3.3°C.
- Frankfurt: Marine west coast, the yearly average temperature is 12.3°C during office time, with a maximum of 34.1°C and a minimum of -9.9°C.
- Houlton: Humid continental, the yearly average temperature is 7.7°C during office time, with a maximum of 32.8°C and a minimum of -24.7°C.

In this comparison, we notice a similar pattern to the previous ones. Air temperature and walls temperature accuracy do not vary much depending on the location and climate (between 0.5°C and 0.6°C). For window's inner surface temperature, the case with internal shading device shows a better accuracy in the case of Houlton, which has the coldest climate. The hotter the location the worse is the accuracy.

As of the mean bias, the blackbox model consistently underestimates the temperature in the hotter climates. This effect is most pronounced in the case where we have an external or no shading device. In Frankfurt and Houlton, the bias is -0.3°C, while in

Alicante is -0.5°C and in Accra -0.6°C. The model tends to underestimate the temperature in hotter locations

The worse accuracy and negative bias noticed in this comparison agree with the previous result, where higher irradiation causes the same effect.

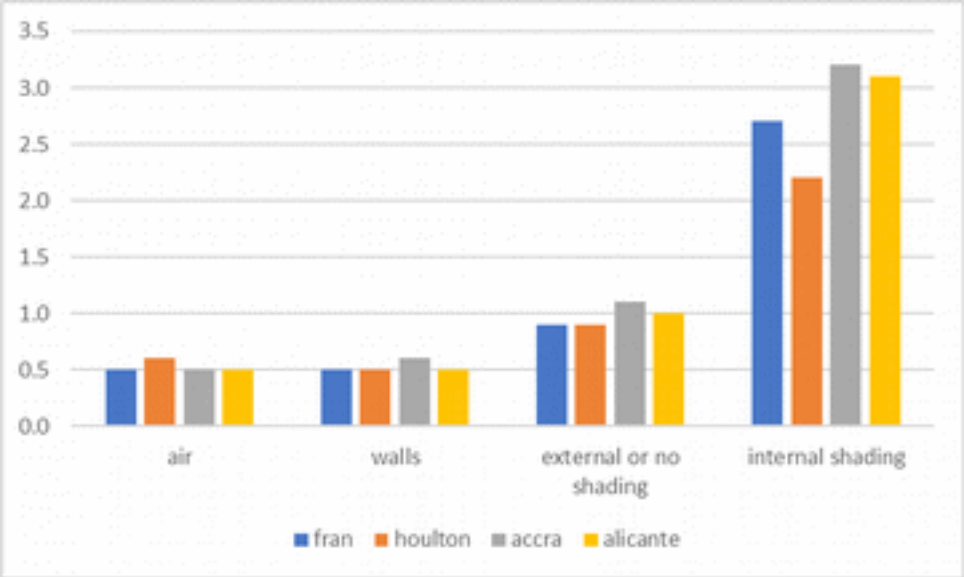

Figure 57 : Root mean square error of the temperature (°C) depending on the location.

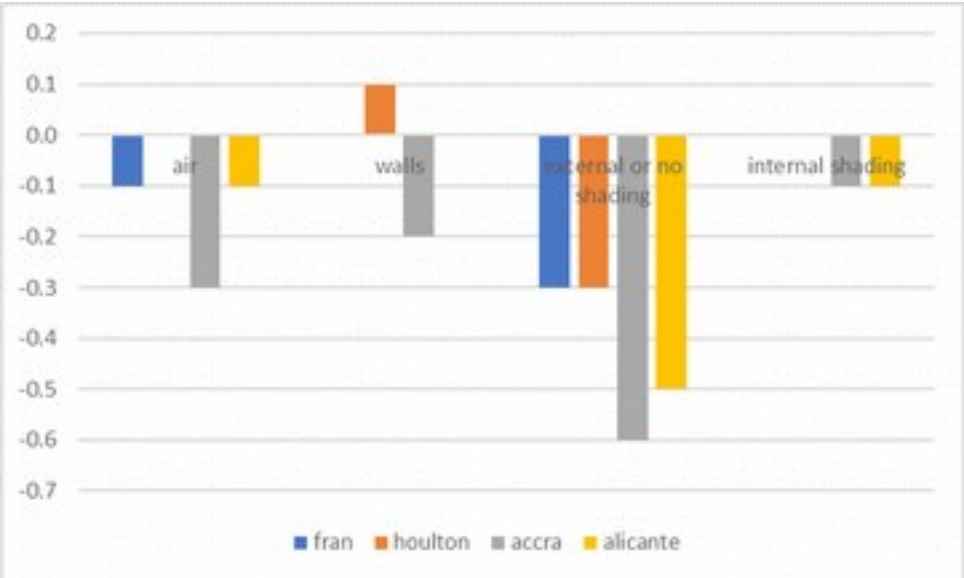

Figure 58 : Mean bias error of the temperature (°C) depending on the location.

To further analyze the impact of the climate on the model's accuracy, we chose to study the correlation between the accuracy of the model, and the available meteorological data.

The meteorological data studied is direct normal irradiance, diffuse horizontal irradiance and outdoor air temperature. Our analysis show that albeit the inner temperature accuracy has a low degree of correlation (<=0.3) with meteorological, data, the low degree of correlation is consistent in the case of direct normal irradiance. The accuracy indices are positive, which confirms the precedent findings. The hotter locations, have a higher rmse, due to a higher normal irradiance.

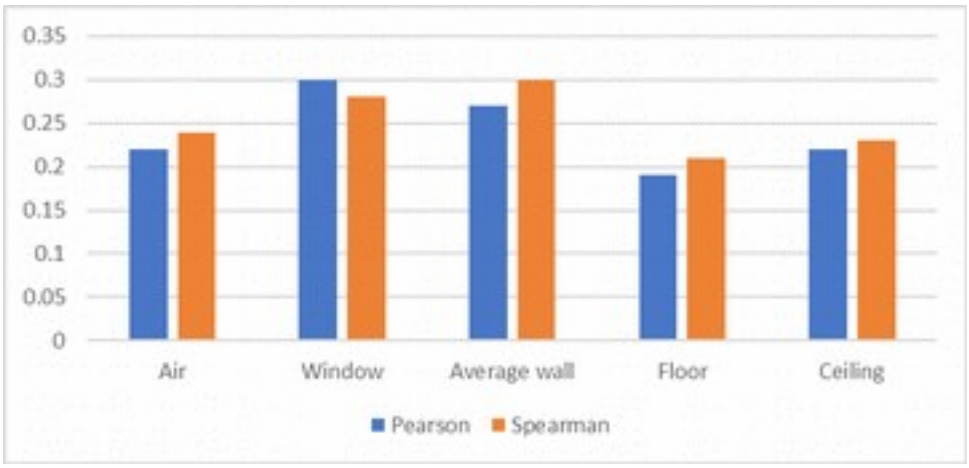

Figure 59 : Correlation between direct normal irradiance and inner temperature accuracy

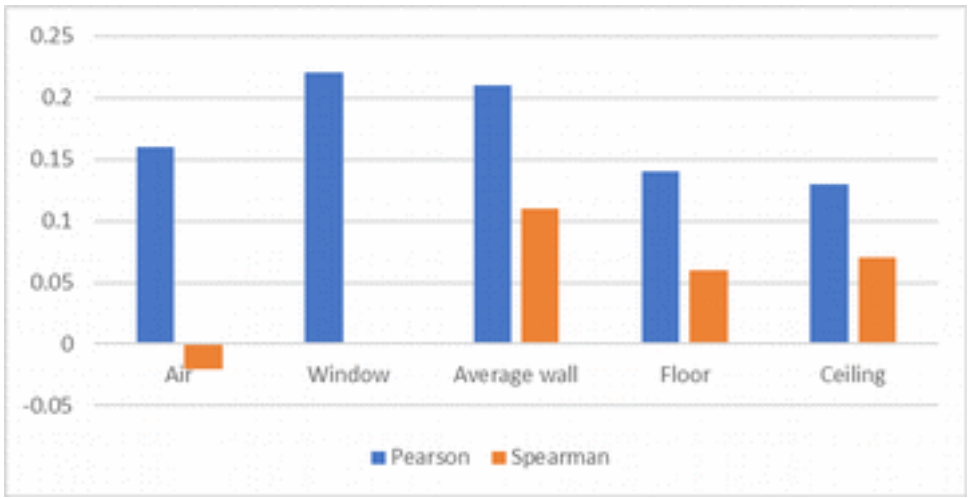

Figure 60: Correlation between direct horizontal irradiance and inner temperature accuracy

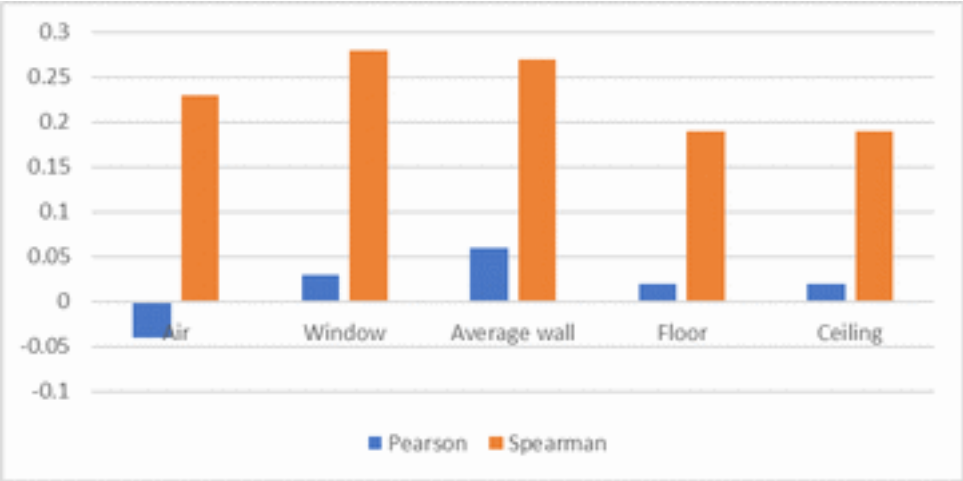

Figure 61 : Correlation between outdoor air temperature and inner temperature accuracy

4.6 Kappa's impact

Across all our studies, we noted that the inner's window temperature has a worse accuracy in the case of the usage of inner shading device. One of the possible suggested factors was the usage of kappa (c.f. 4.1). The coefficient κ is a value between 0 and 1 that represents the fraction of the outward going energy that is reflected by the shading device and absorbed by the glazing unit. In this study we will evaluate the impact of the usage of different values of this coefficient on the window's inner temperature accuracy.

Our findings (Figure 62) show that kappa has a major impact on the accuracy and bias of the method. The accuracy goes from 3.9°C to 2.8°C, and the bias goes from -1°C to 0°C. In the other side, the optimal values are achieved at kappa=1, which doesn't correspond to the physical reality of the system, as normal glazing units can't absorb the totality of the outward flowing energy.

Other paths should therefore be investigated to improve the blackbox, as the calculation of the inner's layer absorbance from measurements, or to better take in consideration the boundary conditions as in ISO 15099.

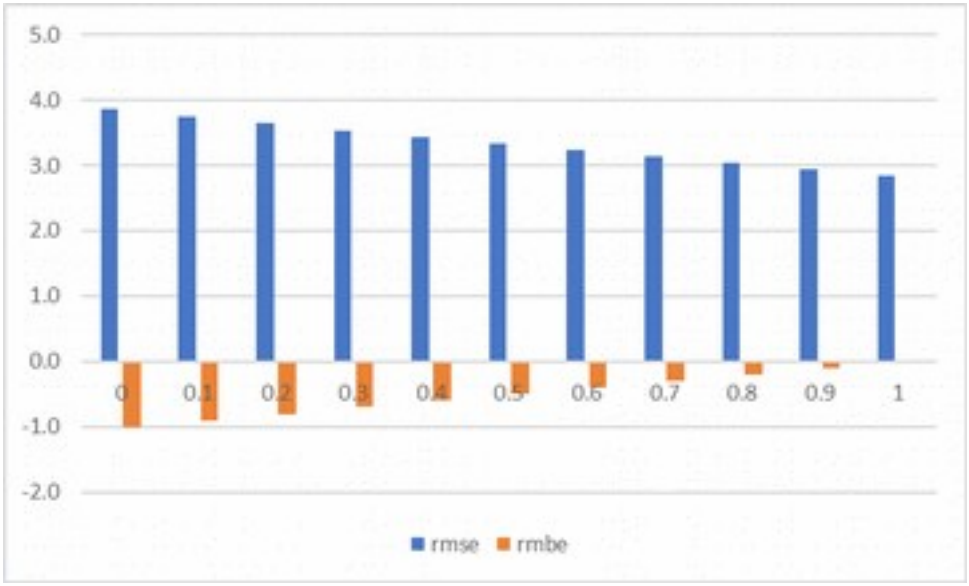

Figure 62: Variation of the rmse and rmbe of the temperature of the inner surface of the window in the case of inner shading device.

4.7 Sensitivity analysis

Our study relied on simulations where we compare results of the exact CFS in two different models. In practice, measured data of the CFS will have some random errors. In literature, the U-value has a usual accuracy of +- 0.3 $Wm^{-2}K^{-1}$ and the g-value an accuracy of +- 0.3 $Wm^{-2}K^{-1}$. We therefore conducted a sensitivity analysis to evaluate the possible impact of measurement errors on the calculated air, walls and window temperatures.

Our findings show a linear relation (Figure 63 and Figure 64) between the error temperature uncertainty and the g-value uncertainty. This has been true for the two cases: CFS with internal shading device and CFS with external or no shading device.

With an internal shading device, an error of 0.1 in the g-value has a noticeable impact of 1°C on the calculated window temperature, 0.6°C on the walls and 0.5°C on the air. The impact of an error of 0.03 that usually correspond to the measurements is 0.3°C on the window, 0.2°C for the walls and the air, which can be neglected for most use cases. With an external or no shading device, the results are very similar.

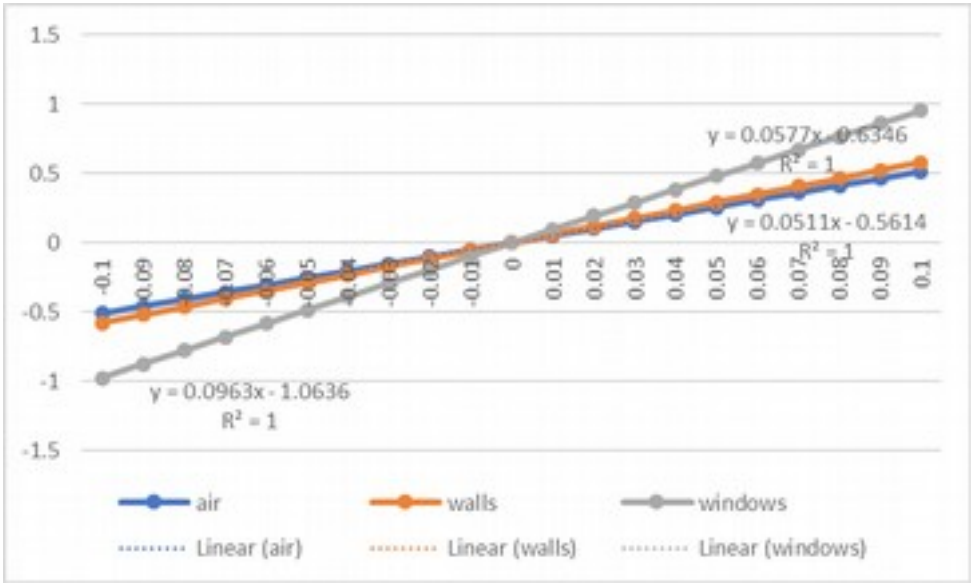

Figure 63: Relation between the error on temperature (°C) and the error on g-value with an internal shading device.

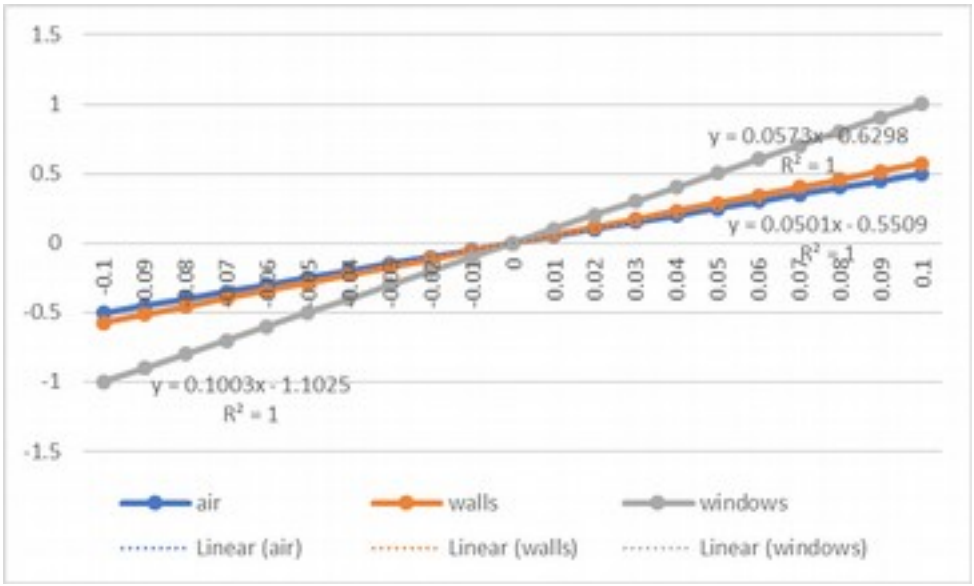

Figure 64: Relation between the error on temperature (°C) and the error on g-value with an external or no shading device.

As of the error on the U-value, the same pattern as the error on the g-value has been found (Figure 65 and Figure 66). The error on temperature is different in its magnitude and less impactful overall. The error on air temperature and wall stays inferior to 0.1°C, while the error on the window's temperature goes up to 0.1°C.

For most use cases, measurement errors on U-value shouldn't impact the final result, while the error on g-value can be more noticeable.

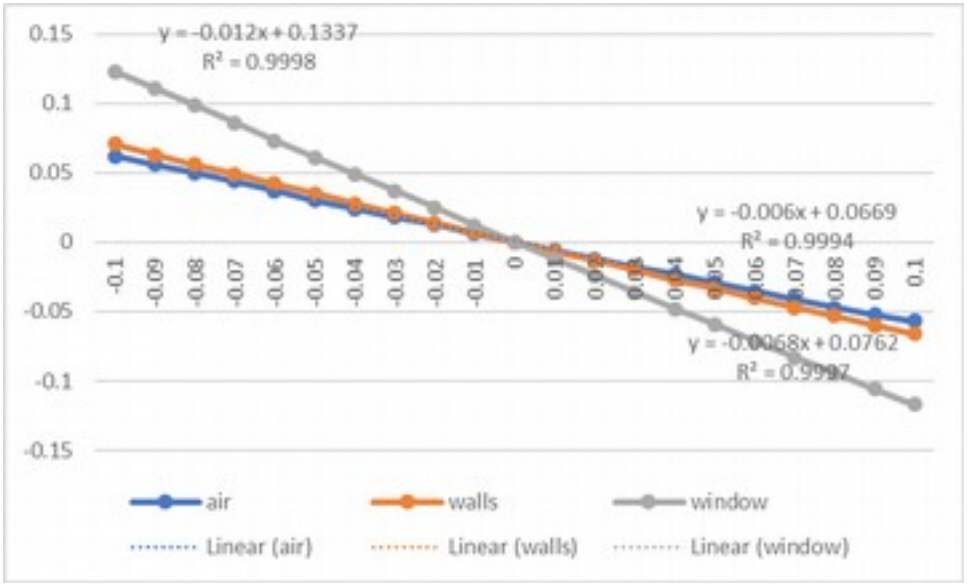

Figure 65: Relation between the error on temperature (°C) and the error on U-value with an internal shading device.

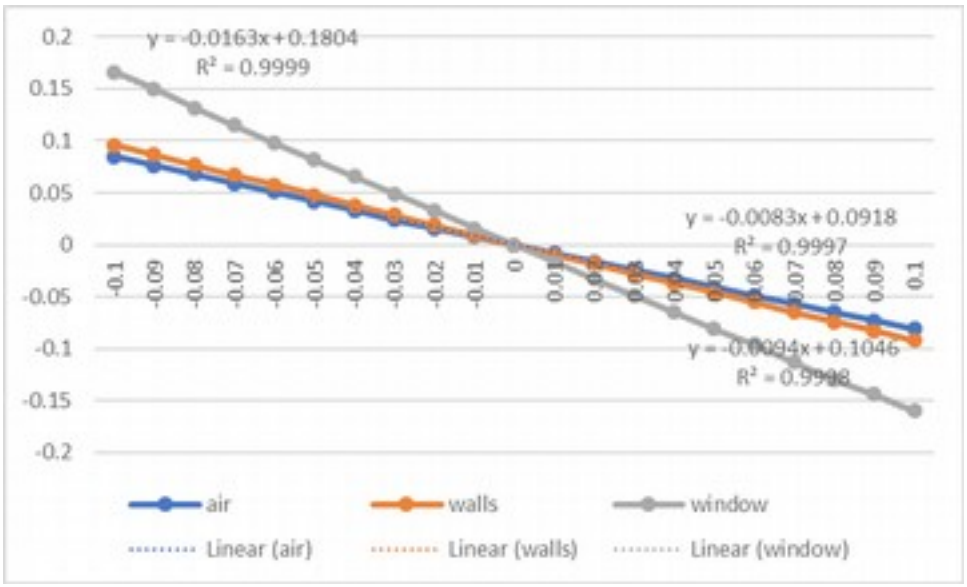

Figure 66: Relation between the error on temperature (°C) and the error on U-value with an external or no shading device.

4.8 Thermal comfort

The adaptive model, as prescribed by ASHRAE, is based on the operative temperature and a range value based on the mean outdoor temperature. It prescribes fundamentally

two ranges, a range for 80% acceptability (most commonly used in practice) and 90% acceptability. These ranges are defined as follow:

$$T_{max,90\%} = 0.31 * T_{outdm} + 20.3 \quad (0)$$

$$T_{min,90\%} = 0.31 * T_{outdm} + 15.3 \quad (0)$$

$$T_{max,80\%} = 0.31 * T_{outdm} + 21.3 \quad (0)$$

$$T_{min,80\%} = 0.31 * T_{outdm} + 14.3 \quad (0)$$

The mean outdoor temperature is a weighted average of the outdoor temperature between the 7 to 30 precedent days. In our research we used data over 7 days with the following formula:

$$T_{outdm} = (1-0.7) * [t_{d-1} + 0.7 * t_{d-2} + 0.7^2 ¿ t_{d-3} + \ldots + 7^6 * t_{d-7}] \quad \textbf{(0)}$$

To ensure that the Blackbox's model is sufficiently accurate for such operations, which is expected from the precedent results, we will conduct a binary classification test

In our case, we consider a single occupant in a room without ventilation. The operative temperature can be approximated as follow [DOE2018]:

$$t_0 = \frac{mean\,radiant\,temperature + air\,dry\,bulb\,temperature}{2} \quad \textbf{(0)}$$

The mean radiant temperature for an occupant in the geometrical center of the room can be approximated as follow [DOE2018]:

$$MRT = \frac{average(surfaces\,temperature) + floor\,temperature}{2} \quad \textbf{(0)}$$

Energy plus can calculate automatically the operative and mean radiant temperature, although these results aren't usable in the case of interior shading device. Therefore, we will exclude interior shading from the accuracy assessment of thermal comfort. Simulations only cover the working hours, from 8:00 to 18:00.

90% acceptability	**Positive**	**Negative**	**Overall**
True	96%	>99%	>99%
False	<1%	4%	<1%
80% acceptability	**Positive**	**Negative**	**Overall**
True	94%	>99%	99%
False	<1%	6%	1%

Table 17: Binary classification of thermal comfort assessment with blackbox model for double glazing units without shading or with external shading

The thermal comfort assessment compared to Energy plus shows an overall accuracy of 99% or more for both the 90% and 80% acceptability range. Its false positive rate is very low, while its false Negative is higher (4% for 90% acceptability, 6% for 80% acceptability), it is still not significant.

As of the case with internal blinds/shadings, it is important to assess first the impact of the window's surface error on the operative temperature. We can write the root mean square error of the operative temperature can be written as follows (assuming 4 walls and one window):

$$Rms\,e_{optemp} = \sqrt{\frac{\sum Rms\,e^{2}_{surface}}{28^{2}} + \frac{Rms\,e^{2}_{ground}}{4^{2}} + \frac{Rms\,e_{air}}{2^{2}}} \qquad (0)$$

Discarding the error related to the air, the walls, the ground and ceiling, it can be simplified to:

$$Rms\,e_{optemp} = \frac{Rms\,e_{window}}{28} \qquad (0)$$

In our study, we established a 2.8 K error on window's surface temperature, which translates to 0.1 K error on operative temperature. The final error induced by the blackbox model in this case is therefore not significant. We also made a binary classification test for this case (Table 18), which didn't show much divergence from the other cases.

90% acceptability	**Positive**	**Negative**	**Overall**
True	96%	>99%	>99%
False	<1%	4%	<1%
80% acceptability	**Positive**	**Negative**	**Overall**
True	95%	>99%	99%
False	<1%	5%	1%

Table 18 : Binary classification of thermal comfort assessment with blackbox model for double glazing units with internal shading

4.9 Summary

In our research, we chose the blackbox Model as a BIM compatible model for the thermal characterization of the complex fenestration system. This model has been chosen as it theoretically can cover a large set of CFS, derivable from measured data while being BIM compatible.

In order to validate this choice, we studied the accuracy of the model on the basis of a comparison with Energy plus. We use an hour by hour simulation over a year in 128 different cases with different orientations, locations and fenestration systems in order to minimize the bias related to the testing system.

We concluded that the uncertainty of the calculated temperature of the air and walls is usually inferior to 0.6°C. As of the accuracy of the temperature of the inner layer of the CFS, we distinguish between two cases: If an internal shading device is used, the uncertainty is approximately of 3°C, otherwise, it is estimated to be around 1°C. This may or may not be acceptable depending of the application.

One of the possible applications studied is the thermal comfort of the occupant. The blackbox model has been to achieve an accuracy of 99% over the tested data-set, which leads us to believe that it is perfectly suitable for thermal comfort assessment, within the constraint and limitations of the adaptive model of ASHRAE 55. Future research may choose to focus on studying its accuracy for Fanger's PMV/PPD model, although some of its parameters are still not possible to fully integrate within the current IFC limitations.

In the case of internal shading devices, the difference in the inner layer temperature proved to be significant but didn't have much impact on the thermal comfort aspect, nor on the temperature of the air or the other walls.

From our comparison, we can conclude that the blackbox model can be used instead of the ISO 15099 when the latter is applicable. Although it should be noted that ISO 15099 itself has some limitations, that do not theoretically impede the blackbox model, for CFS with three-dimensional structures or air permeable layers.

5 EXAMPLE OF APPLICATIONS

The workflow developed in this thesis aims to answer practical questions concerning the energy efficiency of modern buildings. In this chapter, we will provide some examples of questions, usually met in the design phase, that our workflow helps to answer.

5.1 CFS decision based on its optical performance

One of the most important questions of the design phase in the ability to provide daylighting without glare. Most people prefer natural sun light to artificial lightning. To maximize the number of hours of comfortable natural lighting, solar control device as venetian blinds are traditionally used. The problem that then arise is how to reach the global optimum. The number of hours with natural light has to be maximized, while the incoming luminance should be reduced to avoid glare.

Such analysis is usually done at room levels, where the architects can try to find the best shading device for the fenestration system. With the new BIM methods, and the recently developed databases of complex fenestration systems as Complex Glazing Database [CGD2018], it is possible to compare, automatically, multiple CFS.

In our example, we consider a 4 m x 5 m x 3 m room with 50% glazing ratio (Figure 67). The user is in the center of the room. Multiple shading device have been considered in this comparison:

- Double glazing unit without shading
- Double glazing unit with external venetian blinds tilted at 45°

- Double glazing unit with external shades
- Double glazing unit with external venetian blinds tilted at 20°

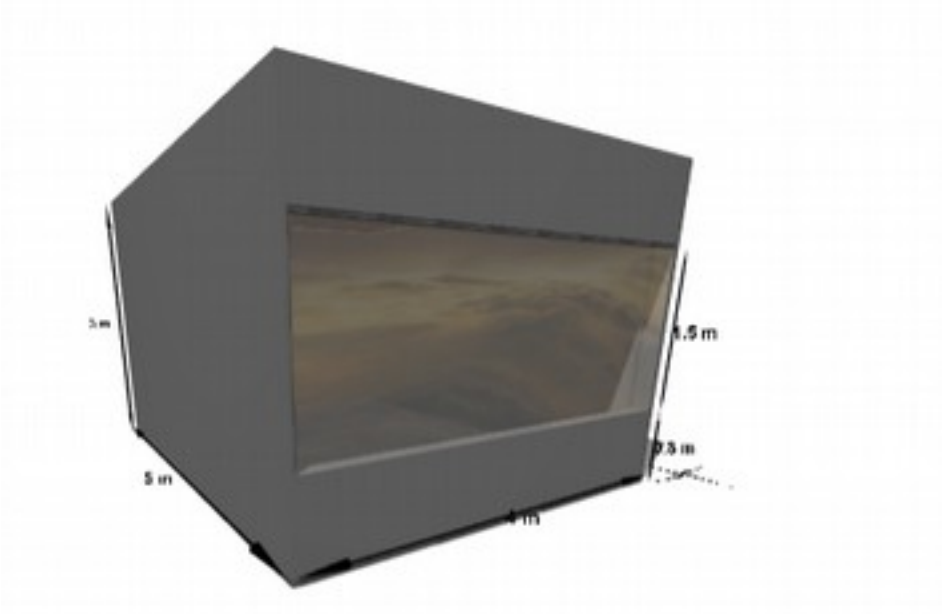

Figure 67: model of the virtual room

The simulation has been done yearly, in hour by hour steps, from 8h to 18h each day in Malaga. We calculated, in each timestep, both horizontal luminance for daylight autonomy, and DGP. DGP is usually read within the 4 following categories depending on its value:

- Imperceptible glare (DGP<0.35)
- Perceptible glare (0.4>DGP>=0.35)
- Disturbing glare (0.45>DGP>=0.4)
- Intolerable glare (DGP>=0.45)

Our results (Figure 68) show that using double glazing unit without any shading device gives the highest daylight autonomy at the cost of higher glare. At the other hand of the spectrum, venetian blinds with a tilt angle at 45° did eliminate every glare source, at the cost of a much lower daylight autonomy. The shades and the venetian blinds tilted at 20° offered the best compromise between glare protection and daylight autonomy.

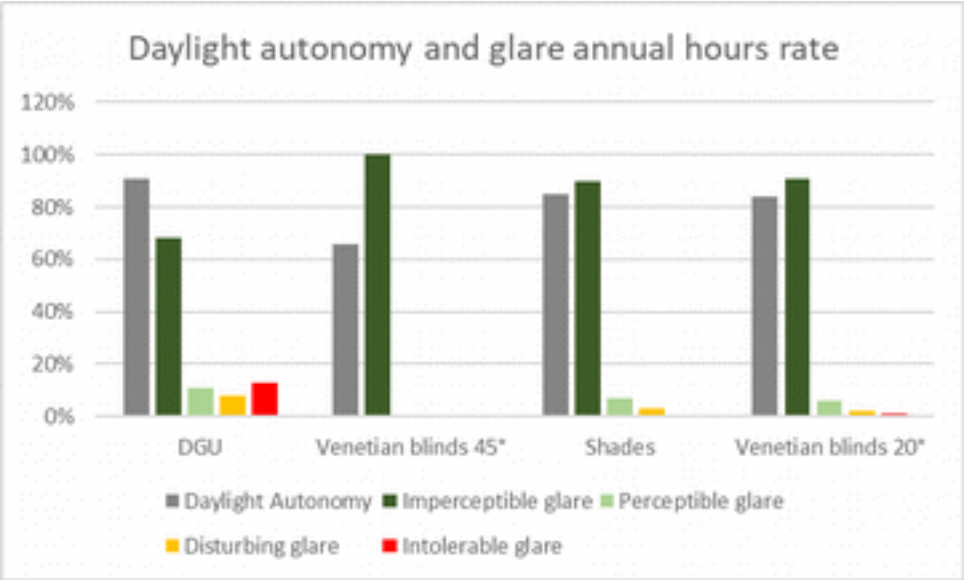

Figure 68: Comparison of daylight autonomy and glare perception between the CFS.

5.2 Building orientation decision based thermal comfort

Another optimization parameter is the building orientation. Depending on the location, some buildings may suffer from a too warm or too cold weather. Such buildings can see their thermal performance improved by opting for a different building orientation.

In this example, we will compare different building orientations in order to achieve the highest possible number of hours of thermal comfort. The CFS used is a double-glazing unit with external venetian blinds tilted at 55°. The building is located in Lyon.

Our results (Figure 69) show that there is a great discrepancy on the percentage of annual comfortable hours depending on the building orientation. North-oriented façade seem to offer the highest rate of comfortable hours (19% to 20%). We can deduce that these comfortable hours gain are mainly in summer where overheating is avoided, thanks to the lesser irradiance in the northern side of the building.

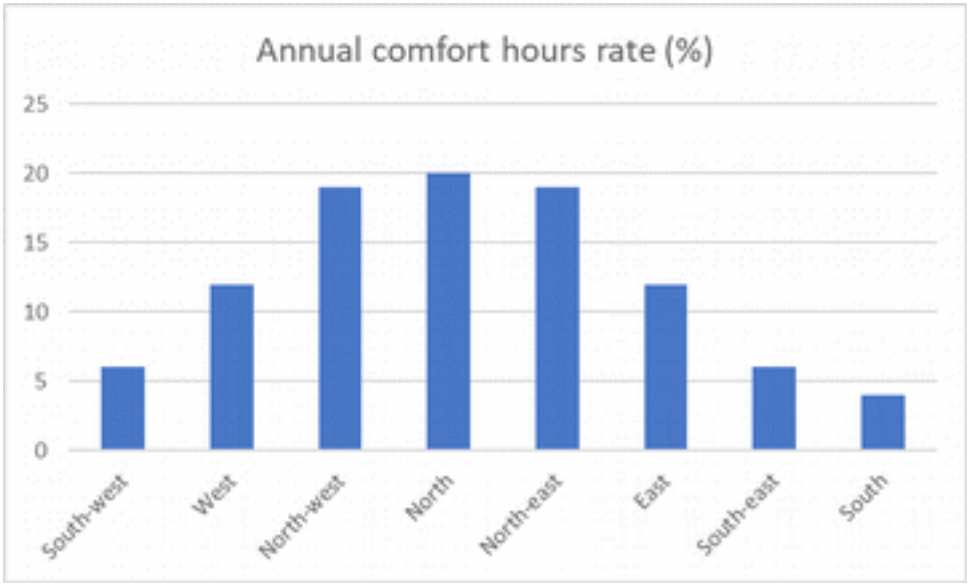

Figure 69: Percentage of thermally comfortable hours between 8h and 18h yearly

5.3 Building Integrated Photovoltaic analysis

While this thesis focuses on complex fenestration systems with passive technologies, the designed methodology was general to be extended to other work domains. The resulting IFC2RAD program has been successfully used in the evaluation of multiple real-world scenarios. In this section, we will present an extension of our work that was possible through a collaboration with the BIPV department of Fraunhofer ISE. We were able to use our methodology to process IFC file designed by architects to generate a geometry and material representation of the building and associate it afterwards with an internally developed engine that models each solar cell as a two-diode system [EIS2018]. This workflow has been successfully applied on three different buildings, but for confidentiality reasons and to preserve industrial secrets, only one building will be presented in this dissertation.

The afore mentioned building is a 4-level building in Freiburg, Germany. Its façade is oriented south-west. The input data was an IFC file with the material and geometry description of the building and its surrounding. The data relative to the PV cells was available independently of the file.

The goal is to evaluate the irradiance at each cell. To do so some modification was necessary for the IFC. First, we had to correct the transparent material of the surrounding (Figure 70). We applied a Lambertian surface to them with 20% reflectance.

Moreover, we filtered out through IFC2RAD the trees that were present in the model, as they don't exist in reality and were only put for aesthetical reasons. To do this filtering, we identified the "Globally Unique Identifier" of each tree in an IFC viewer software, IFCQuery, and supplied this Identifiers to IFC2rad.

The last step was to regenerate a second radiance file where all elements have been filtered out with IFC2RAD except the photovoltaics module. The goal was to generate a sensor automatically of each module. This filtering was done by identifying the material used by the modules. This material was unique to them. All and only the modules have this material, which made this filtering easily possible.

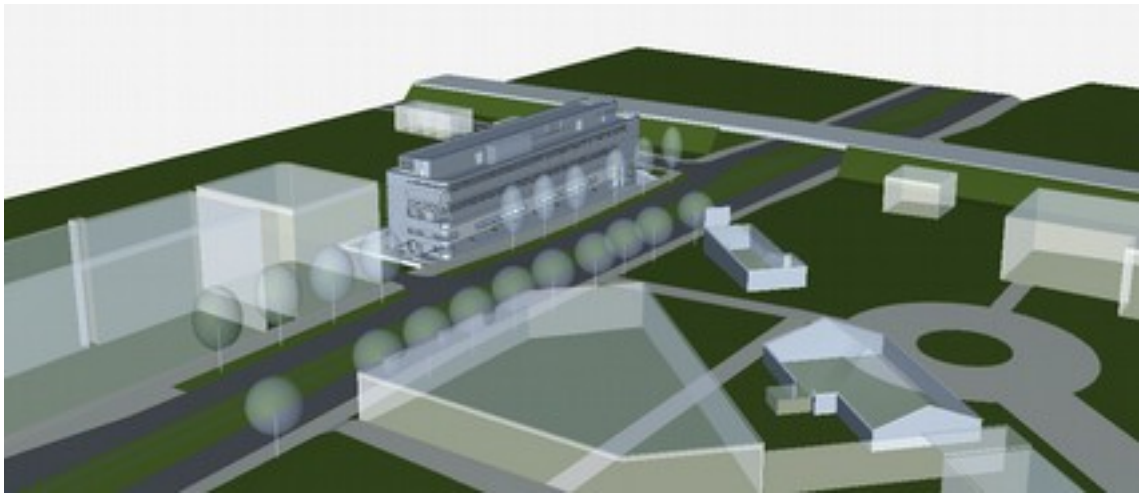

Figure 70: Building and surrounding representation in the IFC file.

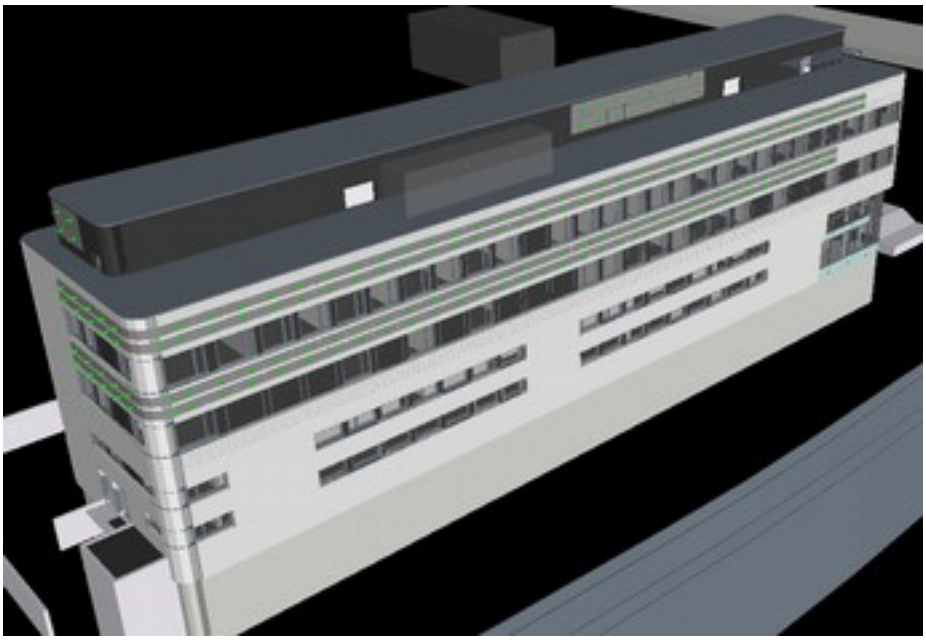

Figure 71: Building and surrounding model in radiance. In green are the sensor points position and direction visualized.

When the radiance and sensor files have been generated (Figure 71), it was possible to analyze the irradiance of each module. The south-east façade modules all receive the same irradiance, between 850 and 950 kWh/m²/a. The exception is on the roof, where a technical box on the south-west of the modules shades partially the modules. The south-west façade, which is very close to the neighboring building, suffers from the shading, which leads to a significant disparity between the irradiance received by the modules depending on their position. North-west façade receives much lower irradiance than the other facades, at approximately 400kwh/m²/a.

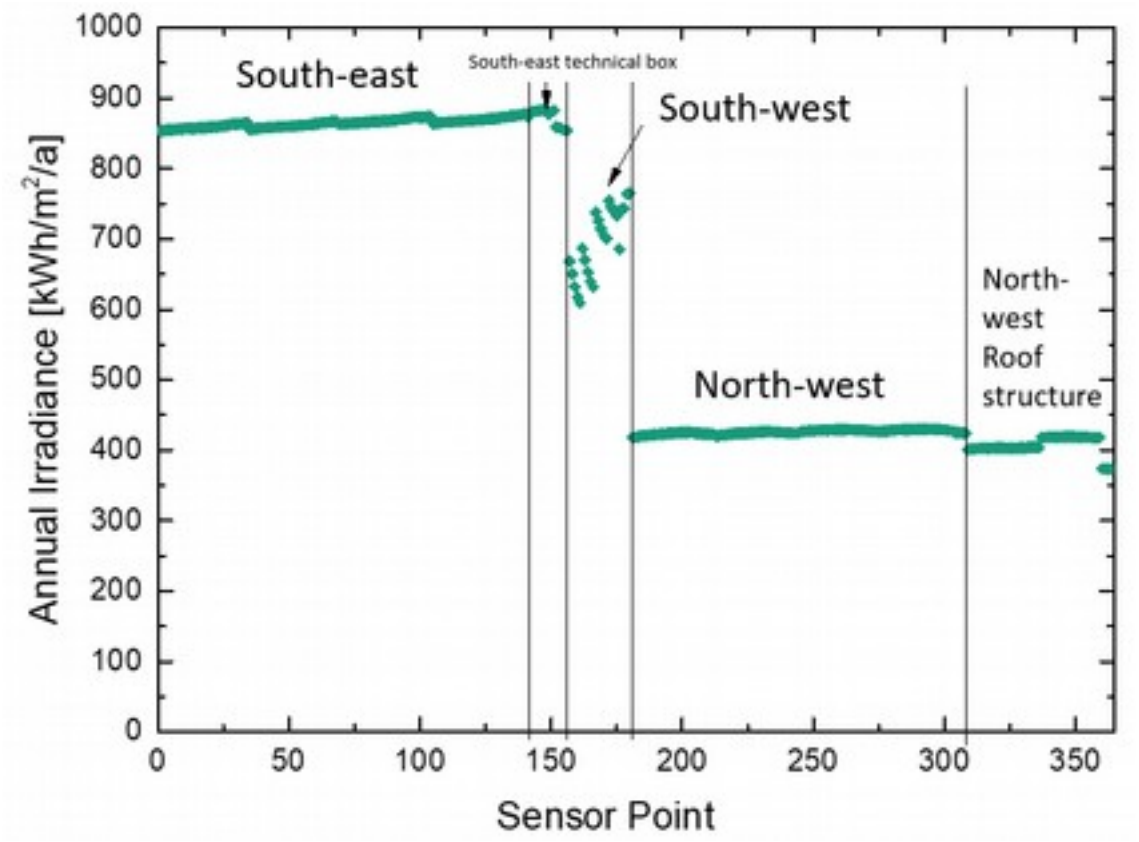

Figure 72: Annual irradiance calculated at each sensor point.

From the irradiance calculation, the annual yield it was possible to calculate the annual yield of the modules (Table 19). The modules were divided into 12 subsystems, with 18 modules in each subsystem (Figure 73). The reported number are only approximate of the reality for confidentiality matters. The modules in the South-East façade yield 25000 kWh considering the 8 modules on the façade. The module on the roof facing South-East yields 2500 kWh. The north-east façade yields considerably less, between 800 and 1100 kWh.

Sub-system	Annual Yield [kWh]
1-8 (total)	25000
9	2500
10	1000
11	800
12	1100

Table 19: Annual yield of the subsystems.

Figure 73 : Sub-systems positions.

This analysis step is often performed in the design phase by architects. It is meant to ensure the cost-efficiency of the modules, in addition to optimize their performance. Such analysis is often very time consuming, and thus expensive. The usage of IFC files here enabled substantial time-savings, as recreating the geometry of the building and neighboring environment, and identifying the relative position of the modules, has been done automatically. Overall, we think that such workflow offers not only a huge opportunity for time and cost saving, but also a reduction of errors that may be induced by human mistakes.

CONCLUSION

The design of the building has become increasingly more complex as the standards for better energy efficiency became stricter. More and more optimization goes towards each individual building element to see how it interacts with the whole. In our research we focused on a single component, the fenestration system.

Modern fenestration system with passive technologies aim to offer better energetical regulation. They use different shading and solar control technologies in order to optimize the incoming energy flux. These systems, called Complex Fenestration Systems, deal with many different parameters, as daylighting, visual comfort, thermal performance and thermal comfort.

The performance of the CFS is therefore the result of a complex interaction between the fenestration system, the building and the environment. To evaluate the result of these interactions, specialized tools have to be used. Problems arise as these tools multiple data from multiple sources that use different tooling. In a real-world project, nobody possesses all the data centralized in one format about the building. Therefore, any specialist of building performance needs to first gather data, and second to remodel it in the right format for its tools. This step is very time consuming and error prone. It has proven to be a major challenge in designing high performance buildings.

To face the complexity of building the design, Building Information Modelling has been developed as a mean to represent and share models within the architecture, engineering and construction industry. These new, rich and smart models provide an opportunity for cost and time savings, and robustness against human errors. These models unfortunately still suffer from their relative youngness.

Building Information Modelling have several limitations. Ranging from lacking support of important data to geometrical errors in the building's model. In this context of the current limitations of BIM, the choice of a correct representation of the thermal and optical representation of the window is crucial. We identified the B-directional Scattering Distribution Function as BIM compatible to model the optical behavior,

along with the Blackbox model to model the thermal aspect. In this thesis we focused therefore on five axes:

- BIM analysis to identify the necessary criteria for BIM compatible methodologies
- Choosing from literature BIM compatible methodologies
- Integrating BIM with these models in a simulation software
- Validation of the optical proposed workflow
- Validation of the thermal proposed workflow

To integrate BIM with optical or thermal simulation software, the presented work presented a set of geometrical algorithms and IFC data processing methodologies that allow a fully automated simulation. The methodology processes the geometry to make it simulation software compatible. It also links it with the thermal and optical information contained in IFC. This methodology has proven in real world application to offer huge time saving opportunity.

While during the study these methodologies have been successfully tested on non-complex geometries, BIM authoring software (software used to generate BIM models) still do not handle IFC correctly. Consequently, they produce geometrical errors during the export phase that may hinder the possibility of a fully automated simulation. Future work will focus on correcting such errors that can be met in IFC files.

Moreover, we studied the possibility of using BSDF based methodologies for automated simulations and estimation of daylight autonomy and glare from BIM. This research focused on comparing BSDF methodologies with experimental data.

For the validation of the daylight autonomy and horizontal luminance calculation, the study showed that BSDF based methods have a dependence on the resolution of the BSDF. The three-phase method that uses the traditional 145x145 patch has a significant worse accuracy to predict horizontal luminance than the higher resolution tensor-tree. On the other side, the error on the horizontal luminance calculation didn’t have any noticeable impact on the daylight autonomy metric. It leads us to believe that despite its accuracy limitation, it still performs correctly to asses this metric.

methods showed a much better accuracy and agreement with experimental data. The effect of the discretization of the sky has been studied and has been demonstrated to not have any significant effect on the results. Another raised concern was the accuracy/calculation speed trade-off.

Matrix based methods excel when there is a high number of time-steps, which is their raison d'être. In the case of the 5-phase method, it also offers a good accuracy for most workflows. On the other hand, a low time steps count favors the usage of Enhanced simplified DGP without matrix usage. The calculation time is highly dependent on the computer characteristics. The authors are convinced that in an automated simulations contest, the best practice would be to run a script that benchmarks the machine's calculation time for each metric and methodology. For the subsequent tests, the user should input manually the time constraints and the desired accuracy, let the program automatically choose the best methodology for his case based on the machine's performance.

A last question raised was how generally applicable these findings are given the wide range of CFS products. Some geometrical parameters of the CFS have been varied in order to give a better overview of the limitation of these results. Scale parameter had no impact on the results. The peak angle amplitude and maximum direct-direct transmittance had a significant impact on the studied accuracy in extreme cases. These extreme cases are on the other hand very theoretical and aren't widespread among CFS products. Most venetian blinds for example do not have such extreme characteristics and can be modeled therefore with BSDF data.

Another possible research path to be investigated would be data quality. For our simulations, we relied on BSDF calculated from geometry. In a scenario without geometry that we advocate, BSDF should ideally be measured. However, it is still unknown what the BSDF resolution should be, and measurements accuracy's constraints.

The third axis of this thesis resolves around about the validation of the proposed thermal workflow based on the Blackbox model. Air and walls temperature showed an agreement with the current reference ISO 15099 in a 0.6°C range. The inner layer of the fenestration system showed a dependence on the position of the shading device. Fenestration system with inner shading, and thus with a high secondary heat gain coefficient, showed a large error of 2.8°C, while the other systems had an error of 1°C.

While this error is significant for inner shading devices, it didn't prove to have any noticeable effect on the rest of the studied temperatures (air and walls). Moreover, for thermal comfort aspects, it didn't alter the results. Whether the shading device was internal, external or omitted, the methodology showed a good agreement with the ISO 15099.

The study also focused on the correlation aspect with multiple environment factors, as incoming irradiation, external air temperature, building orientation. All these factors correlated very poorly with our results. Leading us to think that the agreement we have with ISO 15099 is general enough.

Overall, this research has led to a workflow that can evaluate the thermal and optical performance of CFS. It has moreover been successfully extended to other foreign technologies as building integrated photovoltaics. We believe that such a methodology is not limited to complex fenestration systems only but can be extended to other domains.

Perspectives and future work

While during the study the proposed methodologies have been successfully tested on non-complex geometries, BIM authoring software (software used to generate BIM models) still do not handle IFC correctly. Consequently, they produce geometrical errors during the export phase that may hinder the possibility of a fully automated simulation. Future work will focus on correcting such errors that can be met in IFC files.

Some research paths were unfortunately not investigated during this thesis. For the optical methodologies, the usage of the daylight coefficient method has not been assessed. This methodology if used with a tensor-tree may have better calculation time and accuracy than the five-phase method. Another possibility is the usage of a high-resolution matrix BSDF which would, theoretically, offer a very noticeable calculation speed improvement over the five-phase method, and better accuracy than the three-phase method.

For the thermal side, an admitted limitation of this study is that we do not go beyond the domain of applicability of the ISO 15099. The promise of the Blackbox model to be able to handle even innovative products with minimal assumptions has therefore not been itself validated.

In our research, we mainly represented our systems considering a steady-state regime. Transitional Flow Regime has to be further studied, to see if there any limitation regarding its BIM compatibility.

The CFS performance is evaluated at the room level. The rooms are always assumed adiabatic and opaque, with the exception of the fenestration system. This assumption is not always valid. Old buildings, and buildings in developed countries, may suffer from poor isolation. Moreover, in office and residential space it is not unusual to leave doors open. The heat/daylight gain or loss with the other zones has therefore to be integrated.

Another limitation of our study, that is valid as much for our optical as for our thermal validation, is that we did not consider the dynamic nature of the CFS characteristics and control strategies. Many shading devices can have their performance changed. For example, venetian blinds can have their tilt angle changed to allow more or less daylight. They are more and more often associated with an automated control strategy. In this research, we mainly focused on the static aspect of its characterization. Further research should investigate how to integrate the control strategy into BIM and take into account human behaviour.

This research would highly benefit from further experimental validation, as much for the optical as for the thermal performance, in order to validate the coverage of this methodology over the wide spectrum of Complex Fenestration Systems.

Moreover, the methodologies and metrics used for daylighting, visual comfort, thermal performance and thermal comfort are mainly relevant to residential and office space. Recent research has been actively focusing on the measurement, digitalization and BIM production of the heritage building, in which our methodologies may not apply.

We mainly focused on rooms at a building level. These models would highly benefit from the urban environment data. The environment data can provide information on the shadowing. Moreover, in urban areas, it is accepted that Urban Heat Island effect raises the exterior air temperature. The effect can go up to 12°C.

Finally, this research should be linked to other works that aims to model the thermal or optical behaviour of other building elements. It can even be extended to model environment components, as street light or trees.

REFERENCES

[AKA1996] Akashi, Yukio, Rikuo Muramatsu, and Sueko Kanaya. "Unified glare rating (UGR) and subjective appraisal of discomfort glare." International Journal of Lighting Research and Technology 28, no. 4 (1996): 199-206.

[ASH2001] Ashmore, Joseph, and Paul Richens. "Computer simulation in daylight design: a comparison." Architectural Science Review 44, no. 1 (2001): 33-44.

[AUC2007] Aucliciens, A., and S. V. Szokolay. "Passive and Low Energy Architecture, International Design Tools and Techniques, University Of Queensland, Department of Architecture, pdf." (2007).

[BAZ1997] Bazjanac, Vladimir, and Drury B. Crawley. "The implementation of industry foundation classes in simulation tools for the building industry." published at escholarship.org, 1997.

[BAZ2001] Bazjanac, Vladimir. Acquisition of building geometry in the simulation of energy performance. No. LBNL-48450. Lawrence Berkeley National Lab.(LBNL), Berkeley, CA (United States), 2001.

[BAZ2010] Bazjanac, Vladimir. "Space Boundary Requirements for Modeling of Building Geometry for Energy and Other Performance Simulation." In CIB W78: 27th International Conference. Cairo, Egypt., 2010.

[BED2017] Beddiar, Karim, and Fabien Imbault. "BIM et énergétique des bâtiments". Dunod, 2017.

[BIA2018] Bian, Yu, and Yuan Ma. "Subjective survey & simulation analysis of time-based visual comfort in daylit spaces." Building and Environment (2018).

[BLI1977] Blinn, James F. "Models of light reflection for computer synthesized pictures." In ACM SIGGRAPH computer graphics, vol. 11, no. 2, pp. 192-198. ACM, 1977.

[BOU2016] Boudhaim, Marouane, Thibault Pflug, Bruno Bueno, Monica Siroux and Tilmann E. Kuhn. “thermal and optical modeling of complex fenestration systems within the context of building information modeling”. Conference paper at ASIM 2016.

[BOU2017] Boudhaim, Marouane, Bruno Bueno, Monica Siroux and Tilmann E. Kuhn. “A BIM-compatible Framework to Assess the Thermal and Optical Performance of Envelope Systems”. Conference paper at ECOS 2017.

[BRE1988] Bretagnon, Pierre, and Gérard Francou. "Planetary theories in rectangular and spherical variables-VSOP 87 solutions." Astronomy and Astrophysics 202 (1988): 309-315.

[BSM2017] BuildingSMART, http://buildingsmart.org/ last accessed on 01 February 2017

[BUE2015] B. Bueno, J. Wienold, A. Katsifaraki, T.E. Kuhn, Fener: a radiance-based modelling approach to assess the thermal and daylighting performance of complex fenestration systems in office spaces, Energy Build. 94 (2015) 10–20,

[BUE2017] B. Bueno, J.M. Cejudo-Lopez, T.E. Kuhn,A general method to evaluate the thermal impact of complexfenestration systems in building zones. Energy and Buildings 155 (2017) 43–53 53

[CAR2014] Cellai, G., C. Carletti, F. Sciurpi, and S. Secchi. "Transparent building envelope: windows and shading devices typologies for energy efficiency refurbishments." In Building Refurbishment for Energy Performance, pp. 61-118. Springer, Cham, 2014.

[CGD2018] Complex glazing database, lbnl, https://windows.lbl.gov/software/cgdb, last visited may 2018.

[CHO1984] Choi, U. S., R. Johnson, and S. Selkowitz. "The impact of daylighting on peak electrical demand." Energy and Buildings 6, no. 4 (1984): 387-399.

[CLA1985] Clark, R. P., and Otto Gustaf Edholm. Man and his thermal environment. Edward Arnold, 1985.

[COD2015] Cody M. Rose; Vladimir, Bazjanac (2015): An algorithm to generate space boundaries for building energy simulation. In: Engineering with Computers 31 (2), S. 271–280. DOI: 10.1007/s00366-013-0347-5.

[DAN2016] Dan Sunday: http://geomalgorithms.com, last accessed on 12 July 2016

[DEA1998] De Dear, Richard, and Gail Schiller Brager. "Developing an adaptive model of thermal comfort and preference." (1998).

[DOE2012] Thomas Doerr "Passive Solar Simplified: Easily design a truly green home for Colorado and the West",CreateSpace Independent Publishing Platform, 2012.

[DOE2018] Energy Plus engineering reference, https://energyplus.net/sites/default/files/pdfs_v8.3.0/EngineeringReference.pdf,

[DONG2017] Dong, B., K. P. Lam, Y. C. Huang, and G. M. Dobbs. "A comparative study of the IFC and gbXML informational infrastructures for data exchange in computational design support environments." In Tenth International IBPSA Conference, pp. 1530-1537. 2007.

[EIN1979] Einhorn, H. D. "Discomfort glare: a formula to bridge differences." Lighting Research & Technology 11, no. 2 (1979): 90-94.

[EIS2018] Johannes Eisenlohr, Christian Eller, Christian Leifgen, Marouane Boudhaim, Tilmann E. Kuhn. "FLEXIBLE FILTERING OF HETEROGENEOUS DATA USING THE EXAMPLE OF THE DESIGN AMD SIMULATION OF BUILDING INTEGRATED PHOTOVOLTAICS", proceedings of BAUSIM 2018.

[EUR2017] European Commission, Energy Efficiency/Buildings, https://ec.europa.eu/energy/en/topics/energy-efficiency/buildings, last visited june 2017.

[FAN1970] Fanger, Poul O. "Thermal comfort. Analysis and applications in environmental engineering." Thermal comfort. Analysis and applications in environmental engineering. (1970).

[FOL1974] Folk Jr, G. E. "Adaptation and heat loss: the past thirty years." Heat Loss from Animals and Man. JL Monteith and LE Mount (ed.), Butterworths, London (1974): 119-146.

[FOL1981] Folk, G. E. "Climatic change and acclimatization." Biometeorology, thermal physiology and comfort (1981): 157-168.

[FON1999] Fontoynont, M., Laforgue, P., Mitanchey, R., Aizlewood, M., Butt, J., Carroll, W., Hitchock, R., Erhorn, H., De Boer, J., Dirksmöller, M. and Michel, L., 1999. Validation of daylighting simulation programs. IEA-SHC-Task-21/Annex-29..

[FRI1993] Frisancho, A. Roberto. Human adaptation and accommodation. University of Michigan Press, 1993.

[FUC1980] Fuchs, H., Kedem, Z. M., & Naylor, B. F. (1980). “visible surface generation by a priori tree structures”. Computer Graphics (ACM), 14(3), 124-133.

[GAL2002] Galasiu, Anca D., and Morad R. Atif. "Applicability of daylighting computer modeling in real case studies: comparison between measured and simulated daylight availability and lighting consumption." Building and Environment 37, no. 4 (2002): 363-377.

[GEI2016] Geisler-Moroder, David, Eleanor S. Lee, and Gregory J. Ward. Validation of the Five-Phase Method for Simulating Complex Fenestration Systems with Radiance against Field Measurements. Lawrence Berkeley National Lab.(LBNL), Berkeley, CA (United States), 2016

[GOL1974] Goldsmith, R. "Acclimatisation to cold in man–fact or fiction? Heat loss from animals and man: assessment and control." Proceedings of the 20th Easter School in Agricultural Science, Univ. of Nottingham, London (1974).

[GRY1989] Grynberg, Anat(1989). "Validation of RADIANCE." Lawrence Berkeley Laboratory, Berkeley LBID 1575. Available from: https://eetd.lbl.gov/sites/all/files/publications/lbid-1575.pdf

[HEL2006] Hellwig, R. T., Sabine Brasche, and W. Bischof. "Thermal Comfort in Offices–Natural Ventilation vs. Air Conditioning." In Proceedings of congress Comfort and Energy Use in Buildings–Getting it Right, Winsor. 2006.

[HES2012] Heschong, Lisa, Van Den Wymelenberg, Marilyne Andersen, N. Digert, L. Fernandes, A. Keller, J. Loveland et al. Approved Method: IES Spatial Daylight Autonomy (sDA) and Annual Sunlight Exposure (ASE). No. EPFL-STANDARD-196436. IES-Illuminating Engineering Society, 2012.

[KAJ1986] Kajiya, James T. "The rendering equation." ACM Siggraph Computer Graphics. Vol. 20. No. 4. ACM, 1986.

[KAT2017] Katsifaraki, Angelina, Bruno Bueno, and Tilmann E. Kuhn. "A daylight optimized simulation-based shading controller for venetian blinds." Building and Environment 126 (2017): 207-220.

[KHO1996] Khodulev, Andrei, and Edward Kopylov. "Physically accurate lighting simulation in computer graphics software." Keldysh Institute of Applied Mathematics, Russian Academy of Sciences. Moscow State University. Moscow (1996).

[KLE1994a] Klems JH. 1994. A new method for predicting the solar heat gain of complex fenestration systems: I. Overview and derivation of the matrix layer calculation. ASHRAE Trans. 100(1): 1065–1072.

[KLE1994b] Klems JH. 1994. A new method for predicting the solar heat gain of complex fenestration systems: II. Detailed description of the matrix layer calculation. ASHRAE Trans.100(1):1073–1086

[KUH2011] Kuhn, Tilmann E.; Herkel, Sebastian; Frontini, Francesco; Strachan, Paul; Kokogiannakis, Georgios (2011): Solar control. A general method for modelling of solar gains through complex facades in building simulation programs. In: Energy and Buildings 43 (1), S. 19–27. DOI: 10.1016/j.enbuild.2010.07.015.

[KUH2017] Kuhn, Tilmann E. "State of the art of advanced solar control devices for buildings." Solar Energy 154 (2017): 112-133.

[LEE2018] Lee, Eleanor S., David Geisler-Moroder, and Gregory Ward. "Modeling the direct sun component in buildings using matrix algebraic approaches: Methods and validation." Solar Energy 160 (2018): 380-395.

[LIL2014] Lilis, G. N., G. I. Giannakis, G. D. Kontes, and D. V. Rovas. "Semi-automatic thermal simulation model generation from IFC data." In Proc. of European Conference on Product and Process Modelling, Vienna, Austria, pp. 503-510. 2014.

[LIL2015] Lilis, G. N., G. I. Giannakis, and D. V. Rovas. "Detection and semi-automatic correction of geometric inaccuracies in IFC files." proc. of Building Simulation IBPSA conference. 2015.

[MAR1995] Mardaljevic, John. "Validation of a lighting simulation program under real sky conditions." International Journal of Lighting Research and Technology 27.4 (1995): 181-188.

[MAR2000] Mardaljevic, J. (2000). “Daylight simulation: validation, sky models and daylight coefficients” (Doctoral dissertation, © John Mardaljevic).

[MAR2001] Mardaljevic, John. "The BRE-IDMP dataset: a new benchmark for the validation of illuminance prediction techniques." Transactions of the Illuminating Engineering Society 33.2 (2001): 117-134.

[MAT2017] Regular grids: http://mathworld.wolfram.com/Grid.html last accessed on 01 February 2017

[MAY1993] Mayer, E. "Objective criteria for thermal comfort." Building and environment 28, no. 4 (1993): 399-403.

[MCN2012] McNeil, Andrew, and E. S. Lee. "A validation of the Radiance three-phase simulation method for modelling annual daylight performance of optically complex fenestration systems." Journal of Building Performance Simulation 6.1 (2013): 24-37.

[MCN2013] McNeil, A. (2013). The Five-Phase Method for Simulating Complex Fenestration with Radiance. http://radiance-online.org/learning/tutorials/fivephasetutorialfiles/Tutorial-ivePhaseMethod_v2.pdf, 1-23

[MCN2013] McNeil, Andrew, et al. "A validation of a ray-tracing tool used to generate bi-directional scattering distribution functions for complex fenestration systems." Solar Energy 98 (2013): 404-414.

[NAB2006a] Nabil, Azza, and John Mardaljevic. "Useful daylight illuminance: a new paradigm for assessing daylight in buildings." Lighting Research & Technology 37, no. 1 (2005): 41-57.

[NAB2006b] Nabil, Azza, and John Mardaljevic. "Useful daylight illuminances: A replacement for daylight factors." Energy and buildings 38, no. 7 (2006): 905-913.

[OCH2011] Ochoa, C.E., Aries, M.B.C., Hensen, J.L.M. 2011. State of the art in lighting simulation for building science: a literature review. Journal of Building Performance Simulation, Article in Press. DOI: 10.1080/19401493.2011.558211

[PEA1895] Pearson, Karl. "Note on regression and inheritance in the case of two parents." Proceedings of the Royal Society of London 58 (1895): 240-242.

[PER1990] Perez, Richard, Pierre Ineichen, Robert Seals, Joseph Michalsky, and Ronald Stewart. "Modeling daylight availability and irradiance components from direct and global irradiance." Solar energy 44, no. 5 (1990): 271-289.

[PER1993] Perez, Richard, Robert Seals, and Joseph Michalsky. "All-weather model for sky luminance distribution—preliminary configuration and validation." Solar energy 50, no. 3 (1993): 235-245.

[PHO1975] Phong, Bui Tuong. "Illumination for computer generated pictures." Communications of the ACM 18, no. 6 (1975): 311-317.

[PYS2018] PySolar documentation, "docs.pysolar.org", last visited july 2018.

[RAD2017] https://www.radiance-online.org/learning/tutorials/fivephasetutorialfiles/Tutorial-FivePhaseMethod_v2.pdf, last visited february 2017

[RAD2018] https://www.radiance-online.org/learning/tutorials/matrix-based-methods, last visited august 2018

[REI2001] Reinhart, Christoph F., and Oliver Walkenhorst. "Validation of dynamic RADIANCE-based daylight simulations for a test office with external blinds." Energy and buildings 33.7 (2001): 683-697.

[REI2006] Reinhart, Christoph F., John Mardaljevic, and Zack Rogers. "Dynamic daylight performance metrics for sustainable building design." Leukos 3, no. 1 (2006): 7-31.

[ROO2001] Karlsson, J., M. Rubin, and A. Roos. "Evaluation of predictive models for the angle-dependent total solar energy transmittance of glazing materials." Solar Energy 71, no. 1 (2001): 23-31.

[SPE1904] Spearman, Charles. "The proof and measurement of association between two things." The American journal of psychology 15, no. 1 (1904): 72-101.

[STE2013] Stevanović, Sanja. "Optimization of passive solar design strategies: A review." Renewable and Sustainable Energy Reviews 25 (2013): 177-196.

[SUK2016] Suk, Jae Yong, Marc Schiler, and Karen Kensek. "discomfort glare metrics." (2016)

[SZO2014] Szokolay, S. V. "Introduction to architectural science: the basis of sustainable design. 2014."

[TAM1992] Filippo Tampieri. “Newell's Method for Computing the Plane Equation of a Polygon”. In Graphics Gems III, Academic Press, 1992, pp. 231–232.

[TSA2003] Tsangrassoulis, Aris, and Vassilis Bourdakis. "Comparison of radiosity and ray-tracing techniques with a practical design procedure for the prediction of daylight levels in atria." Renewable Energy 28, no. 13 (2003): 2157-2162.

[UBB1998] Ubbelohde, M. Susan, and Christian Humann. "Comparative evaluation of four daylighting software programs." Proceedings of ACEE Summer Study on Energy Efficiency in Buildings, Pacific Grove, CA (1998): 23-28.

[WAR1994a Ward, Gregory J. "The RADIANCE lighting simulation and rendering system." Proceedings of the 21st annual conference on Computer graphics and interactive techniques. ACM, 1994.

[WAR2011] Ward, Gregory, et al. "Simulating the daylight performance of complex fenestration systems using bidirectional scattering distribution functions within radiance." Leukos 7.4 (2011): 241-261.

[WIE2006] Wienold, Jan, and Jens Christoffersen. "Evaluation methods and development of a new glare prediction model for daylight environments with the use of CCD cameras." Energy and buildings 38.7 (2006): 743-757.

[WIE2017] Wienold, Jan, et al. "Comparison of luminance-based metrics in different lighting conditions." Proceedings of the CIE 2017, Midterm Meeting, Jeju Island, Korea. No. EPFL-CONF-232380. CIE, Vienna, 2017.

[WIEN2004] Wienold, Jan. "Evalglare–A new RADIANCE-based tool to evaluate daylight glare in office spaces." 3rd International RADIANCE workshop 2004. 2004.

[WIEN2009] Wienold, Jan. "Dynamic daylight glare evaluation." In Proceedings of Building Simulation, pp. 944-951. 2009.

[WOO2016] Jeong, WoonSeong; Son, JeongWook (2016): An Algorithm to Translate Building Topology in Building Information Modeling into Object-Oriented Physical Modeling-Based Building Energy Modeling. In: Energies 9 (1), S. 50. DOI: 10.3390/en9010050.

[WYM2014] Van Den Wymelenberg, Kevin, and Mehlika Inanici. "A critical investigation of common lighting design metrics for predicting human visual comfort in offices with daylight." Leukos 10.3 (2014): 145-164.

CIE (1995). Publication No. 117, Discomfort glare in interior lighting, Commission Internationale de l'Eclairage, Vienna, Austria

IES Committee on Recommendations for Quality and Quantity of Illumination. Subcommittee on direct glare (1966). Outline of a standard procedure for computing visual comfort ratings for interior lighting: Report No. 2, Illuminating Engineering, 61, No. 10.

ISO 6707-1:1989, “Building and civil engineering -- Vocabulary -- Part 1: General terms”, published on: 1989-08

ISO 16739:2013, “Industry Foundation Classes (IFC) for data sharing in the construction and facility management industries”, published on 2013-04.

Performances Optiques Et Thermiques Des Systèmes De Fenestration Complexes Dans Le Contexte Du BIM

I. Introduction

L'efficacité énergétique du bâtiment occupe une place importante dans la phase de planification des projets de construction. La façade, intermédiaire entre le bâtiment et l'environnement extérieur, joue un rôle clé pour déterminer les performances énergétiques du bâtiment. Les systèmes de fenestration complexes (CFS) sont donc généralement utilisés pour améliorer son efficacité. L'étude des performances de la façade inclut généralement la consommation d'énergie, l'éclairage naturel et les aspects de confort visuel et thermique afin de choisir le meilleur CFS.

Une évaluation précise de l'impact du CFS sur ces aspects (performance optique, thermiques, confort optique et thermique) nécessite des simulations avec des données basées sur la géométrie du bâtiment et les propriétés optiques et thermiques de tous les éléments. En pratique, on ne modélise la plupart du temps que les murs, le sol, le plafond et le système de fenestration.

Cette évaluation est dans la plupart des cas gérée par des architectes, mais de plus en plus de bâtiments complexes d'un point de vue architectural s'avèrent être un défi complexe et sont sous-traités à des experts. Ces simulations s'avèrent être un défi majeur même pour les experts du milieu en pratique. Il y a plusieurs problèmes à résoudre avant de pouvoir effectuer des simulations :

- La caractérisation optique disponible du CFS est généralement insuffisante. Il faut que les propriétés du CFS soient mesurées ou calculées à partir de modèles 3D très détaillés qui ne sont souvent pas fournis. Car ces

modèles n'ont soit pas été effectués dans un logiciel 3D, soit sont considérés comme des secrets industriels. Dans le cas où ces modèles sont accessibles, ils représentent souvent la conception idéale sans les imperfections dues à la fabrication. Par exemple, une déviation de ± 5 ° a été observée entre les angles d'inclinaison des lamelles . Les mesures expérimentales sont généralement le seul moyen d'obtenir des données fiables et de caractériser le système de fenestration.

- Le défi ne s'arrête pas à la modélisation du CFS lui-même. Créer un modèle énergétique du bâtiment (BEM) entier est une tâche très complexe et chronophage. La préparation des données d'entrée peut prendre jusqu'à 80% du temps passé dans un projet. La géométrie des bâtiments est généralement disponible sous la forme d'un plan d'architecte dans un logiciel de CAO 2D. Ces plans ne sont pas directement utilisables dans de nombreux moteurs de simulation nécessitant des modèles 3D. De plus, les matériaux des éléments de construction ne sont souvent pas directement intégrés dans les modèles CAO mais fournis dans une documentation séparée.

Pour résoudre ces problèmes, de récents efforts se sont orientés vers l'utilisation de modèles plus riches tels que le Building Information Modeling (BIM). Ces modèles offrent une opportunité pour l'automatisation et l'économie de coûts. Les performances de plusieurs modèles de CFS peuvent facilement être comparées dans la phase de conception du bâtiment afin de choisir le produit le plus performant. Malheureusement, le BIM souffre de plusieurs limitations. Le choix de la méthodologie et des modèles à intégrer est important. La problématique de la thèse est donc la suivante : **Est-il possible d'évaluer les performances optiques et thermiques des CFS à partir du BIM ?** Cette question, soulève implicitement d'autres questions :

- Existe-t-il des modèles compatibles avec le BIM dans la littérature ? Sur quels critères faut-il se baser pour les choisir ?
- Comment peut-on intégrer ces modèles au BIM ?
- Quelle serait la précision d'une telle méthodologie ?

II. MODÈLES DE CFS

Après évaluation du BIM durant cette thèse, plusieurs limitations ont été constatées. Par conséquent, trois critères ont été définis pour le choix d'une méthodologie compatible avec le BIM :

- **Indépendant de la représentation géométrique** : le BIM souffre actuellement de plusieurs limitations en pratique quand il s'agit de représenter les données géométriques. Un modèle compatible avec le BIM doit donc obligatoire résider au niveau sémantique du BIM et pas au niveau géométrique.
- **Applicabilité globale** : Les modèles ne doivent pas être limités à un sous-ensemble limité des systèmes de fenestration complexes, mais couvrir le spectre le plus large possible de CFS. En pratique, cela veut dire que le modèle minimalise le nombre d'hypothèses sur le produit qu'il représente.
- **Mesurable** : Les données d'entrée du modèle doit être mesurable à partir du système de fenêtres complexes. Cette caractéristique est généralement requise en pratique car les données à la disposition de l'architecte, et parfois du fabricant, sont insuffisantes pour une modélisation correcte du BIM.

En prenant en compte ces trois critères, deux modèles ont été choisis dans la littérature pour représenter les CFS :

- Le « B-directional Distribution Function » pour la représentation optique
- Le « Blackbox Model » pour la représentation thermique

La précision de ces modèles a été évaluée durant cette étude. En outre, une méthodologie a été développée pour transformer le BIM en modèle compatible avec les logiciels de simulation thermique et optique.

II. BIM AU BEM

Durant notre étude, nous avons réussi à mettre en place une méthodologie pour transformer un BIM en format IFC (Industry Foundation Classes) en modèle compatible avec des logiciels de simulation thermique et optique tels que Radiance/Fener/Energy Plus.

La méthodologie s'appuie sur 6 différentes étapes :

- **Division du bâtiment en espaces adiabatiques** : En se basant sur l'algorithme de Binary Space Partition Tree, il est possible de diviser le BIM en différents espaces isolés (thermiquement ou optiquement).
- **Transformation géométrique** : La géométrie telle qu'utilisée dans le BIM s'appuie, en majorité sur une modélisation implicite. Il faut alors la transformer en géométrie explicite en énumérant les coordonnées des sommets délimitant chaque surface.
- **Distinguer les salles « modèle »** : Les salles « modèle » sont des salles qui peuvent représenter un ensemble de salles au comportement thermique ou optique identique. Des salles sont dites avec le même comportement si elles ont la même géométrie, orientation, matériaux et systèmes de fenestration.
- **Distinguer les surfaces intérieures et extérieures** : Les calculs optiques ou thermiques nécessitent généralement de distinguer les surfaces exposées à l'environnement extérieur des surfaces intérieures où résident généralement les occupants.
- **Créer des points de calculs** : Une fois les surfaces intérieures et extérieures identifiées, l'algorithme les discrétise en plusieurs points de calcul, généralement appelés dans la littérature « sensor points ».
- **Convertir au format approprié** : Une fois toutes ces transformations effectuées, l'algorithme réécrit les surfaces et points de calcul dans le format adéquat.

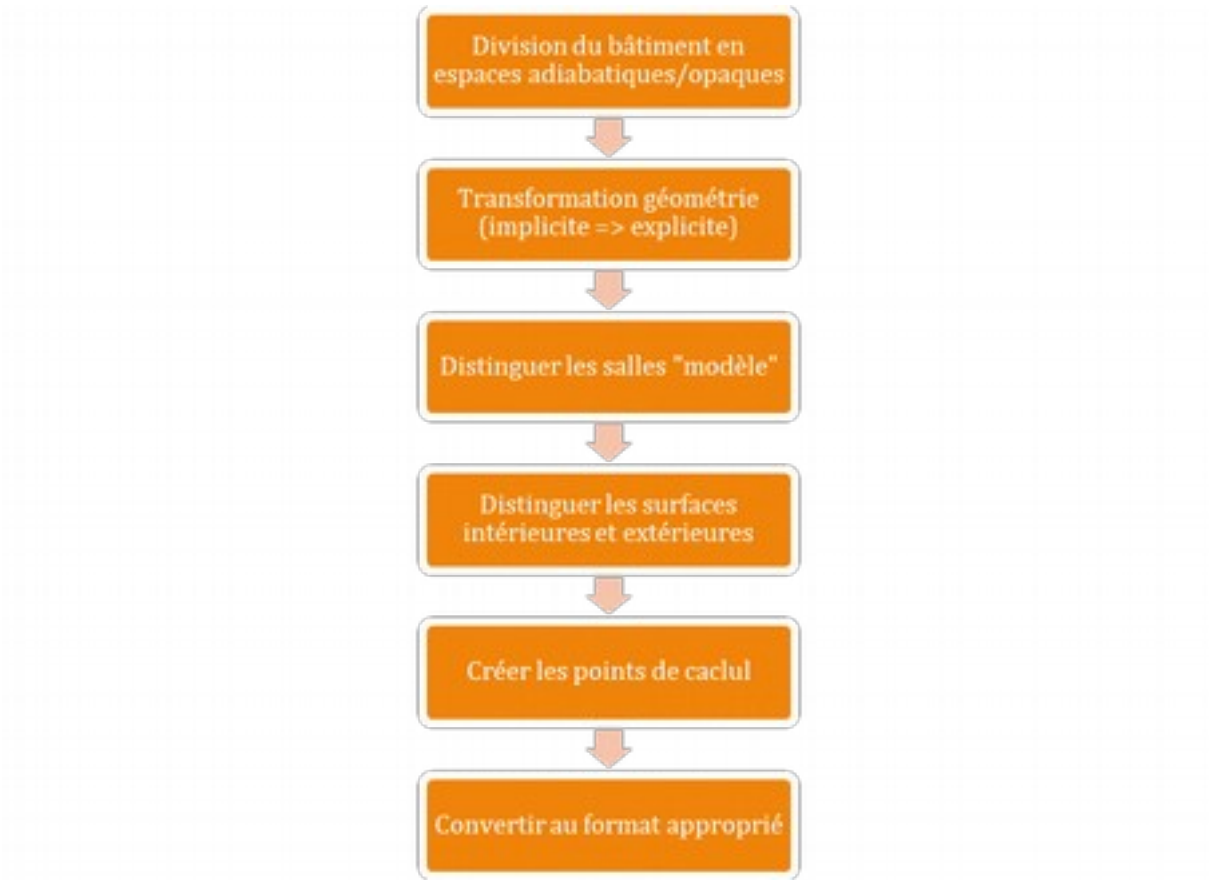

Figure 74: Méthodologie de transformation d'un BIM en format IFC en format compatible avec les logiciels de simulation.

Cette méthodologie a été développée dans un nouveau logiciel appelé Ifc2rad, qui a déjà été utilisé avec succès sur plusieurs bâtiment réels.

III. PERFORMANCES OPTIQUES

Le BSDF a été choisie pour représenter le comportement optique des CFS. Dans la littérature deux méthodes existent principalement pour utiliser, la three-phase method, et son extension la five-phase method. Ces méthodes matricielles se basent sur la discrétisation de l'environnement intérieur, extérieur, et le ciel. Une troisième méthodologue analogue serait d'utiliser le BSDF sans discrétiser l'environnement. Dans notre étude nous avons comparé les trois approches.

L'ensoleillement est surtout utilisé pour déterminer l'autonomie à partir de la lumière naturelle. Il se calcule principalement à partir de la luminance horizontale. Le système

est dit autonome (et donc indépendant de l'éclairage artificiel) à partir du palier de 300 lux. Pour l'ensoleillement, nous avons effectué de luminance horizontale sur plusieurs jours en utilisant différentes variations de notre système de fenestration complexe.

Nous avons utilisé une fenêtre à double vitrage durant plusieurs jours ensoleillés où nous avons mesuré la luminance horizontale. Certains jours les mesures ont été effectuées sans stores vénitiens, et durant d'autres nous avons utilisé les stores. Ces stores ont été utilisés avec un angle d'inclinaison de 5°, 40° et 70°.

Avec la luminance horizontale, nous avons pu calculer le facteur notre indicateur d'ensoleillement, la « Daylight Autonomy ». L'indicateur a été utilisé avec un palier de 300Lux. Nous estimons alors qu'une luminance horizontale supérieure ou égale à 300 Lux équivaut à une situation d'autonomie en ensoleillement.

Nous obtenons, après un test de classification binaire comparant la Daylight Autonomy mesurée et calculée, les résultats suivants.

	Three-phase method		Five-phase method		Sans discrétisation	
Évaluation	Positive	Negative	Positive	Negative	Positive	Negative
Correcte	>99%	>99%	>99%	>99%	>99%	>99%
Fausse	<1%	<1%	<1%	<1%	<1%	<1%

Table 1: Évaluation de l'autonomie en ensoleillement à partir des méthodes basées sur BSDF.

La luminance horizontale mesurée, permet d'estimer correctement, dans plus de 99% des cas, la situation d'autonomie en ensoleillement, peu importe la méthodologie utilisée. Nous concluons donc que les trois méthodes sont assez précises pour calculer le taux d'ensoleillement annuel, peu importe le CFS qu'on a utilisé expérimentalement.

Pour le confort optique, nous nous sommes principalement focalisés sur l'éblouissement. De nombreux indices existent pour évaluer la perception de l'éblouissement, comme la Daylight Glare Probobility (DGP), Daylight Glare Index (DGI), Unified Glare Index (UGR) et Visual Comfort Probability (VCP). De nombreuses études ont essayé d'évaluer leur exactitude. Certaines études évaluent le DGP comme le meilleur indice pour évaluer l'éblouissement due à la lumière naturelle, d'autres ont conclu que toutes les mesures existantes montrent une mauvaise performance après une analyse statistique, tandis que d'autres études statistiques montrent une meilleure performance globale pour certains indices, y compris le

DGP. Dans l'état de l'art, l'évaluation de la perception de l'éblouissement n'est pas un problème totalement résolu, mais le DGP est considéré dans la littérature comme l'un des indicateurs les plus performants.

Le DGP est calculé par la formule suivante :

$$DGP = c_1 . E_V + c_2 . \log\left(1 + \sum_i^n \frac{L_{s,i}^2 . \omega_{s,i}}{E_v^c . P_i^2}\right) + c_3 \quad (3)$$

- E_v : éclairement vertical des yeux (lux)
- L_s : Luminance de la source (cd / m²)
- ω_s : Angle solide de la source
- P: Indice de position
- c1 = 5,87 * 10^{-5}
- c2 = 9,18 * 10^{-2}

Le DGP prend en compte essentiellement deux composantes, la luminance verticale et le contraste dans l'environnement. La composante de contraste est généralement calculée à partir d'une photo représentant ce que verrait l'occupant. Cette photo en pratique est soit prise avec une caméra CCD, soit plus souvent calculée avec le ray-tracing. Ce calcul par la simulation du rendu photo-réaliste pour le DGP est très lent. Deux variantes simplifiées ont alors été développées : l'eDGP (qui prend en compte de façon simplifiée le contraste), et le sDGP (qui prend pas en compte le contraste).

Durant notre étude, des mesures expérimentales ont été effectuées pour comparer le DGP/eDGP/sDGP estimé par la simulation avec le DGP mesuré. La simulation se base sur les trois différentes méthodologies sus-citées : la Three-phase method, la Five-phase method et le rendement à base de tensor-tree sans calcul matriciel.

Nous avons pu établir que la three-phase method est principalement limitée dans les cas où le sujet est soumis aux radiations directes du soleil). La Five-phase method et la méthode sans calcul ne souffrent pas de cette limitation.

Cela est principalement dû au fait qu'elles utilisent un BSDF avec une résolution angulaire supérieure, qui permet de mieux représenter l'apport direct du soleil.

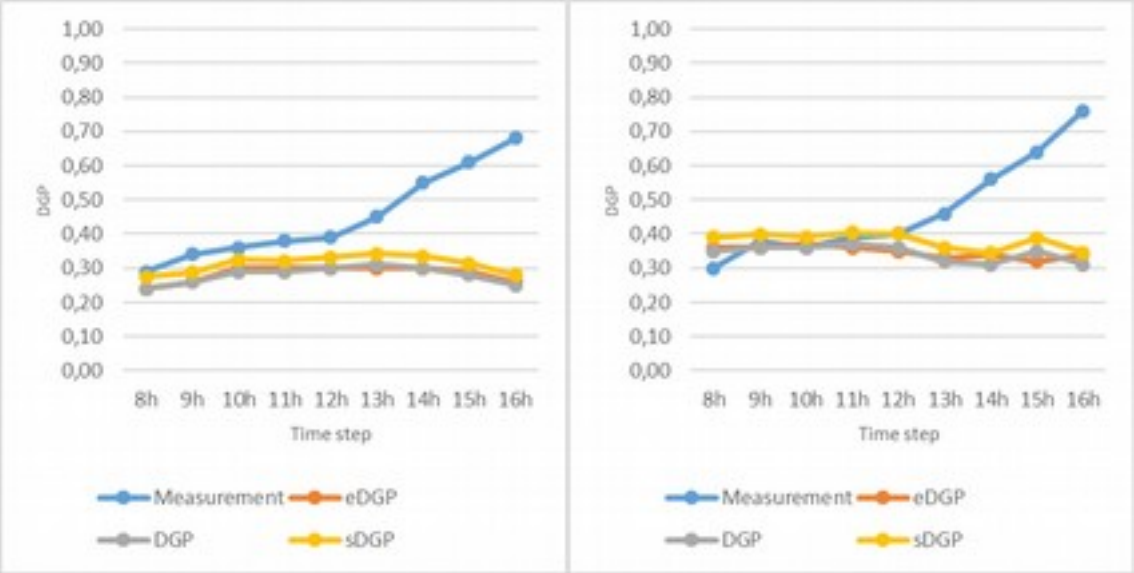

Figure 75: Calcul du DGP/eDGP/sDGP avec la three-phase method et les mesures de DGP le the 04/09/2015 à gauche, et le 05/09/2015 à droite. A partir de 13h le sujet commence à être partiellement soumis aux radiations directes du soleil.

Afin de tester les limites de notre étude sur l'éblouissement, nous avons choisi de faire varier certains paramètres du CFS. Deux paramètres ont eu un effet notable sur les résultats présentés :

Transmittance directe-directe

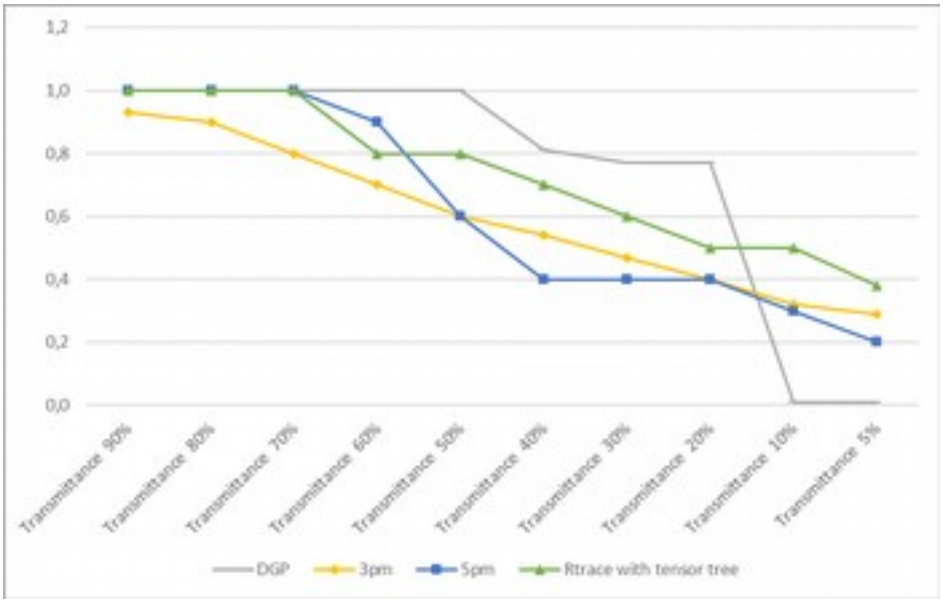

Figure 76: Comparaison des différents DGP en fonction de la transmittance directe-directe.

Notre premier facteur est la transmittance directe-directe. Le DGP calculé montre une corrélation inhabituelle par rapport à la transmittance. Dans les transmissivités élevées,

il prédit un DGP de 1, car l'utilisateur est sous irradiation directe. Dans les transmittances faibles, la capacité du moteur de ray-tracing à trouver la source de lumière est plus faible. A partir de 10 % il est incapable de trouver correctement la source de lumière.

Il convient de noter que le cas des faibles transmittances où Radiance ne parvient pas toujours à trouver la source lumineuse est essentiellement théorique. Les stores vénitiens ont par exemple tendance à avoir des lames plates avec un rayon de courbure relativement élevé, ce qui leur confère une grande transmittance.

Les méthodes basées sur BSDF montrent une relation linéaire avec le transmittance. En excluant la transmittance inférieure à 10%, où notre référence ne peut être utilisée, Rtrace avec un Tensor-tree est la méthodologie qui a la meilleure précision.

Amplitude d'angle de pic

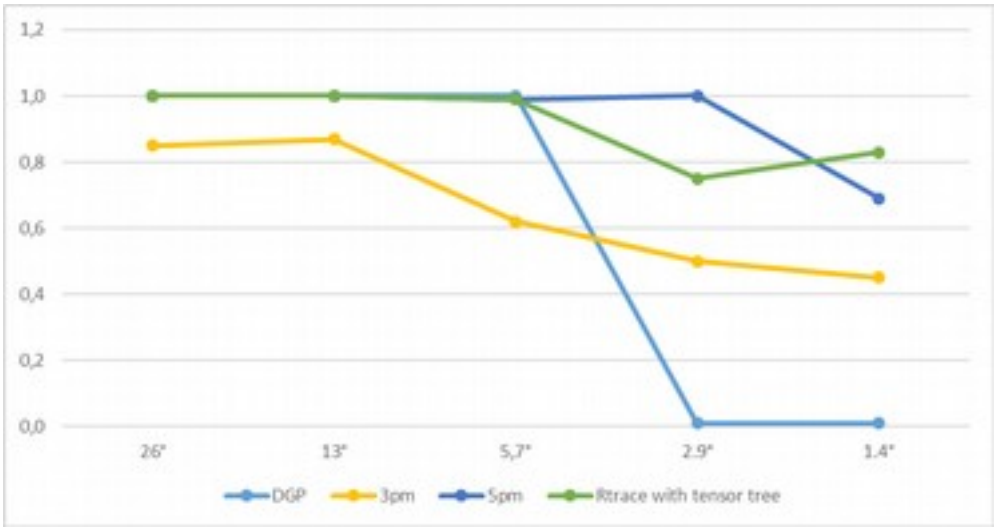

Figure 77:Comparaison des différents DGP en fonction de l'amplitude de l'angle de pic.

Le calcul de DGP montre toujours le même problème à trouver la source lumineuse pour les angles les plus faibles. Les angles très bas ne sont que théoriques car généralement, les stores vénitiens ont des angles >10°.

Les méthodes basées sur BSDF ont montré globalement une meilleure prédiction du DGP dans le cas des angles bas, en particulier ceux à base de Tensor-tree. Pour les angles les plus hauts, les méthodes avec Tensor-tree présent le même DGP que la référence. Elles ont dans tous les cas étudiés, une meilleure précision que la méthode Three-phase

IV. PERFORMANCES THERMIQUES

Pour les performances thermiques, nous avons effectué une étude théorique qui compare la température calculée des surfaces du bâtiment et de l'air avec une simulation basée sur la référence actuelle, l'ISO 15099. La comparaison théorique a été faite en se basant sur 4 CFS différent, à 4 régions et avec 8 orientations différentes. Nous avons essayé de faire varier aux maximum ces paramètres afin d'éviter au maximum les biais dans nos résultats.

Nous avons conclu que le calcul des températures de l'air a un écart quadratique moyen de 0.6°C. Les surfaces intérieures du bâtiment ont le même écart. L'exception notable est la température de la surface intérieure du système de fenestrations complexes.

L'erreur sur les systèmes de fenestration dépend de la position du dispositif du système de contrôle solaire. Quand il n'y a pas de dispositif ou que le dispositif est à l'extérieur, l'écart est de 1°C, alors que quand il est à l'intérieur l'écart est de 2.8°C.

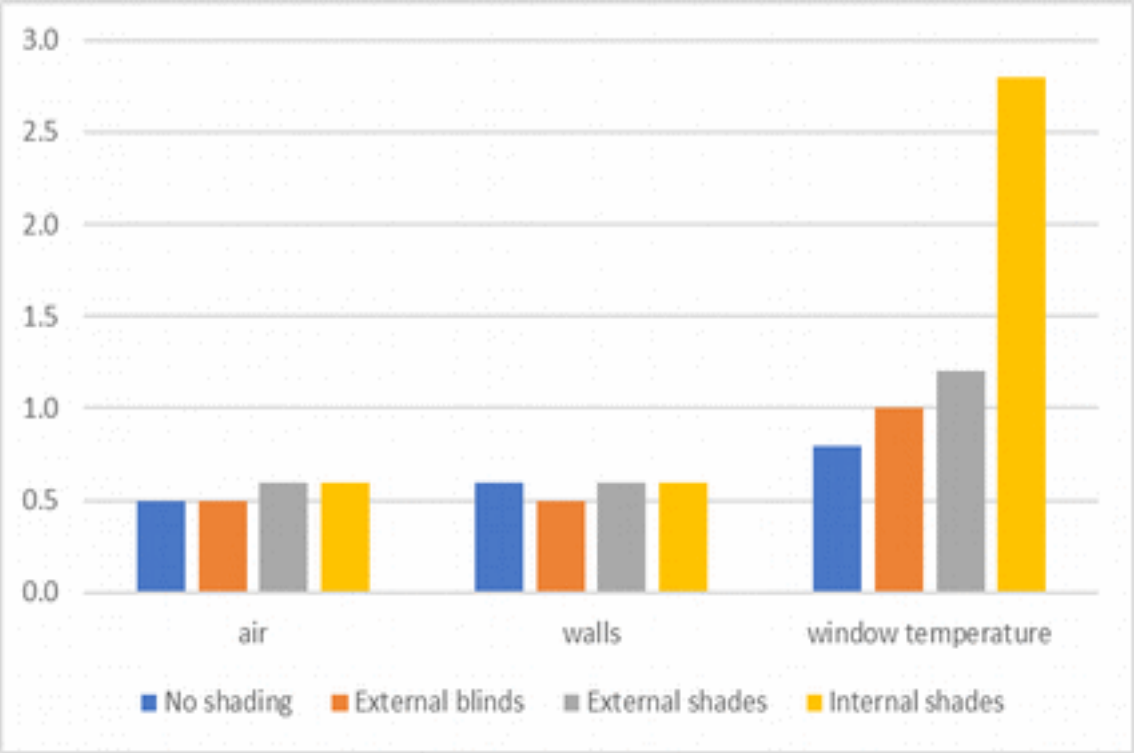

Généralement, pour les calculs de chauffage et de rafraichissement on se base sur la température de l'air. La température des surfaces est surtout utile pour le confort thermique. Nous avons évalué durant notre étude l'erreur engendrée sur l'estimation du confort thermique par les écarts sur la température des surfaces des systèmes de

fenestration. Nous avons conclu que son impact était très réduit. En se basant sur le modèle adaptif pour le confort thermique, le Blackbox Model pouvait prédire correctement le confort ou l'inconfort dans plus de 95% des cas.

V. CONCLUSION ET PERSPECTIVES

Cette thèse s'est articulée autour de l'évaluation des performances thermiques et optiques des CFS à partir du BIM. Le BIM, nouvelle technologie pour la modélisation de bâtiment, offre de nouvelles possibilités, pour lesquelles nous avons développé une méthodologie pour évaluer les performances optiques et thermiques des CFS.

Ces performances se sont concentrées sur 4 axes:

- Éclairage naturel
- Confort visuel
- Performances thermiques
- Confort thermique

Pour l'éclairage naturel, les modèles proposés prédisent correctement à 99% les conditions d'éclairage, peu importe la méthode utilisée. Tandis que pour l'éblouissement, la méthode Three-phase qui utilise le BSDF de Klems a un écart d'approximativement 26% en moyenne. Les méthodes à base de Tensor-tree ont un écart moyen d'approximativement 10%. Le choix de la méthode utilisée dépend donc de trois facteurs : les données disponibles, la précision désirée et le temps de calcul alloué.

Pour les performances thermiques, l'utilisation du Blackbox model permet de calculer la température de l'air et du mur avec un écart moyen d'environ 0.6°C. Ce modèle ceci-dit, du fait de son utilisation de couches virtuelles, accuse un plus gros écart pour le calcul de la température de la couche intérieure de la fenêtre. Les fenêtres avec un système d'ombrage intérieures accusent des écarts en moyenne de 2.8°C. Les fenêtres avec un système d'ombrage extérieur ou sans système d'ombrage ont des écarts moyens de respectivement 0.8°C et 2.6°C. Pour le confort thermique, ces écarts ne sont pas problématiques vu que le modèle prédit correctement la satisfaction des occupants à 99%.

Certaines question restent cependant ouvertes à la fin de cette these. Les performances thermiques ont été calculées dans un régime permanent, mais le régime transitoire n'a pas été évalué. Le modèle blackbox étudié montre rapidement ses limites pour estimer

la température de la couche intérieure du CFS. Plusieurs pistes d'améliorations peuvent être envisagées comme une meilleure prise en compte des conditions limites, une mesure expérimentale de l'absorbance de la couche Pour le confort visuel, l'indice étudié suppose une personne avec un champ de vision statique. Une future étude devrait se concentrer sur la prise en compte du comportement humain.

Marouane BOUDHAIM

Performances optiques et thermiques des systèmes de fenestration complexes dans le contexte du BIM

Résumé

L'efficacité énergétique du bâtiment occupe une place importante dans la phase de planification des projets de construction. La façade, intermédiaire entre le bâtiment et l'environnement extérieur, joue un rôle clé pour déterminer les performances énergétiques du bâtiment. Les systèmes de fenestration complexes (CFS) sont donc généralement utilisés pour améliorer son efficacité. L'étude des performances de la façade inclut généralement la consommation d'énergie, l'éclairage naturel et les aspects de confort visuel et thermique afin de choisir le CFS optimal.
Pour résoudre ces problèmes, de récents efforts se sont orientés vers l'utilisation de modèles plus riches tels que le Building Information Modeling (BIM). Ces modèles offrent une opportunité pour l'automatisation et l'économie de coûts. Les performances de plusieurs modèles de CFS peuvent facilement être comparées dans la phase de conception du bâtiment afin de choisir le produit le plus performant.
Dans cette thèse, nous présentons tout d'abord une méthodologie pour transformer le modèle architectural du BIM en modèle énergétique compatible avec plusieurs logiciels de simulation. Nous présentons aussi des modèles optique et thermique compatibles avec le BIM. Ces modèles sont validés par une comparaison avec des données expérimentales et des données théoriques issues des normes actuelles.

Mots-clés : BIM, système de fenestrations complexes, thermique du bâtiment, confort optique, confort thermique, éclairage naturel.

Résumé en anglais

The energy efficiency of the building occupies an important place in the planning phase of construction projects. The facade, intermediate between the building and the external environment, plays a key role in determining the energy performance of the building. Complex fenestration systems (CFS) are therefore generally used to improve its efficiency. The facade performance's evaluation typically includes energy consumption, natural lighting, visual and thermal comfort aspects in order to choose the optimal CFS.
To solve these problems, recent efforts have focused on using richer models such as Building Information Modeling (BIM). These models provide an opportunity for automation and cost savings. The performance of several CFS models can easily be compared in the design phase of the building to choose the best performing product.
In this thesis, we first present a methodology to transform the architectural model of the BIM into a Building Energy Model compatible with several simulation software. We also present optical and thermal models compatible with BIM. These models are validated by comparison with experimental data and theoretical data from current standards.

Keywords: BIM, Complex Fenestration Systems building thermal design, optical comfort, thermal comfort, daylighting.